Imaging Hippocampal Hemodynamics in Schizophrenia

By

Pratik Talati

Dissertation

Submitted to the Faculty of the

Graduate School of Vanderbilt University

in partial fulfillment of the requirements

for the degree of

DOCTOR OF PHILOSOPHY

in

Neuroscience

December, 2015

Nashville, TN

Approved:

Bruce D. Carter, Ph.D.

Manus J. Donahue, Ph.D.

Brandon A. Ally, Ph.D.

Stephan H. W. Heckers, M.D., M.Sc.

Dedicated to my family and friends

ACKNOWLEDGEMENTS

This work would not be possible without the support of many members within the Vanderbilt community. First and foremost, I would like to thank Dr. Stephan Heckers, my thesis advisor, for spending countless hours mentoring me through my graduate school training. I'd also like to thank Drs. Swati Rane Levendovszky and Manus J. Donahue for their mentorship and technical expertise with the imaging methods. I'm also grateful to Drs. Bruce Carter and Brandon Ally for providing valuable feedback while serving on my thesis committee. Finally, I'm grateful to the members of the Heckers Lab and the Psychiatric Neuroimaging Program for creating a great work environment.

I would not be able to complete this project without the support of the Vanderbilt Medical Scientist Training Program under National Institute for General Medical Studies (T32 GM07347), the National Institute of Mental Health (R01 MH070560, F30 MH102846), the Vanderbilt Institute for Clinical and Translational Research (UL1 TR000445 from NCATS/NIH), and the Vanderbilt University Graduate School Dissertation Enhancement award.

TABLE OF CONTENTS

LIST OF TABLES

Table Page

LIST OF FIGURES

Figure Page

LIST OF ABBREVIATIONS

AIF	arterial input function
ASL	arterial spin labeling
CA	cornu Ammonis
cASL	continuous arterial spin labeling
CBF	cerebral blood flow
CBV	cerebral blood volume
DSC	dynamic susceptibility contrast
DSM	Diagnostic and Statistical Manual of Mental Disorders
iVASO	inflow-based vascular-space-occupancy
MRI	magnetic resonance imaging
MTT	mean transit time
pASL	pulsed arterial spin labeling
pCASL	pseudocontinuous arterial spin labeling
PET	positron emission tomography
PLD	post-labeling delay
ROI	region of interest
SNR	signal to noise ratio
SS	steady state
SVD	singular value decomposition

CHAPTER I

INTRODUCTION

Introduction

The hippocampus is a bilateral medial temporal lobe structure that is responsible for declarative memory and spatial navigation (Morris, Garrud et al. 1982; Eichenbaum 2004). It runs along the base of the temporal horns of the lateral ventricles and is composed of the cornu Ammonis (CA) and the dentate gyrus, which form "two interlocking, U-shaped laminae" (Duvernoy 2013). A computer rendering of the human brain obtained from magnetic resonance imaging (MRI), with part of the temporal lobe removed to highlight the human hippocampus *in vivo*, is shown in Figure 1.

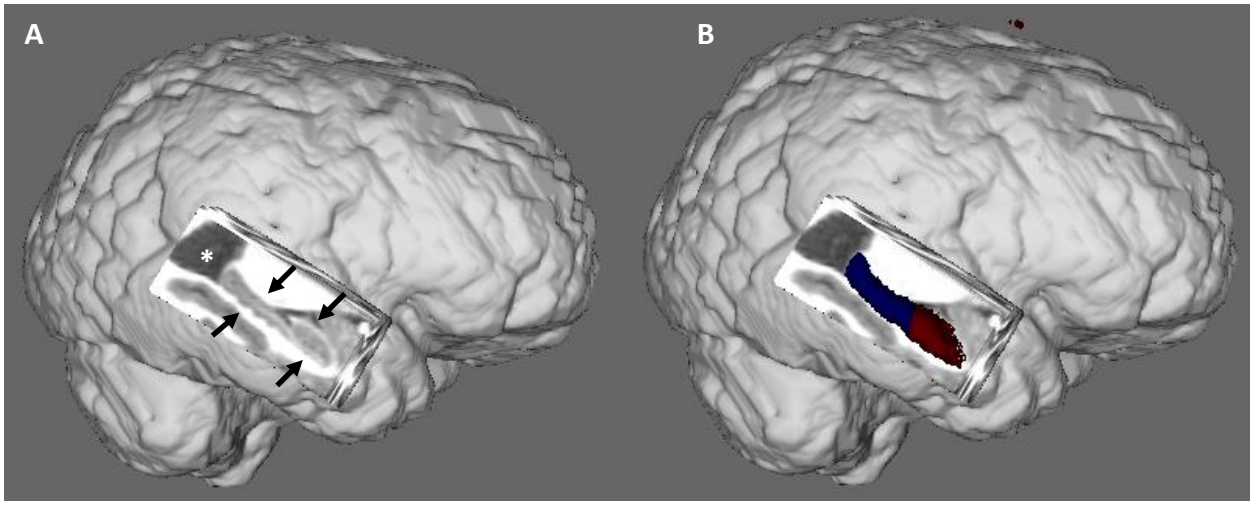

Figure 1 View of the hippocampus from outside of the brain
Figure 1A shows the right hippocampus (outlined by black arrows) and the temporal horn of the lateral ventricle (white asterisk) as seen when looking into the temporal lobe from the outside of the brain. Figure 1B illustrates the anterior (red) and posterior (blue) hippocampus for the same subject.

The human hippocampus can be examined along two axes: longitudinal and transverse. The longitudinal axis is shown in Figure 1A and can be used to easily visualize the anterior and posterior parts, as illustrated in Figure 1B. The anterior hippocampus contains the uncus, which

is defined as a folding over and rotation of the anterior portion of the hippocampus that occurs during brain development (Gloor 1997). Thus, the anterior hippocampus is defined as containing more than one cut through the hippocampus (due to the uncus) in the coronal view (Duvernoy and Bourgouin 1998). From the lamellar hypothesis of hippocampal organization, the hippocampus can also be viewed as a series of independent, transverse slices stacked along the longitudinal axis (Andersen, Bliss et al. 1971). Each transverse slice of the hippocampus contains several subfields, including the subiculum, CA1-4, and the dentate gyrus. These regions are connected to the entorhinal cortex through an intrinsic system called the tri-synaptic pathway. The entorhinal cortex receives inputs from polymodal association cortices (Insausti 1993) and sends excitatory, glutamatergic projection fibers via pyramidal cells to the hippocampus and dentate gyrus. As shown in Figure 2, the glutamatergic fibers either project directly to the CA1 subfield (direct pathway) or project indirectly to the CA1 subfield by traveling through the dentate gyrus and CA3 subfield (indirect pathway) (Amaral and Witter 1989). Fibers from the CA1 subfield then project to the subiculum and other brain regions. Together, the transverse and longitudinal axes can allow for the hippocampus to be examined through a three-dimensional coordinate system (e.g., left anterior CA1, right posterior subiculum), which can be useful when investigating various diseases that involve the hippocampus.

Importantly, the CA subfields are only definitively identified through neurohistological examination of its pyramidal neurons. The CA1 is a continuation of the subiculum and is the largest subfield (Simic, Kostovic et al. 1997). The pyramidal cells are triangular, small, and well-spaced out in this subfield. In contrast, the CA2 subfield contains densely packed, ovoid

pyramidal neurons (Duvernoy 2013). CA3 is similar to CA2 except the neurons are not packed as tightly. Another feature that helps characterize the CA3 is the presence of the "mossy" axons or fibers from the dentate gyrus between the pyramidal and RLM layers, which forms a unique layer called the stratum lucidum. Finally, the CA4 is located in the concavity of the dentate gyrus. The pyramidal neurons are large and ovoid interspersed among the "mossy" fibers.

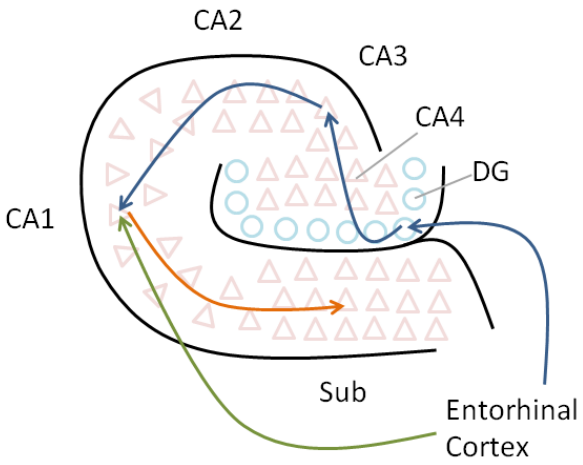

Figure 2 Hippocampal tri-synaptic pathway
This cartoon of the hippocampus in the transverse axis illustrates projections directly from the entorhinal cortex to the CA1 subfield (green) and indirect projections (blue) to the CA1 through the dentate gyrus (DG) and the CA3 subfield. The CA1 then projects to other subfields (orange), including the subiculum (Sub). The red triangles represent pyramidal cells in the CA and the blue circles represent cells in the dentate gyrus.

Just as the hippocampus can be partitioned into several structural units, it is currently accepted that the hippocampus is divided into several functional modules, with each subfield of the hippocampus participating in a different task (Small, Schobel et al. 2011). The entorhinal cortex functions in brief memory retention (Brickman, Stern et al. 2011) and the subiculum is responsible for memory retrieval. The CA1 subfield is responsible for input integration (comparing old and new stimuli), the CA3 is responsible for pattern completion (retrieving information based on partial cues)(Fellini, Florian et al. 2009), and the dentate gyrus is

responsible for spatial pattern separation (distinguishing between similar events at different time periods)(Schmidt, Marrone et al. 2012). These modules can work together to process and route multisensory information for long term storage in the cortex. For example, input from the entorhinal cortex to the dentate gyrus is associated with learning, and CA3 and CA1 are responsible for short and intermediate-term retrieval, respectively, while backprojections to neocortical regions help with long term memory retrieval (Kesner and Rolls 2015).

The hippocampus is able to carry out its function through a delicate balance of pyramidal cells and interneurons that contain gamma-aminobutyric acid (GABA). Approximately 90% of all neuronal cells in the hippocampus are pyramidal neurons, and the rest are GABAergic interneurons (Heckers and Konradi 2010). This is in contrast to the neocortex, which has six layers with 70-80% excitatory pyramidal cells and 20-30% interneurons (Markram, Toledo-Rodriguez et al. 2004). Hippocampal interneurons synchronize pyramidal cell activity and generate oscillatory rhythms (e.g. theta, gamma) that are crucial for hippocampal function, especially memory (Cobb, Buhl et al. 1995; Markram, Toledo-Rodriguez et al. 2004).

Testing models of hippocampal dysfunction using neuroimaging

Neuroimaging methods can be implemented to study patients with neuropsychiatric disorders (Table 1). This allows for insight into clinical diseases by testing hypotheses about hippocampal dysfunction and monitoring outcomes.

Structural neuroimaging provides information about hippocampal volume and shape. Segmentation protocols generate estimates of hippocampal volume, which are further defined into anterior and posterior regions based on anatomical landmarks in the coronal view. This

method is not sensitive to subtle changes within a region and can be complemented with shape analyses to investigate precise hippocampal morphological changes in neuropsychiatric diseases (Styner, Oguz et al. 2006). While subfields are only inferred from shape analyses, higher resolution imaging, typically in the coronal or oblique coronal view, is used to interrogate hippocampal subfields directly (Thomas, Welch et al. 2008). Findings from hippocampal post-mortem studies in neuropsychiatric disorders provide a contextual framework for structural imaging findings. For example, reduced hippocampal volume can be attributed to cell loss (such as in Alzheimer's disease or epilepsy) or reduced neuropil in the context of no pyramidal cell loss, as seen in schizophrenia.

Table 1 Neuroimaging methods to study the hippocampus in neuropsychiatric diseases

Neuroimaging method	Measure	Pathology	Examples
Structural Imaging (T1)	Brain volume, shape	Cell loss, neuropil changes, white matter pathology	Alzheimer's disease, epilepsy, schizophrenia
Steady State Cerebral Blood Volume (SS CBV)	Blood volume	Abnormal metabolism, angiogenesis	Epilepsy, schizophrenia, vascular disease
Dynamic Susceptibility Contrast (DSC)	Blood volume, blood flow, mean transit time	Abnormal metabolism, angiogenesis, flow	Alzheimer's disease, epilepsy, schizophrenia,
Arterial Spin Labeling (ASL)	Blood flow, blood volume*, arterial arrival time*	Abnormal flow, metabolism,* angiogenesis*	Alzehimer's disease, epilepsy, vascular disease
Inflow-Based Vascular-Space-Occupancy (iVASO)	Blood volume, arterial arrival time#	Abnormal metabolism, angiogenesis	Vascular disease

Table 1 illustrates the relative value of different imaging methods to study neuropsychiatric conditions.
*only multi-postlabeling delay ASL
#only multi-inversion time iVASO

Functional neuroimaging can be used to study hemodynamic parameters, including blood volume; blood flow; arterial arrival time (time for blood water to reach the capillary bed); and mean transit time (time for blood to pass through a tissue), the ratio of blood volume to blood flow. These functional methods have different spatial resolutions, ranging from less than 1 mm to 3-4 mm. This means that some methods only assess regional (anterior, posterior) hippocampal hemodynamics (e.g. arterial spin labeling, inflow-based vascular-space-occupancy) while others provide information at the level of hippocampal subfields (e.g. steady state cerebral blood volume).

Hemodynamic parameters from functional imaging provide an indirect measure of underlying neural activity. Increased neuronal metabolic activity leads to vasodilation and increased blood flow to meet metabolic demand. This process is quite complex and involves both neurons and astrocytes. Molecularly, activation of pre-synaptic neurons leads to glutamate release, which activates post-synaptic neuronal N-methyl-D-aspartate (NMDA) receptors, resulting in calcium influx and subsequent nitric oxide generation through activation of nitric oxide synthase (Attwell, Buchan et al. 2010). The release of nitric oxide leads to increased blood vessel diameter (blood volume) and subsequent increase in blood flow. Astrocytes are located near neural synapses and have end-foot processes that surround blood vessels, making them ideal for regulating blood volume and flow into a metabolically active brain region (Attwell, Buchan et al. 2010). While the molecular signaling pathway is still uncertain, one popular theory proposes that pre-synaptic glutamate release binds to metabotropic glutamate receptors on astrocytes. This raises intracellular calcium levels and generates arachidonic acid and other vasoactive substances that regulate blood vessel diameter

and, consequently, blood flow (Howarth 2014). Taken together, blood volume and blood flow can serve as good proxies of neural activity.

Abnormalities in blood volume and blood flow occur in disease processes based on underlying cellular (e.g. cell loss in Alzheimer's disease) or vascular pathology (e.g. ischemic stroke) and can be studied using imaging methods. For example, in schizophrenia, post-mortem studies support the finding of GABAergic interneuron pathology in the hippocampus (Konradi, Yang et al. 2011; Heckers and Konradi 2014). Interneurons modulate pyramidal cell activity, and interneuron dysfunction can lead to excitation-inhibition imbalances and, and in effect, increased activity within the hippocampus. It has been suggested that the functional output of hippocampal hyperactivity would lead to dopaminergic dysfunction in the ventral tegmental area based on the polysynaptic connectivity between the two regions (Grace 2010; Lodge and Grace 2011). This may lead to the positive and negative symptoms seen in schizophrenia. Functional imaging methods can test this hypothesis by examining hippocampal blood volume and blood flow. It's important to note that while blood volume provides information about changes in basal metabolism due to physiological or pathological conditions (Small, Schobel et al. 2011), another possibility could be due to angiogenesis (Dunn, Roche et al. 2004). Just as with structural imaging, functional imaging needs to be supplemented with contextual information from the literature to make inferences about hippocampal function. In schizophrenia, there have been no reports of hippocampal angiogenesis, suggesting that increased blood volume is due to increased metabolism.

The next section provides a summary of the neuroimaging methods used in this study to investigate the hippocampus in schizophrenia.

MRI methods to study the hippocampus

Structural Imaging: Manual Segmentation

Overview: Although labor intensive, manual segmentation is considered the gold standard in the field and can provide valuable information about hippocampal volume. It requires extensive knowledge about hippocampal anatomy and training to verify accuracy and precision. Tracings are typically generated from a T1-weighted structural image, which has a typical resolution of 1x1x1 mm^3 on a 3T MRI scanner. Recently there have been efforts to push towards sub-millimeter resolution at this field strength, and subfield-level investigations are possible at higher field strengths (e.g. 7T).

Approach: After a structural image is acquired, the image is read into a program such as 3DSlicer to view and trace the hippocampus in three different orientations (coronal, sagittal, and axial). This program also calculates the volume of the traced structure. The hippocampus can be further divided into the anterior and posterior regions based on the presence of more than one cut through the hippocampus in the coronal view (Duvernoy and Bourgouin 1998) to generates 4 different regions of interest (ROIs): right anterior (RA), right posterior (RP), left anterior (LA), and left posterior (LP). Although the size of each person's hippocampus is variable, typically the anterior hippocampus ranges from 1700-2500 mm^3 while the posterior hippocampus ranges from 1100-1800 mm^3.

Figure 3 shows a manually-segmented bilateral hippocampus in one subject in the coronal (Figure 3A), sagittal (Figure 3B), and axial (Figure 3C) planes. These manually segmented hippocampal regions of interest (ROIs) can then be overlaid on functional imaging sequences to answer specific questions about hippocampal function.

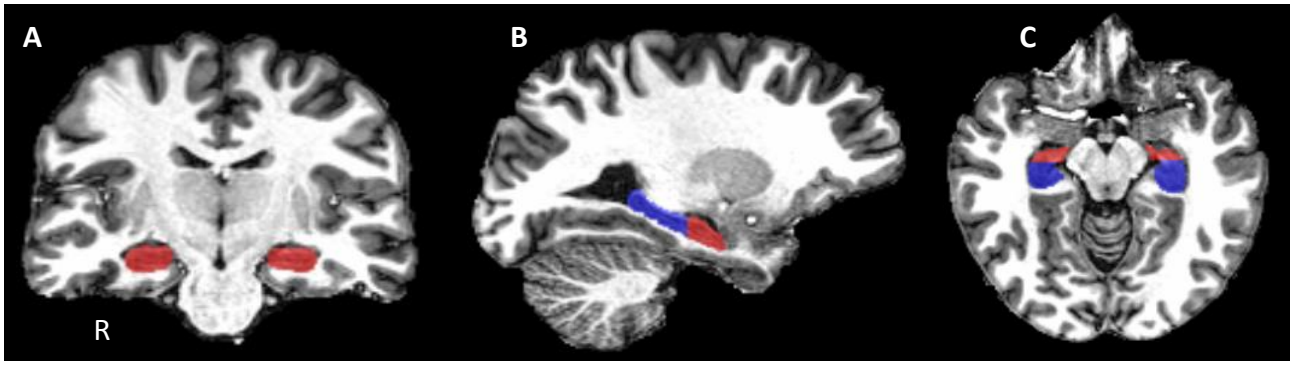

Figure 3 Manual segmentation of the hippocampus
The left panel illustrates manual segmentation of the hippocampus viewed in the coronal orientation. The red denotes the anterior hippocampus and the blue denotes the posterior hippocampus. The middle panel illustrates the tracings in the sagittal view. Finally, the right panel illustrates the left and right hippocampus in the axial view. Note that this view is the only one that allows for full visualization of both bilateral anterior and posterior tracings. R denotes the right side of the brain.

Invasive Functional Imaging: Steady State Cerebral Blood Volume

Overview: Steady state cerebral blood volume (SS CBV) is one of the most accurate MRI methods available to quantify CBV. It correlates well with positron emission tomography (PET) studies using fludeoxyglucose F-18 glucose (Gonzalez, Fischman et al. 1995), a gold standard in the field. This leads many to believe that SS CBV is a marker of basal metabolism in the brain. Importantly, this method utilizes high resolution imaging with the typical resolution of $0.8x0.8x4\ mm^3$.

Approach: This functional imaging method combines MR techniques with exogenous paramagnetic contrast agents, such as gadolinium chelates, to provide measures of CBV. It does so by measuring differences in signal intensity before contrast administration (Figure 4A) and after it has reached equilibrium within the vasculature (Figure 4B) on T1-weighted images. It is assumed that the blood brain barrier is intact and the contrast agent only affects the relaxation rates of the intravascular (and not extravascular) component (Schwarzbauer, Syha et al. 1993; Kuppusamy, Lin et al. 1996). Absolute CBV maps (Figure 4C) can be obtained by normalizing

CBV values by the difference in signal obtained in a region with pure blood such as the superior sagittal sinus (Lin, Celik et al. 1999). This is illustrated in Equation (1):

$$CBV = \frac{S_{par,post} - S_{par,pre}}{S_{ss,post} - S_{ss,pre}} * 100 \qquad \textbf{(1)}$$

where $S_{par,post} - S_{par,pre}$ is the difference between the post- and pre-contrast signal in the parenchyma and $S_{ss,post} - S_{ss,pre}$ denotes the difference between the post- and pre-contrast signal in the superior sagittal sinus. Importantly, this is the only MR method that utilizes high spatial resolution imaging (sub-millimeter), which can be used to investigate CBV changes in the hippocampus and its much smaller subfields (Small, Schobel et al. 2011). The best orientation for subfield-level investigation is acquiring images perpendicular to the long axis of the hippocampus.

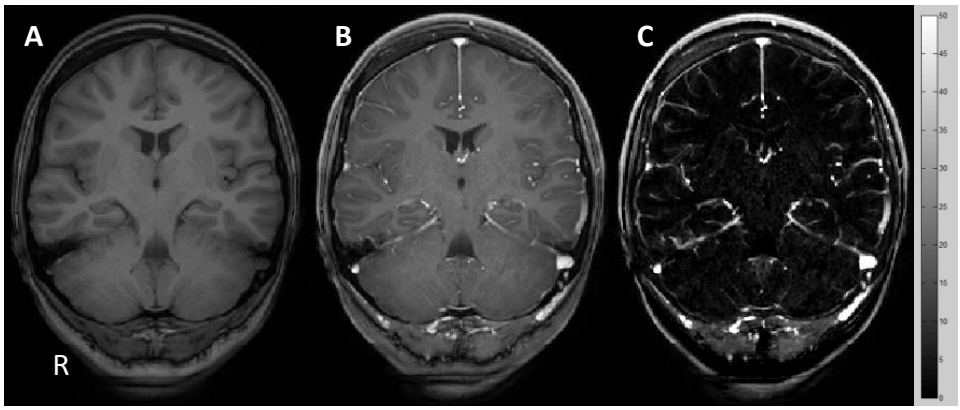

Figure 4 Steady state CBV imaging
Figure 4A and B illustrate pre- and post-contrast images obtained after administration of a gadolinium-containing contrast agent, respectively. Note that the vasculature is bright on these images. Figure 4C is the subsequent CBV map. R denotes the right side of the brain.

While this method has strengths in spatial resolution, it comes at a cost of poor temporal resolution. In addition, the model does not take into account water exchange effects between the intravascular and extravascular compartments, which results in an overestimation

of CBV (due to gadolinium's effect on shortening T1 relaxation of intravascular hydrogen protons in water).

Invasive Functional Imaging: Dynamic Susceptibility Contrast

Overview: Dynamic susceptibility contrast- (DSC-) MRI is a popular method that characterizes several different hemodynamic parameters, including CBV, cerebral blood flow (CBF) and mean transit time (MTT). Supplementing CBV with other hemodynamic parameters is important because CBF provides information about brain perfusion, and MTT is the time it takes for blood to pass through a tissue. Together these three measures provide insight into brain hemodynamics, and physiological relationships between these parameters can be uncoupled in disease processes. This method has good spatial (1-3 mm) and temporal (< 2 sec) resolution (Wintermark, Sesay et al. 2005) to rapidly track a contrast agent as it circulates through the vasculature.

Approach: This method acquires a succession of T2*-weighted images using echo planar imaging to track changes in the blood transverse relaxation time (R_2*=1/T2*) caused by a paramagnetic contrast agent circulating through the brain vasculature (before it reaches equilibrium). Figure 5 shows an image of a brain before (Figure 5A), during (Figure 5B) and after (Figure 5C) bolus circulation through the vasculature. Note that the signal decreases and subsequently recovers due to the contrast agent's effect on T2* shortening of intravascular hydrogen protons in water.

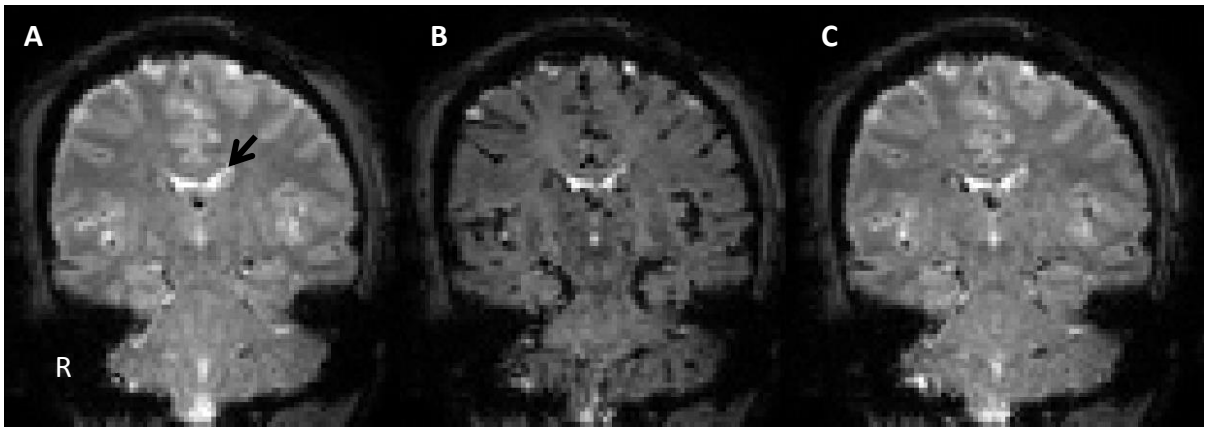

Figure 5 Dynamic susceptibility imaging
Figure 5A shows a T2*-weighted image of the brain before contrast administration. Note that the lateral ventricles are bright on this image (black arrow), as expected. Figure 5B is an image acquired after contrast administration. Note the signal loss around the major vessels in the brain. Figure 5C illustrates the signal recovery after the first pass of the contrast agent. R denotes the right side of the brain.

From the approximately linear relationship between the change in transverse relaxation signal and tissue contrast agent concentration, the signal over time curve can be converted to a concentration over time curve (Ostergaard 2004) using the following relationship:

$$C_t(t) = \frac{-log\left(\frac{S(t)}{S_0}\right)}{TE} \qquad \textbf{(2)}$$

where $C_t(t)$ is the tissue contrast agent concentration at a time t, *TE* is the echo time, $S(t)$ is the signal intensity at a time *t*, and S_0 is the baseline signal intensity at a voxel. The concentration of tissue contrast agent can be expressed as a function of the CBF multiplied by the convolution of the arterial input function ($C_a(t)$, the amount of contrast entering a tissue of interest) and the residual tissue concentration ($R(t)$, the concentration of contrast remaining in the tissue at a time *t*), as illustrated in Equation (3):

$$C_t(t) = CBF * C_a(t) \otimes R(t) \qquad \textbf{(3)}$$

The convolution function is denoted by $\otimes$. In order to obtain CBV, CBF, and MTT, Equation (3) is deconvolved after measuring the arterial input function (AIF). While there are several

deconvolution strategies, previous work illustrates that singular value decomposition (SVD) deconvolution of tissue curves, a model-independent method, generates the best estimates of hemodynamic parameters (Ostergaard, Sorensen et al. 1996; Ostergaard, Weisskoff et al. 1996).

Regional CBF is calculated as the peak value of the deconvolved tissue impulse response (*CBF*R(t)*). Regional CBV is the ratio of the area under the tissue ΔR_2^* curve to the area under the AIF ΔR_2^* curve. Finally, mean transit time (MTT) is calculated under the central volume theorem (Stewart 1893) and is illustrated in Equation (4) below:

$$MTT = \frac{CBV}{CBF} \quad \textbf{(4)}$$

Absolute CBV and CBF values are typically obtained by selecting a region of normal appearing white matter for each subject. Assuming a white matter CBF of 22 ml/100g/min and a CBV of 2 ml/100g (Ostergaard, Sorensen et al. 1996), the regional values are then scaled to obtain absolute CBF and CBV measures.

This method is dependent on arterial input function selection (Calamante 2013). Ideally, the artery that provides blood flow to the brain region of interest should be selected. For the hippocampus, the posterior cerebral artery is ideal but can be difficult to reliably select depending on the slice acquisition. Furthermore, this method has reasonable signal to noise ratio and utilizes echo planar imaging, which is subject to geometric distortions (Shiroishi, Castellazzi et al. 2015).

Noninvasive Functional Imaging: Inflow-Based Vascular-Space-Occupancy

Overview: A recently-developed inflow-based vascular-space-occupancy (iVASO) method uses blood water as an endogenous contrast agent to generate CBV values. This method specifically measures arterial CBV instead of total (arterial *and* venous) CBV measured by the contrast-enhanced steady state CBV method. Arterial CBV comprises approximately 20-30% of total CBV (Ito, Kanno et al. 2001; Kim, Hendrich et al. 2007) and is the vascular compartment that experiences the most changes after neural stimulation (Hillman, Devor et al. 2007; Kim, Hendrich et al. 2007; Chen, Bouchard et al. 2011). The typical in place resolution is around 2-3 mm, with 4-5 mm out of plane slice thickness.

Approach: The iVASO method acquires two single-slice images: a control image that contains tissue and blood signals and a null image that contains only tissue signal (the blood signal is nulled) (Donahue, Sideso et al. 2010). The control image is acquired by first performing a slice-selective inversion pulse that inverts both the blood and tissue water magnetization in the imaging slice. This is immediately followed by a second slice-selective inversion pulse that restores the blood and tissue water magnetization. The label image is acquired in a slightly different manner. A spatially nonselective inversion pulse inverts brain tissue and blood water magnetization, which is then followed by a slice-selective inversion to restore the magnetization in the imaging slice (Hua, Qin et al. 2011). The inverted ('labeled') blood water outside of the imaging slice flows into the imaging slice while undergoing T1 relaxation. The labeled image is then acquired when the longitudinal magnetization of blood water is zero (at the TI of blood water). As such, the labeled image is also called the null image because the signal from the blood is zero. The difference between the control and null image contains only

arterial blood because the tissue signals cancel out. Figure 6A shows a structural image containing the left and right hippocampus, Figure 6B shows a typical iVASO image, and Figure 6C illustrates the calculated aCBV map from the difference image.

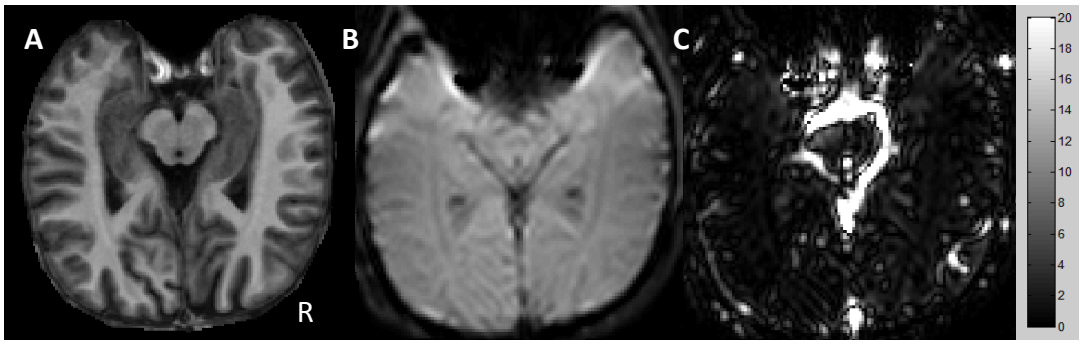

Figure 6 Inflow-based vascular-space-occupancy
Figure 6A shows a typical, single-slice image obtained through the long axis of the left and right hippocampus. Figure 6B is an example iVASO image obtained in the same orientation. Figure 6C illustrates a typical aCBV map from the difference iVASO image. Note that the vasculature is white and the Circle of Willis can be appreciated in this view. R denotes the right side of the brain.

Arterial CBV can be calculated using Equation (5) (Donahue, Sideso et al. 2010):

$$aCBV = \frac{\Delta S}{AM_b^0 C_b \left(\frac{TI}{\tau}\right) E1E2} \qquad \textbf{(5)}$$

where ΔS is the difference between the control and the null image, A is a constant dependent on the scanner gain, M^0_b is the steady state magnetization of blood water, C_b is the blood water density (0.87ml/ml) (Herscovitch and Raichle 1985), TI is the inversion time, τ is the arterial arrival time, $E1 = 1 - e^{(-TR/T1b)}$, and $E2 = e^{(-TE/R2b^*)}$ where $R2_b^*$ is the R2* of blood water. $T1_b$ = T1 of blood water (1.627s), τ = 500 ms for the hippocampus, R2* of arterial blood water = $16s^{-1}$ and of venous blood water = $21s^{-1}$. AM^0_b can be calculated from the first control image using a sagittal sinus ROI and a correction for differences between arterial and venous $R2^*$ as outlined by Petersen et al (Petersen, Lim et al. 2006). Since the time for the labeled blood to arrive to the imaging place (τ, arterial arrival time) is different in cortical and subcortical structures (Wang, Alsop et al. 2003; Li, Sarkar et al. 2013), collecting iVASO data over different inversion

times can be used to estimate arterial CBV and the arterial arrival time in a brain region (Hua, Qin et al. 2011).

There are some notable limitations to this method. First, while this method is non-invasive, it only acquires a single slice through a brain region, which means that there can be coregistration issues with whole brain data if the slice planning is at an oblique angle. Second, this method has poor SNR, requiring many control and label images for averaging. (Hua, Qin et al. 2011).

Noninvasive Functional Imaging: Arterial Spin Labeling

Overview: Arterial spin labeling (ASL) is a clinical method that measures absolute CBF in brain regions such as the hippocampus. Similar to iVASO, this method also uses blood water as an endogenous contrast agent to acquire control and labeled images and requires averaging across several control-label pairs to obtain optimum SNR (although typically poorer than iVASO). The typical resolution of this method is 3-4 mm in plane and 6-8 mm out of plane.

Approach: There are several different methods to label the blood water in ASL. One method, called continuous ASL (cASL) requires special hardware to administer a continuous radiofrequency (RF) pulse lasting one to three seconds through a labeling plane. Another method, called pulsed ASL (pASL), uses a single short pulse lasting 10-20 ms to invert a thick slab of arterial spin water flowing through the labeling plane. The strengths and limitations of these two methods based on SNR, labeling efficiency, and hardware limitations have made a third method, pseudocontinuous ASL (pCASL), more favorable. This method uses over a thousand radiofrequency pulses applied at a rate of around one per millisecond, to generate

perfusion images that can be easily implemented in a clinical scanner and has been recommended to study clinical populations (Alsop, Detre et al. 2014). In each of these three methods, it is important that the labeling plane is perpendicular to the carotid vessels in the neck to maximize labeling efficiency.

In order to quantify CBF using the pCASL sequence, there are several assumptions that are made. First, the entire labeled blood water reaches the target tissue before image acquisition. Second, the labeled blood water does not leave the target tissue before image acquisition. Third, the labeled blood water spins undergo blood T1 relaxation. If these assumptions are met, CBF can be calculated by the following equation (Alsop, Detre et al. 2014):

$$CBF = \frac{6000\lambda(\Delta S)e^{\frac{PLD}{T_{1b}}}}{2\alpha T1_b S_{M0}\left(1-e^{\frac{\tau}{T_{1b}}}\right)} \quad \textbf{(6)}$$

In Equation (6), the factor 6000 is a conversion factor from mL/g/s to mL/100g/min, λ is the blood/brain partition coefficient (0.9 mL/g), ΔS is the difference between the control and label images, $T1_b$ is the T1 of blood (at 3T = 1650 ms), *PLD* is the post-labeling delay, α is the labeling efficiency (0.85 for pCASL), S_{M0} is the baseline magnetization scan, and τ is the labeling duration. The PLD is a compromise between the T1 signal decay that occurs at longer PLDs and ensuring the labeled blood waters reach tissues with the longest arterial transit time, which may be an issue at shorter PLDs. This is particularly a concern in patients with steno-occlusive arterial disease. Figure 7 illustrates hippocampal coverage of CBF maps generated from pCASL. It is important to note that this method differs from the iVASO method in several regards: First, ASL provides full brain coverage while iVASO currently is restricted to a single slice. Second,

iVASO label images are obtained at the time of blood water nulling while ASL label images are obtained at a fixed time (called the post-labeling delay) that may include some inverted and nulled blood water. Third, ASL measures perfusion by allowing labeled blood water to interact with tissue blood water in the capillaries while the iVASO method is designed to acquire label images while the blood is still in the arteries and arterioles (before exchange occurs in the capillaries).

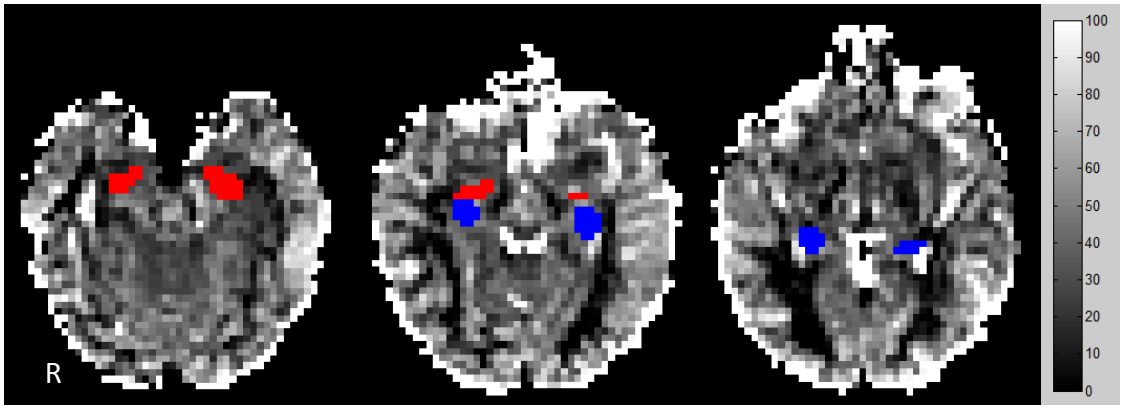

Figure 7 Arterial spin labeling (pCASL)
Figure 7 illustrates a representative CBF map illustrating coverage of the hippocampus. Note that the anterior (red) and posterior (blue) hippocampus are each contained within two axial slices. R denotes the right side of the brain.

ASL can now assess across several hemodynamic parameters due to recent advances. This method acquires ASL images across multiple, long (two to three seconds) PLDs to obtain simultaneous measurements of whole brain CBF, arterial CBV, and arterial transit time (Wang, Alger et al. 2013). This sequence is still relatively new and has the potential to replace the invasive DSC-MRI method since it collects similar hemodynamic parameters. However, there are some limitations that make it difficult to implement to study the hippocampus and its subfields. First, it has worse spatial resolution compared to DSC-MRI, which would make it difficult to resolve hemodynamic parameters in small, subcortical brain regions such as

hippocampal subfields. Second, this method is limited by the range of selected PLDs, which can be influenced by various disease processes. Finally, by design, multi-PLD ASL acquires images at longer PLDs, which means that fewer control and label pairs are collected (Wang, Alger et al. 2013) in the same scanning time as a single PLD ASL sequence. Since SNR is related to the square root of the number of dynamic images acquired, fewer control and label pairs would result in images with lower SNR.

Structural and Functional Imaging: Summary

In summary, there are several different MRI methods to investigate hippocampal hemodynamics (CBV, CBF, and MTT). Each method has its strengths and limitations, and this is outlined with regards to hippocampal investigation along the longitudinal and transverse axes in Table 2.

Furthermore, it is important to note that gadolinium-containing invasive imaging methods have many limitations, especially in clinical populations. Some participants cannot receive contrast administration if their kidney function test (serum creatinine) is abnormal or if they are predisposed to disease conditions that affect the kidney (such as diabetes or hypertension) due to the potential risk of nephrogenic system fibrosis. Furthermore, there may be difficulties with dose restrictions, intravenous access, and contrast tolerance while in the scanner. These methodological challenges also make it difficult to implement in longitudinal studies, which is why development of reliable, non-invasive methods has become important in imaging science.

Table 2 Resolution of imaging methods to investigate the human hippocampus

Neuroimaging method	Anterior/Posterior?	Subfield?
Structural T1	Yes	Yes
Steady State Cerebral Blood Volume (SS CBV)	Yes	Yes
Dynamic Susceptibility Contrast (DSC)	Yes	No
Arterial Spin Labeling (pCASL)	Yes	No
Inflow-Based Vascular-Space-Occupancy (iVASO)	Yes	No

Table 2 summarizes the different methods reviewed to investigate the human hippocampus. Note that while most methods can extract information along the long axis of the hippocampus (anterior, posterior), the steady state CBV method is the only functional method with sufficient spatial resolution to investigate subfields.

Applications of hippocampal imaging to schizophrenia

The reviewed imaging methods can be applied to any clinical population with notable hippocampal pathology. While there are many diseases that affect the hippocampus, this section focuses on hippocampal pathology in schizophrenia. Before reviewing this literature, a brief introduction to schizophrenia is merited.

Schizophrenia overview

Schizophrenia is a heterogeneous clinical syndrome with a lifetime prevalence of approximately 1% in the general population (Perala, Suvisaari et al. 2007) and usually presents in early adulthood (Helgeland and Torgersen 2005). According to the Diagnostic and Statistical Manual of Mental Disorders (DSM)-V, a diagnostic system in Psychiatry, people with schizophrenia need to have two out of the five following symptoms for at least a one month time period (or less if successfully treated): delusions, hallucinations, disorganized speech,

disorganized behavior, and negative symptoms. Notably, at least one of the two symptoms must be the delusions, hallucinations, or disorganized speech (Tandon, Gaebel et al. 2013). Furthermore, there must be a period of social or occupational dysfunction, and there must be continuous signs of disturbance for at least six months, which includes at least one month of symptoms (or less if successfully treated). Individuals between the one and six month time period would be considered to have schizophreniform disorder, and most of these individuals convert to schizophrenia. Even after treatment, many of these individuals do not completely recover and are frequently hospitalized or dependent on medications. For this reason, these illnesses have been termed "chronic disorders of the young" (Manji, Kato et al. 2012) and are projected to be a significant health burden in industrialized and rapidly industrialized regions when measured via disability-adjusted life years (Lopez, Mathers et al. 2006).

Hippocampal structural and functional changes in schizophrenia

It has been well established in the literature that with the advent of *in vivo* MRI techniques, the most notable findings in individuals with chronic schizophrenia include enlarged lateral ventricles and reduced medial temporal lobe volume (Shenton, Dickey et al. 2001; Honea, Crow et al. 2005), including reduced hippocampal volume (Altshuler, Bartzokis et al. 2000; Heckers 2001; Shenton, Dickey et al. 2001). Meta-analyses of functional deficits in schizophrenia have illustrated significant memory impairment (Heinrichs and Zakzanis 1998; Aleman, Hijman et al. 1999), with abnormal hippocampal recruitment (Weiss, Schacter et al. 2003). Resting PET scans have shown increased hippocampal regional CBF in medication-naïve

patients, which may be normalized by antipsychotic treatment (Medoff, Holcomb et al. 2001; Lahti, Weiler et al. 2009).

Given the different functions within each hippocampal subfield, it comes as no surprise that researchers use high-resolution spatial imaging techniques to test hypotheses involving subfield-dependent pathology in schizophrenia. Examination of subfield-dependent functional activity within the hippocampus arose out of an apparent conundrum: resting-state (baseline) PET scans showed increased hippocampal regional CBF, a correlate of neural activity (Medoff, Holcomb et al. 2001), while functional tasks illustrated decreased task-dependent hippocampal activation. In order to resolve this apparent paradox, it was recently suggested that the two are related: decreased hippocampal activation is due to increased baseline perfusion (Heckers, Rauch et al. 1998; Tamminga, Stan et al. 2010). Several lines of investigation support this idea, although the literature is quite mixed on the individual subfields. One group has suggested increased activity within the CA3 subfield (Tamminga, Southcott et al. 2012)**.** If this occurs in the context of a partial dentate gyrus failure, which would create specious associations, then CA3 hyperactivity can lead to increased pattern completion, resulting in delusions or psychosis (Tamminga, Southcott et al. 2012). Another group has implicated CA1 subfield hyperactivity in schizophrenia (Schobel, Lewandowski et al. 2009).

Through the use of steady state CBV mapping, a proxy of neural metabolism, one group was able to illustrate several key findings in schizophrenia: CBV was increased in the anterior CA1 subfield of the hippocampus, CA1 CBV correlated with positive symptoms (delusions) in schizophrenia, and antipsychotic medications did not likely confound the results (Schobel, Lewandowski et al. 2009). Shape-based analyses have also reported structural findings in the

left anterior CA1 subfield and linked this deformity to antipsychotic dosage and symptom severity in schizophrenia (Zierhut, Grassmann et al. 2013). These findings have significant implications given the CA1 subfield's function in novelty detection. Hyperactivity within the CA1 subfield can lead to incorrect assessment between memories that are stored in the hippocampus and new memories that are processed through the entorhinal cortex. Since all parts of the tri-synaptic pathway need to be intact for proper hippocampal function, dysfunction in the CA1 subfield can lead to memory disturbances seen in schizophrenia (Heckers, Rauch et al. 1998; Preston, Shohamy et al. 2005; Armstrong, Williams et al. 2012).

Recent efforts have tried to study individuals much earlier in the disease. A cross-sectional study that characterized hippocampal and amygdaloid volumes in different psychiatric diagnoses did not find hippocampal volume changes in first episode schizophreniform patients but found a smaller hippocampus in first episode schizophrenia patients (Velakoulis, Wood et al. 2006). The only difference between the two groups was illness duration. This finding has been supported by a recent meta-analysis that found a negative association between illness duration before baseline scan and the effect size in the left and right hippocampus (Olabi, Ellison-Wright et al. 2011), suggesting that duration of illness is an important component to consider when investigating the hippocampus. Along those lines, another group recently published a study illustrating increased CA1 CBV in an ultra-high-risk group that spreads to the subiculum after psychosis onset. The group also showed in the study that increased CBV *preceded* volume loss in the hippocampus (Schobel, Chaudhury et al. 2013), illustrating that baseline hippocampal hyperactivity may lead to volume changes over time. They then recreated a similar pattern of increased CA1 CBV that spread to the subiculum in a ketamine

mouse model and implicated excess glutamate as a driver of hippocampal hypermetabolism (Schobel, Chaudhury et al. 2013). These results suggested increased hippocampal activity that led to volumetric changes over time.

Summary of progress in schizophrenia

Progress in advancing knowledge on hippocampal dysfunction in schizophrenia is occurring on two fronts. First, studies are now investigating patients early in the disease course to determine when changes in hippocampal structure and function occur. Second, given that the hippocampus is a heterogeneous structure, high resolution spatial imaging has been used to examine the hippocampal formation along its longitudinal and transverse axes to better localize findings.

The emerging literature implicates the CA1 subfield as one of the areas initially affected in the disease, and this subfield, as well as the timing of the changes, needs to be better characterized. Therefore, we performed a cross-sectional study in patients in the early stage of psychosis and schizophrenia to better understand hippocampal structure and function using MRI.

Specific Aims

The two aims of this study implemented imaging methods to test hippocampal structure and function in schizophrenia. The first aim was to develop CBV maps of the two regions (anterior and posterior) and four subfields (subiculum, CA1, CA2/3, and hilus) of the hippocampal formation. The second aim was to implement an established non-invasive inflow-

based vascular-space occupancy (iVASO) method to measure arterial CBV in schizophrenia. The overall hypothesis was that hippocampal hypermetabolism in the schizophrenia would lead to increased CBV or CBF.

To test these aims, a cross-sectional study was performed involving healthy controls and patients with early psychosis and chronic schizophrenia. In chronic patients, subfield-level testing was performed using SS CBV and followed up with another study investigating CBV, CBF, and MTT from the concurrently collected dynamic susceptibility contrast data. In early psychosis, we tested for group differences in hippocampal volume, CBF, and CBV. We also investigated hippocampal arterial CBV using the iVASO method in this cohort.

In this study, we characterized physiological CBV gradients along the long axis of hippocampal subfields (Chapter 2) and illustrated increased CA1 CBV, but not CA2/3 CBV, in patients with schizophrenia using the steady state CBV method (Chapter 3). We also used dynamic susceptibility contrast imaging to show an uncoupling between CBV and CBF in schizophrenia (Chapter 4). We then studied patients in the early stage of psychosis. We found no changes in hippocampal volume and blood flow, although we illustrated a strong inverse correlation between anterior hippocampal CBF and volume and a trend towards increased anterior hippocampal CBV (Chapter 5). Finally, we were not able to find group arterial CBV differences using the iVASO method (Chapter 6).

CHAPTER II

ANTERIOR-POSTERIOR CEREBRAL BLOOD VOLUME GRADIENT IN THE HUMAN SUBICULUM

Introduction

The hippocampal formation, an elongated structure in the medial temporal lobe, is crucial for memory formation and affect regulation (Morris, Garrud et al. 1982; Eichenbaum 2004). These functions have been mapped to distinct *subfields* and *regions* within the human hippocampal formation (Small, Schobel et al. 2011). Subfields are defined in coronal sections, whereas regions are defined along the anterior-posterior axis of the hippocampal formation.

The subfields of the hippocampal formation include subiculum, Cornu Ammonis sectors 1-4 (CA1-4) and dentate gyrus. There is considerable evidence for the role of each subfield in the processing of multisensory information towards memory encoding and retrieval. The CA1 sector is associated with input integration (comparing old and new stimuli), the CA3 sector with pattern completion (retrieval of information based on partial cues) (Fellini, Florian et al. 2009), and the dentate gyrus with pattern separation (distinguish between similar events at different time periods) (Schmidt, Marrone et al. 2012). These sector-dependent functions may be due to different glutamatergic projections from the entorhinal cortex (EC). Layer II cells from the EC project to the dentate gyrus and CA3 via the topographically-organized perforant pathway: the lateral EC is connected to septal dentate gyrus and CA3 subfields while the medial EC sends projections to temporal dentate gyrus and CA3 subfields (Witter, Wouterlood et al. 2000). However, the rostal-caudal (long) axis of the dentate gyrus and CA3 subfields do receive some projections from both the medial and lateral EC, allowing for diffuse activation of these subfields by the EC (Amaral and Witter 1989; Witter, Wouterlood et al. 2000). In contrast to the

EC layer II neurons, cells in layer III project to CA1 and subiculum. The lateral EC is connected to the proximal subiculum and distal CA1 (subiculum-CA1 border) while medial EC projections synapse on neurons in the distal subiculum and proximal CA1, allowing for selective input from the EC (Witter, Wouterlood et al. 2000).

There is also growing evidence that the anterior and posterior regions of the hippocampal formation differ anatomically and functionally (Moser, Moser et al. 1993; Moser and Moser 1998; Kjelstrup, Tuvnes et al. 2002; Bannerman, Rawlins et al. 2004) . Along the long axis of the hippocampus, the anterior hippocampus has prominent connections with medial prefrontal cortex, orbitofrontal cortex, and nucleus accumbens. In contrast, the posterior hippocampus has strong connections with dorsolateral prefrontal cortex and retrosplenial/posterior cingulate cortex (Fanselow and Dong 2010). Functionally, the anterior hippocampus is associated with the regulation of mood and affect, while the posterior hippocampus is involved in spatial memory and navigation (Fanselow and Dong 2010; Poppenk and Moscovitch 2011; Demaster, Pathman et al. 2013).

In addition, there are cellular, hemodynamic, and neurochemical differences between the anterior and posterior regions of the human hippocampal formation. For instance, pyramidal cell density increases in an anterior-posterior direction (Mouritzen Dam 1979). This is related to findings from proton magnetic resonance spectroscopy studies, which found a similar anterior-posterior gradient of increasing *N*-acetylaspartate (NAA), choline, and creatine (Cre) levels (King, Glodzik et al. 2008; Ostojic, Kozic et al. 2010). In addition, blood supply differs between the two regions: the anterior hippocampus is perfused by the anterior hippocampal branch of the posterior cerebral artery and branches of the anterior choroidal arteries, while

the middle and posterior hippocampal branches of the posterior cerebral artery perfuse the posterior hippocampus (Huang and Okudera 1997). This may explain differences in perfusion along the long axis of the hippocampus. A rodent arterial spin labeling (ASL) study has illustrated longer arterial transit times (ATT, 316 vs 244 ms) and lower regional cerebral blood flow (rCBF, 158 vs 173 mL/100 g/min) in the anterior compared to the posterior hippocampus (Thomas, Lythgoe et al. 2006). A recent ASL study has shown a similar gradient in humans, with the ATT and rCBF of 546 ms and 39 mL/100 g/min, respectively, in the anterior hippocampus and 443 ms and 70 mL/100 g/min, respectively, in the posterior hippocampus (Li, Sarkar et al. 2013).

Several neurological and psychiatric disorders, including Alzheimer's disease (Hyman, Van Hoesen et al. 1984; Ball, Fisman et al. 1985), Parkinson's disease (Braak, Braak et al. 1996; Galvin, Uryu et al. 1999), and schizophrenia (Heckers 2001; Heckers and Konradi 2010), are associated with abnormalities of the hippocampal formation. Recent studies have explored whether these disorders affect the subfields of the hippocampal formation differentially (Small, Schobel et al. 2011). An initial study by Schobel et al. reported increased cerebral blood volume (CBV) in the CA1 region of the hippocampal formation in subjects who convert from a high-risk state for psychosis to schizophrenia (Schobel, Lewandowski et al. 2009). Recently the same investigators examined CBV along the long axis of the hippocampus and found increased CBV in the anterior but not posterior CA1 region in patients at-risk for schizophrenia (Schobel, Chaudhury et al. 2013).

Given the notable gradients in cell density, proton spectroscopy, and blood flow across the long axis of the hippocampus, we hypothesized that the hippocampal formation has

anatomically unique hemodynamics that reflect the distinct underlying neural activity and chemical structures. Furthermore, it is likely that these distinctions may be subfield specific within the hippocampal formation. While blood oxygen level dependent (BOLD) functional magnetic resonance imaging (fMRI) (Szaflarski, Holland et al. 2004; Restom, Bangen et al. 2007; Bangen, Restom et al. 2009) and arterial spin labeling (Restom, Bangen et al. 2007; Bangen, Restom et al. 2009; Rusinek, Brys et al. 2011) are well-established approaches to evaluate hippocampal function, contrast-enhanced steady state imaging offers a unique advantage to perform sub-millimeter CBV mapping (Lin, Celik et al. 1999). CBV measures microvasculature blood volume and has been well-established as a marker of basal metabolism (Small, Schobel et al. 2011). Steady state CBV utilizes high resolution imaging that reduces partial volume effects, improves segmentation, and allows for CBV measurement in the hippocampal subfields (Small, Schobel et al. 2011). Therefore, we performed contrast enhanced, high resolution T1-based steady state (SS) imaging in 14 healthy controls to examine an anterior-posterior CBV gradient in the human hippocampal formation.

Methods

Participants

14 healthy subjects (nine male, five females; age range: 23-53 years; mean age ± st. dev: 35.14 ± 8.72 years) provided informed consent as approved by the Institutional Review Board (see Table 3 for subject demographics). Using a structured clinical interview (SCID-I/P (First 2002)), we excluded any major medical, psychiatric, or neurological illness. In order to minimize

the risk of nephrogenic systemic fibrosis, serum creatinine was measured before and 24-48 hours after contrast administration to ensure normal kidney function (GFR > 60).

Table 3 SS CBV healthy control subject demographics

Gender (n)	Age (yrs) ± stdev	Race (W/B)	Handedness (L/R)
Males (9)	37.78 ± 9.37	7/2	1/8
Females (5)	30.4 ± 5.27	4/1	1/4

Cerebral Blood Volume Mapping

Imaging was performed using an 8 channel SENSE head coil with a Philips 3T Achieva scanner. T1-weighted pre- and post-contrast images were acquired using a 3D T1 FFE (Lin, Celik et al. 1999) sequence with the following imaging parameters: TR/TE = 20 ms/3.98 ms, FOV = 256 x 256 mm^2, Res = 0.80 x 0.80 x 4 mm^3, slices = 30, SENSE factor = 2.5. Post-contrast images were acquired approximately four minutes after contrast administration (Magnevist ® - Gadopentetate dimeglumine, Bayer Schering Pharma, Germany, 0.1 mmol/kg). Contrast was administered using a power injector (Medrad®, PA, USA) through the antecubital vein with an 18G needle and was followed by a 40 ml saline flush. Images were acquired perpendicular to the long axis of the hippocampus to allow for accurate segmentation of the hippocampal subfields as briefly outlined below and referenced in (Moreno, Wu et al. 2007). Of note, the boundary between subfields can only be determined through histological landmarks and were excluded from the regions of interest (ROIs). We compared the local fractional increase in tissue signal after a gadolinium-containing intravenous contrast agent had equilibrated in the blood and thoroughly perfused the microvasculature.

Analysis

CBV calculations: The pre- and post-contrast steady state images were corrected for subject motion using AFNI (2dimreg) (Cox 1996). Absolute CBV in the brain was measured by subtracting the pre-contrast from the post-contrast image, normalized by the difference in the superior sagittal sinus (Lin, Celik et al. 1999). A 10% regional CBV threshold was used to minimize large epicortical vessel contribution (Lin, Celik et al. 1999). Analysis was completed using Matlab (version 7.13.0., The MathWorks Inc, Natick, Massachusetts).

Hippocampal Segmentation: Manual segmentation of the subiculum, CA1 sector, CA2/3 sector, and the hilus (CA4 with some dentate gyrus contribution) was performed by one rater (PT) using the pre-contrast image. The post-contrast image was used as a guide to ensure epicortical vessels were excluded. A separate ROI was drawn to segment the whole hippocampus (defined as containing the subiculum, CA1-4, and dentate gyrus) in each slice. We chose manual segmentation of each hippocampus in the native space instead of co-registration to a standard space to minimize interpolation in older subjects who may have a smaller hippocampus. We were able to segment all 5 regions of interest in 6 to 8 slices in all subjects. There were some slices in the anterior-most or posterior-most hippocampus that were not included because they could not be segmented due to methodological limitations (unclear subfield boundaries). ROI placement was verified with another rater (SR). In case of discrepancies, both raters redrew the ROI until a consensus was reached.

We used the uncus to delineate the anterior and posterior regions of the hippocampal formation. The uncus can be defined in coronal sections as more than one cut through the hippocampus (Duvernoy and Bourgouin 1998; Woolard and Heckers 2012). We numbered the

coronal series for each subject in such a way that the same section corresponded to the same region of the hippocampal formation. In most subjects, the hippocampal subfields could not be segmented in slices one and eight, and they were not included in the analysis. Three slices (slices two-four) were identified as anterior hippocampus and three slices (slices five-seven) as posterior hippocampus. The transition from slice four to slice five denotes the anterior-posterior boundary of the hippocampal formation.

CBV Gradient Determination: For each aligned slice of the hippocampus, CBV values were calculated in the four subfields and in the whole hippocampus for all subjects. Outliers were detected at each slice using Tukey's method (Tukey 1977). Interquartile range (IQR) was calculated using the 25^{th} and 75^{th} percentile of CBV measurements. Values > 1.5*IQR were considered as outliers. The CBV values for each subfield in each subject were plotted along the x-axis, starting with slice 2 and ending with slice 7. Slices 2-4 denote the anterior hippocampus and slices 5-7 denote the posterior hippocampus. Slopes were calculated using the line of best fit for each individual subject. Each subject's slope was used to generate an average group slope for gradient comparison.

The Statistical Package for Social Sciences software (SPSS version 20, http://www.spss.com) was used to determine whether the CBV slopes/gradients from slice two (the anterior hippocampus) to slice seven (posterior hippocampus) were significant by testing against a null hypothesis of no gradient (slope = 0) using a two-tailed t-test. The Bonferroni method (Lesack and Naugler 2011) was used to correct for multiple comparisons when appropriate. Subsequent correlation analyses were performed between significant CBV gradients and age, race, or gender.

Results

For each subject, we manually segmented ROIs for the whole hippocampal formation and different subfields (subiculum, CA1, CA2/3, and hilus) along the long axis of the hippocampus (see Figure 8 for a representative subject). The CBV values averaged across the long axis of the hippocampus (mean ± standard deviation; units = ml blood/ml parenchyma) for

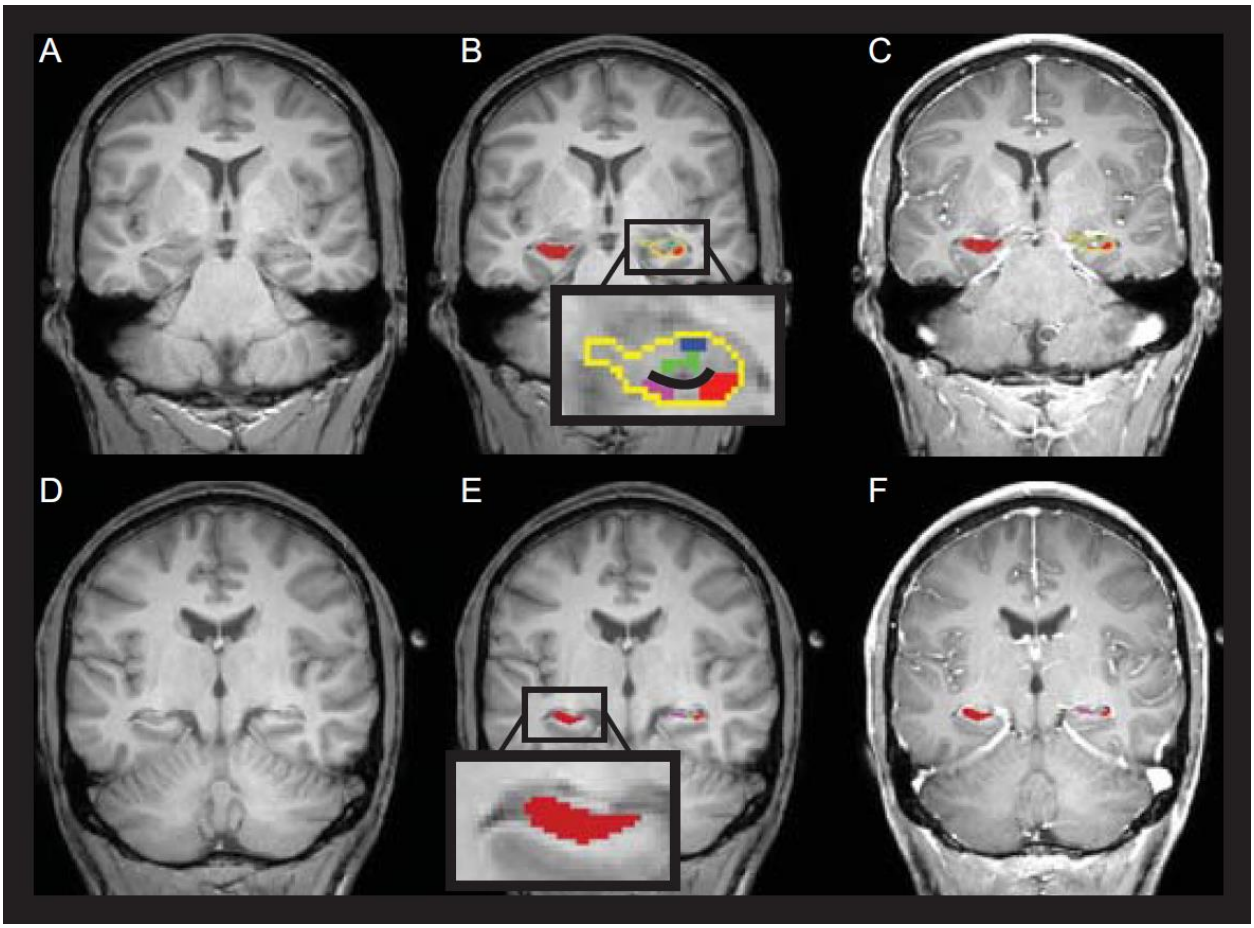

Figure 8 Steady state CBV 3T imaging (radiological orientation)
A: T1-weighted coronal image containing the anterior hippocampus
B: Figure A with hippocampal formation ROI tracing (red) and subfields (purple = subiculum, red = CA1, blue = CA2/3, green = hilus)
C: Post-contrast image with ROIs overlaid from B.
D: T1-weighted coronal image containing the posterior hippocampus
E: Figure E with hippocampal formation ROI tracing and subfields
F: Post-contrast image with ROIs overlaid from E.

whole hippocampal formation, subiculum, CA1, CA2/3, and hilus were 3.22 ± 0.61, 3.07 ± 1.12, 3.58 ± 0.89, 2.84 ± 0.94, 2.89 ± 1.03 (left hippocampal formation) and 3.40 ± 0.57, 3.15 ± 1.24, 2.66 ± 0.83, 3.07 ± 1.21, 3.12 ± 0.91 (right hippocampal formation). These values are similar to those reported previously for cerebral cortex (Sakaie, Shin et al. 2005) and hippocampus (Kuppusamy, Lin et al. 1996).

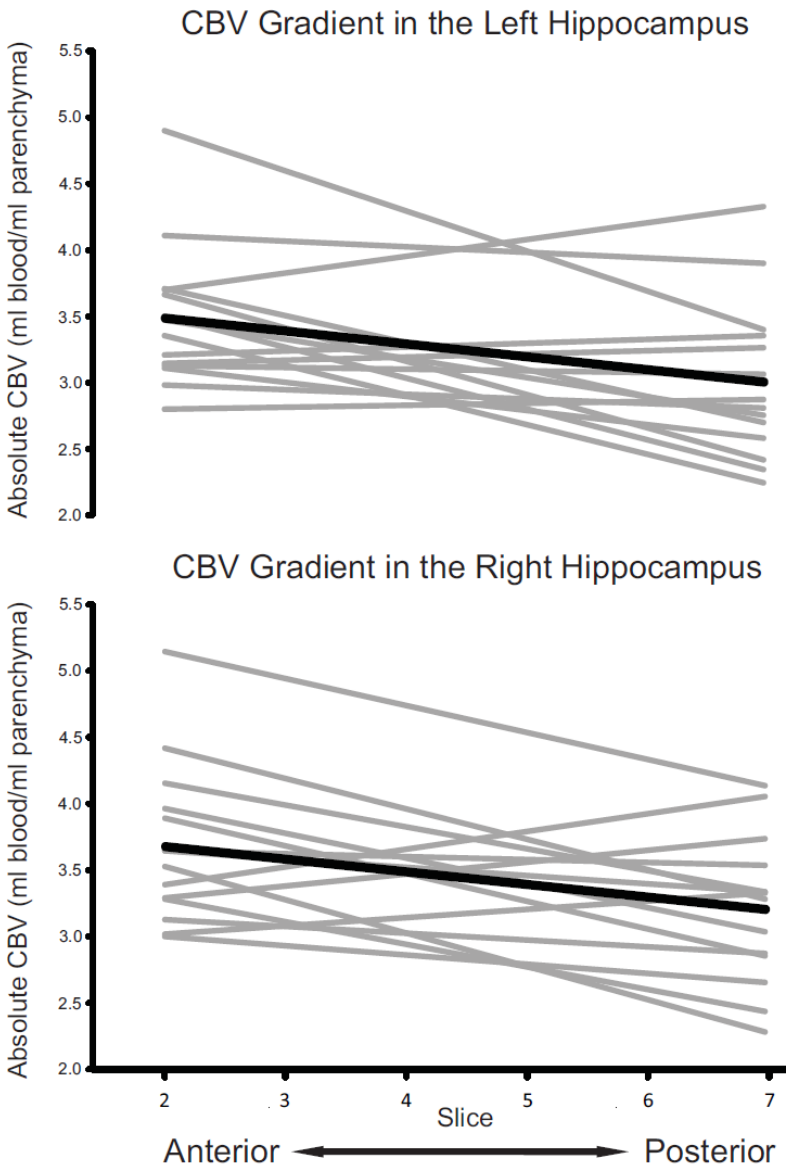

Figure 9 Anterior to posterior SS CBV gradients in the hippocampus. There is a significant anterior to posterior gradient in the left (two tailed t-test, $p<0.01$) and right ($p<0.01$) hippocampus in healthy controls. The gray lines denote slopes for individual subjects, while the black line represents the average slope.

Each subject's CBV values were plotted along the long axis of the hippocampal formation, moving from the most anterior (slice two) to the most posterior slice (slice seven) (Figure 9). A linear fit to the data provided a gradient value for each subject. The group average was used to test the hypothesis of an anterior-posterior CBV gradient.

We found significant gradients in the right (two-tailed t-test, $p<0.01$) and left ($p<0.01$) hippocampal formation. The slope values (mean ± standard deviation; units = (ml blood/ml parenchyma)/4mm^3) were -0.096 ± 0.13 and -0.095 ± 012 for the left and right hippocampus, respectively (Figure 9).

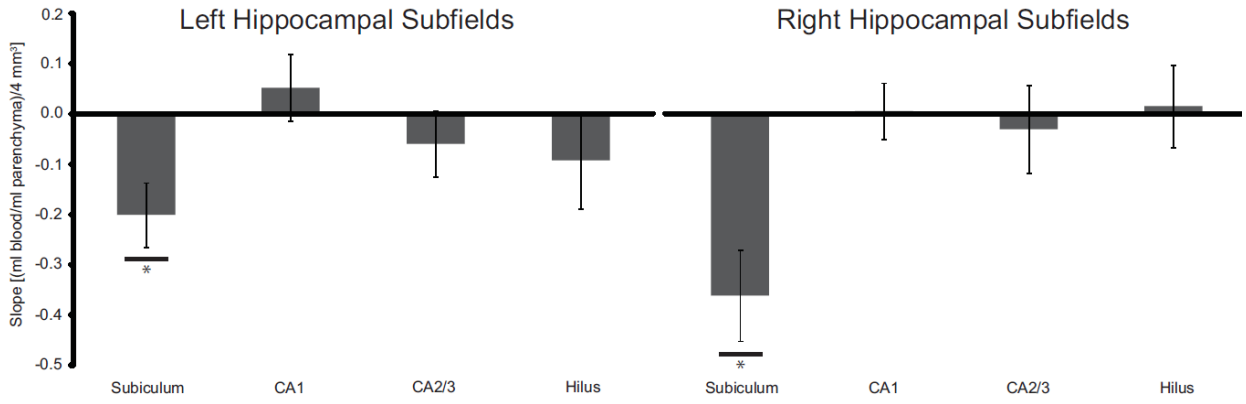

Figure 10 Anterior to posterior SS CBV gradients in hippocampal subfields
There is a significant anterior to posterior gradient in the left (two tailed t-test, $p<0.005$) and right ($p<0.0005$) subiculum, but not other subfields of the hippocampal formation, in healthy controls. Error bars denote standard error of the mean.

We tested whether the CBV gradient differed between the subfields of the hippocampal formation. The slope values for the subiculum, CA1, CA2/3, hilus were -0.20 ± 0.23, 0.05 ± 0.24, -0.06 ± 0.24, -0.093 ± 0.35 in the left hippocampal formation and -0.36 ± 0.33, 0.0065 ± 0.20, -0.030 ± 0.31, 0.016 ± 0.29 in the right hippocampal formation. The results illustrate a significant anterior-posterior CBV gradient in the right subiculum (two tailed t-test, $p<0.0005$, corrected for multiple comparisons) and left subiculum (two-tailed t-test, $p<0.005$, corrected

for multiple comparisons), but not the other subfields (Figure 10). To better characterize the gradients, average subject CBV was calculated for the 5 ROIs for each slice along the long axis of the hippocampus. The line curve trend, along with the line of best fit, for the hippocampal formation and its subfields are shown in Figure 11.

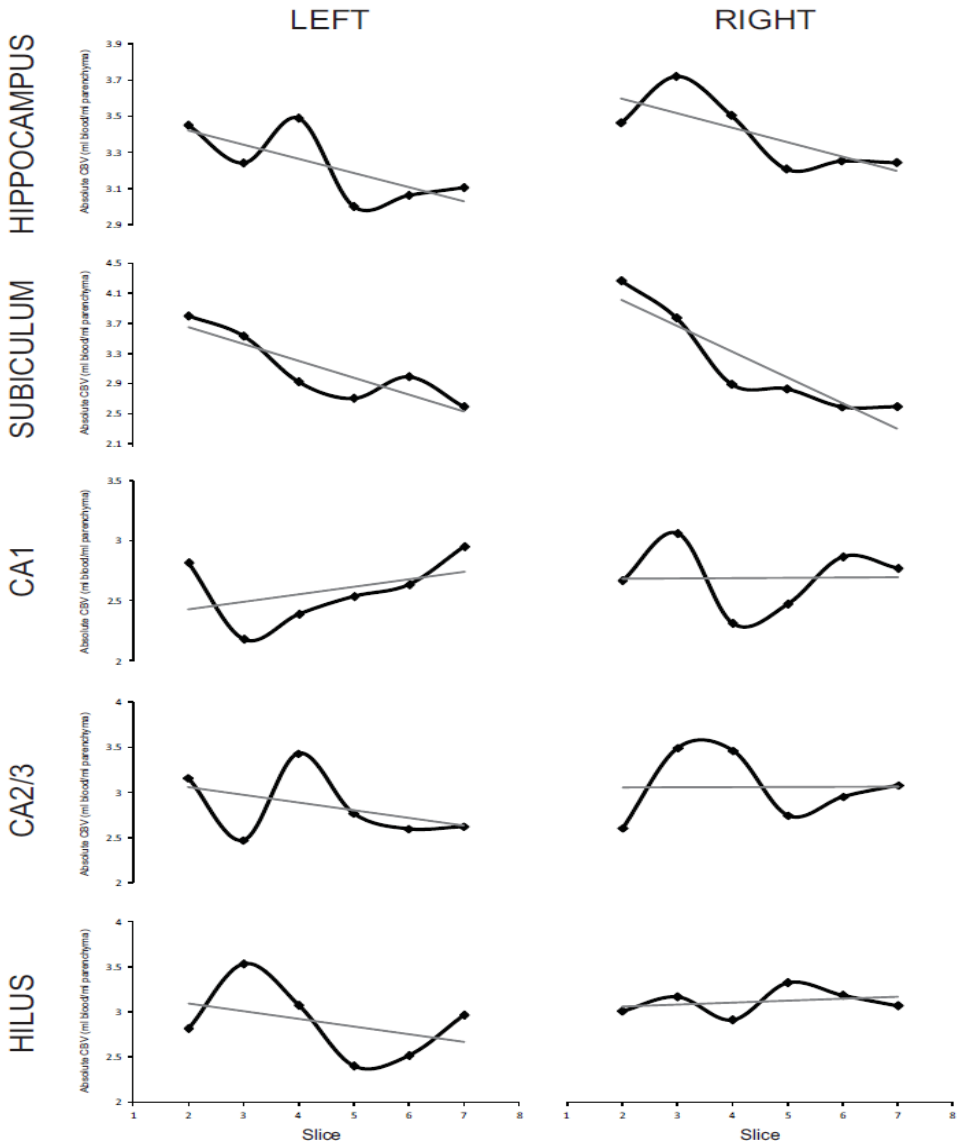

Figure 11 SS CBV values for the hippocampus and subfields along the long axis of the hippocampus

Average group CBV for each slice along the long axis of the hippocampus was calculated for the left (top left panel) and right (top right panel) hippocampus and subfields (subsequent panels). Black line denotes line curve fit to the average group CBV. Gray line denotes line of best fit gradient.

Finally, we investigated whether the significant gradients were influenced by age, gender, or race. Our results indicate that the right and left hippocampal CBV gradients did not correlate with age ($p = 0.449$ and $p = 0.098$) or race ($p = 0.228$ and $p = 0.470$). Right hippocampal CBV did not correlate with gender ($p = 0.830$) but left hippocampal CBV did ($p = 0.033$). The right and left subiculum CBV gradients did not correlate with age ($p = 0.641$ and $p = 0.646$), gender ($p = 0.325$ and $p = 0.080$), or race ($p = 0.948$ and $p = 0.909$).

Discussion

Since CBV is a marker of basal metabolism, the results of this study indicate greater anterior than posterior activity of the human subiculum. Considering the role of the subiculum as the main outflow station of the hippocampal formation (O'Mara 2005), such a gradient might have functional implications (Lisman and Grace 2005). Within the subiculum, burst cells are organized into columns, and regular spiking neurons integrate columnar activity along the transverse axis (Poppenk and Moscovitch 2011). The intrinsic circuitry of the subiculum, mainly the burst cells, may predispose to epileptiform activity and epileptogenesis (Stafstrom 2005). Along the long axis of the subiculum, the ventral (anterior) subiculum projects to the medial entorhinal cortex, amygdala, and the bed nucleus of the stria terminalis while the dorsal (posterior) subiculum projects to the lateral entorhinal, retrosplenial, and perirhinal cortices (Andersen 2007). Functionally, the anterior subiculum plays a major role in inhibiting the stress response through the hypothalamic-pituitary-adrenal (HPA) axis while the posterior subiculum processes information about memory, movement, and spatial direction (O'Mara 2005). Subicular inhibition of the HPA axis is thought to be mediated through γ-aminobutyric acid

(GABA) (Lowry 2002; Herman, Mueller et al. 2004), and tonic inhibition would indeed lead to increased CBV in the anterior subiculum. The posterior subiculum CBV values may be low due to the nature of the study: participants were told to lie still in the scanner and a scan was obtained without performing a task. Thus, many of the key functions of the posterior subiculum may have not been recruited, including memory and spatial direction. Future studies should examine whether task performance modulates the CBV gradient in the subiculum.

Anterior-posterior gradients of the hippocampal formation have been explored in aging, depression, ischemia, and neurogenesis. Normal aging has been reported to cause reductions in posterior, but not anterior, hippocampal volume (Driscoll, Hamilton et al. 2003). In contrast, depression has been linked to anterior hippocampal volume reduction, possibly due to decreased neuropil and glial cell number in CA1 and dentate gyrus (Willard, Friedman et al. 2009; Willard, Riddle et al. 2013). Within CA1, there is a notable anterior-posterior ischemia susceptibility gradient, with the posterior region (dorsal hippocampus in rodents) being more vulnerable to ischemia than the anterior region (ventral hippocampus in rodents) (Ashton, Van Reempts et al. 1989). Finally, in rodents, adult neurogenesis was higher in the dorsal, compared to ventral, dentate gyrus and significantly increased after performing a spatial task (Snyder, Radik et al. 2009). Further studies need to explore how neuropsychiatric disorders such as schizophrenia can disrupt the normal anterior-posterior gradients of basal metabolism in the subiculum.

This study has several limitations. The sample size is small (but consistent with previous CBV imaging studies) and the cohort included both genders, different races, and mostly right-

handed subjects. While our results show that the CBV gradients are independent of age and race, gender was significantly correlated with left hippocampal but not left subicular CBV.

In conclusion, we found a significant anterior-posterior CBV gradient in the human subiculum. Future studies should investigate the functional implications of this gradient for normal hippocampal function and possible alterations in disease states.

CHAPTER III

INCREASED HIPPOCAMPAL CA1 CEREBRAL BLOOD VOLUME IN SCHIZOPHRENIA

Introduction

The hippocampus is dysfunctional in schizophrenia (Ragland, Gur et al. 2001; Weiss, Schacter et al. 2003; Ongur, Cullen et al. 2006; Heckers and Konradi 2010; Ledoux, Phillips et al. 2013). Meta-analyses have concluded that schizophrenia is associated with memory impairment (Heinrichs and Zakzanis 1998; Aleman, Hijman et al. 1999) and that hippocampal recruitment is impaired during the performance of memory tasks (Heckers, Rauch et al. 1998; Weiss, Schacter et al. 2003). However, a notable limitation of such functional studies is that individuals with cognitive deficits may have difficulty performing tasks in a scanning environment.

To circumvent issues associated with cognitive deficits and the limits in the interpretation of neural origins of the BOLD signal (Arthurs and Boniface 2002), several investigators have measured baseline hippocampal activity using non-BOLD methods. Initial baseline 18F-deoxyglucose positron emission tomography (PET) studies of medial temporal lobe activity in schizophrenia provided mixed results (i.e., decreased (Tamminga, Thaker et al. 1992; Nordahl, Kusubov et al. 1996) or increased (DeLisi, Buchsbaum et al. 1989; Gur, Mozley et al. 1995) in schizophrenia). However, several 15O-PET and Single Photon Emission Computed Tomography (SPECT) studies of regional cerebral blood flow (CBF) have established increased hippocampal baseline activity in schizophrenia (Friston, Liddle et al. 1992; Heckers, Rauch et al. 1998; Lahti, Holcomb et al. 2003; Malaspina, Harkavy-Friedman et al. 2004; Lahti, Weiler et al. 2009). A recent resting-state BOLD fMRI study revealed greater right hippocampal activity in

schizophrenia by measuring intrinsic signal intensity fluctuations (Tregellas, Smucny et al. 2014).

Hippocampal hyperactivity has been proposed as a biomarker for schizophrenia (Tregellas 2013), but it is unclear whether it affects all hippocampal subfields. An initial study by Schobel et al. reported increased cerebral blood volume (CBV) in subfield CA1 only (Schobel, Lewandowski et al. 2009). This finding was limited to a single slice of the hippocampal formation, averaged across the right and left hemisphere. A follow up study by the same group explored CBV changes along the long axis of the hippocampal formation in a cohort at high risk for psychosis and demonstrated that increased left anterior CA1 CBV spreads to the subiculum after psychosis onset (Schobel, Chaudhury et al. 2013). In contrast, Tamminga and colleagues predicted increased CBV in the CA3 subfield, as the downstream result of dentate gyrus pathology (Tamminga, Southcott et al. 2012). This model initially emerged as a way to bring together several findings in schizophrenia: smaller hippocampal volume, impaired activation during declarative memory tasks, increased baseline hippocampal perfusion, and reduced dentate gyrus neurogenesis and efferent signaling (Tamminga, Stan et al. 2010). They hypothesized that reduced pattern separation (i.e., the ability to distinguish between similar events at different time periods) and greater pattern completion (i.e., the retrieval of information based on partial cues) results in the production and retrieval of incorrectly coded memories, leading to psychosis. Taken together, the two competing models predict increased CBV either in CA1 or CA2/3.

Here we performed high spatial resolution, contrast-enhanced, T1-weighted steady state MRI in patients with schizophrenia and healthy controls to test these two opposing

models of subfield-specific hyperactivity in the anterior hippocampus in schizophrenia. This method provides the necessary high spatial (sub-millimeter) resolution to parse out subfields of the hippocampal formation (Small, Schobel et al. 2011) and has been implemented in our lab to characterize CBV gradients in different subfields (Talati, Rane et al. 2014).

Methods

Participants

15 healthy subjects and 15 patients with schizophrenia or schizoaffective disorder provided informed consent in a manner approved by the Vanderbilt Institutional Review Board. Patients and healthy controls were group-matched on age, gender, race, education, and parental education. Subjects were recruited from the Vanderbilt Psychotic Disorders Program or the local community and were paid for their participation. All subjects underwent a Structural Clinical Interview for DSM-IV Axis I disorders (SCID, (First 2002)) to confirm the diagnosis, and healthy controls had no major psychiatric, neurological, or medical illness. Serum creatinine was measured in all participants before and after contrast administration to minimize the potential risk of nephrogenic systemic fibrosis.

Cerebral Blood Volume Mapping

A Phillips 3T Achieva scanner with an 8 channel SENSE head coil was used for imaging. A 3D T1 FFE sequence (Lin, Celik et al. 1999) was implemented to acquire T1-weighted pre- and post-contrast images with the following parameters: TR = 20ms, TE = 3.98 ms, Field-of-View = 256 x 256 mm^2, Spatial resolution = 0.80 x 0.80 x 4 mm^3, slices = 30, SENSE factor = 2.5. A power

injector (Medrad®, PA, USA) was used for contrast administration (Magnevist ® - Gadopentetate dimeglumine, Bayer Schering Pharma, Germany, 0.1 mmol/kg) and subsequent 40 mL saline flush through an 18G needle in the antecubital vein. After contrast administration, post-contrast images were acquired approximately 4 minutes later. To allow for accurate segmentation of the hippocampal subfields (Moreno, Wu et al. 2007), images were acquired perpendicular to the long axis of the hippocampus. For each subfield, the regions of interest (ROIs) were centered to avoid border regions with neighboring subfields. We compared the fractional increase in tissue signal after the contrast agent had thorougly perfused the microvasculature and equilibrated in the blood.

Analysis

CBV calculations: AFNI (Cox 1996) was used to correct for subject motion in pre- and post-contrast steady state images. Absolute CBV (units = ml blood/ml parenchyma) was calculated using Equation (7):

$$CBV = \frac{S_{par,post} - S_{par,pre}}{S_{ss,post} - S_{ss,pre}} * 100 \qquad \textbf{(7)}$$

where $S_{par,post} - S_{par,pre}$ is the difference between the post- and pre-contrast signal in the parenchyma and $S_{ss,post} - S_{ss,pre}$ denotes the difference between the post- and pre-contrast signal in the superior sagittal sinus (Lin, Celik et al. 1999). To minimize contribution from large epicortical vessels, a 10% regional CBV threshold was used (i.e., voxels with CBV values greater than 10 were excluded) (Lin, Celik et al. 1999).

Hippocampal Segmentation: The T1-weighted pre-contrast image was used for manual segmentation of the allocortical subfields of the hippocampal formation: subiculum, CA1,

CA2/3, and hilus/dentate gyrus (referred to here as dentate gyrus) (Gloor 1997). The post-contrast image was used to exclude large epicortical vessels. From manual segmentation, 5 ROIs were generated for each slice: hippocampal formation, subiculum, CA1, CA2/3, and dentate gyrus. All segmentations were performed by one blinded rater (PT) and verified by another blinded rater (SR). If there were any discrepancies, the ROI was drawn by both raters until a consensus was reached.

The uncus is defined in coronal sections as more than one cut through the hippocampal formation and was used to delineate between the anterior and posterior regions (Duvernoy and Bourgouin 1998; Woolard and Heckers 2012). The coronal series for each subject was numbered and aligned across all subjects using the presence or absence of the uncus as a guide. From this method, three slices (slices two-four) were labeled as anterior and three slices (slices five-seven) were labeled as posterior for the whole hippocampal formation, subiculum, CA1 subfield, and CA2/3 subfields. Of note, the dentate gyrus CBV analysis only included slices three-seven because the dentate gyrus did not consistently extend into the first two slices of the anterior region. The anterior-posterior boundary was denoted by the transition between slice four to slice five. The final five hippocampal regions of interest were bilateral hippocampal formation, subiculum, CA1, CA2/3, and dentate gyrus (see Figure 12) for segmentation in a representative subject). CBV values were generated for each region and used in the statistical analyses.

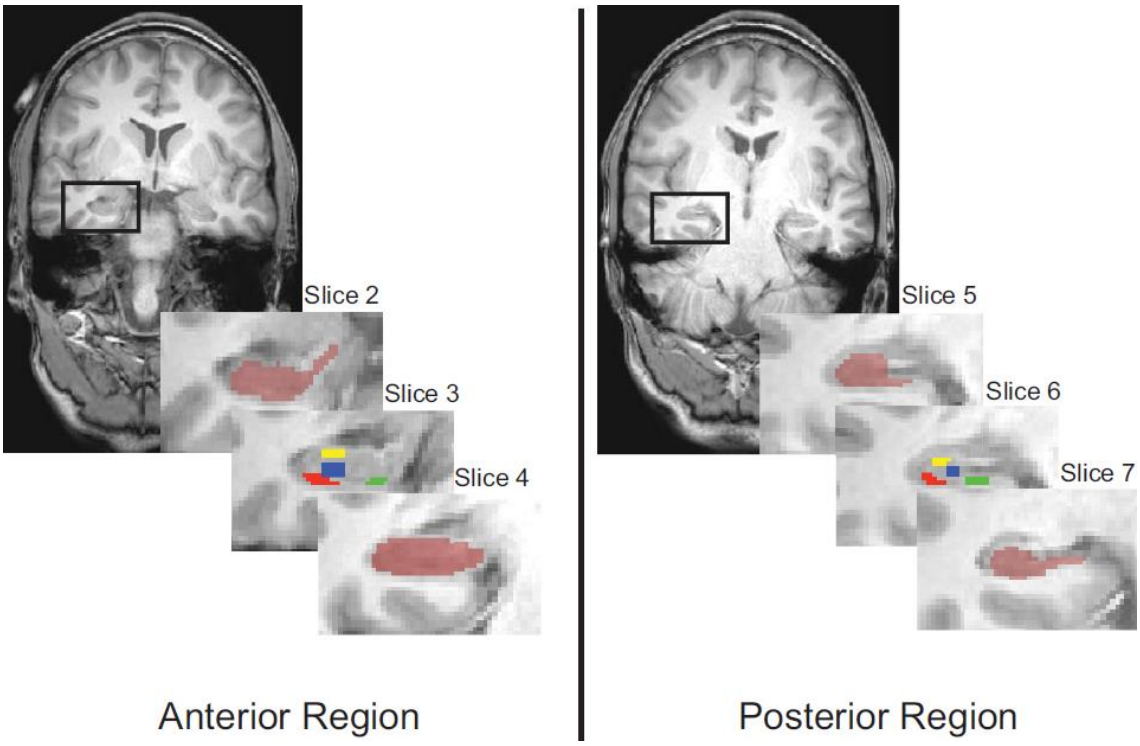

Figure 12 Manual segmentation of the hippocampal formation and subfields for a representative subject with a structural MRI (radiological orientation) for SS CBV
Left: Anterior hippocampal formation (slice 2) outlined in the black box with an inset series of slices through the anterior region. The dark red ROI in slices 2 and 4 illustrate the hippocampal formation ROI while slice 3 denotes the segmented subfields (green = subiculum, red = CA1, yellow = CA2/3, and blue = dentate gyrus).
Right: Posterior hippocampal formation (slice 5) outlined in the black box with an inset series of slices through the posterior region. The dark red ROI in slices 5 and 7 illustrate the hippocampal formation ROI while slice 6 denotes the segmented subfields (green = subiculum, red = CA1, yellow = CA2/3, and blue = dentate gyrus).

Statistical Analyses: Prior to statistical analyses, data were inspected to detect multivariate outliers; one subject in each group was identified as an outlier and removed from the analytic dataset. The remaining 14 healthy controls and 14 patients were group-matched on age, gender, race, subject education, and parental education (see Table 4). The Positive And Negative Symptom Scale (PANSS) was used to assess patient symptom severity across positive, negative, and general psychopathology (Kay, Fiszbein et al. 1987) and is reported in Table 4.

Table 4 SS CBV healthy control and patient demographics

	Controls (n = 14)	Schizophrenia (n = 14)	Statistic	p-value
Age (yrs ± stdev)	34.57 ± 9.32	32.93 ± 10.89	t(26) = 0.43	0.67
Males	9	9	$X^2(1) = 0$	0.65
Race (W/B)	10/4	9/5	$X^2(1) = 0.16$	0.50
Subject Edu. (yrs ± stdev)	15.79 ± 2.69	14.07 ± 2.69	t(26) = 1.69	0.10
Avg. Parental Edu. (yrs ± stdev)	14.57 ± 1.86	13.69 ± 2.13	t(26) = 1.18	0.25
Duration of Illness (yrs ± stdev)	-	8.47 ± 7.92	-	
CPZ equivalent (mg/day)	-	316.36 ± 170.43	-	
PANSS	-	Positive: 15.93 ± 7.13 Negative: 16.00 ± 6.88 General: 29.64 ± 7.35	-	

Fourteen controls and patients with schizophrenia were group-matched on age, gender, race, subject education, and parental education. CPZ denotes chlorpromazine; PANSS denotes Positive and Negative Syndrome Scale.

12 patients were taking a variety of atypical (i.e., aripiprazole, olanzapine, quetiapine, asenapine) and typical (i.e., haloperidol, risperidone, thiothixene) antipsychotic medications at the time of the study. Chlorpromazine equivalent doses were calculated from an international consensus study by Gardner et al (Gardner, Murphy et al. 2010). The chlorpromazine equivalent dose could not be calculated for one subject treated with asenapine, and two subjects were not taking any antipsychotic medications at the time of the study.

To test the primary hypothesis of diagnosis differences in anterior subfield CBV activity, we performed a repeated-measures ANOVA. Diagnosis was the between-subjects factor and subfield (CA1 or CA2/3) was the within-subjects factor. Age and gender were matched between groups and were not included as covariates in the ANOVA. We calculated effect sizes (Cohen's *d* (Cohen 1988)) and followed up with *post-hoc* comparisons to aid in interpretation of findings. *Post-hoc* one-tailed t-tests then investigated group differences in the anterior three slices of the two subfields. As an exploratory analysis, we also tested for group differences in the anterior slices of the subiculum and dentate gyrus. The Statistical Package for Social Sciences software (SPSS Version 20.0. Armonk, NY: IBM Corp.) was used for statistical analyses.

Results

The CBV values ranged from 2.82 – 3.37 (see Table 5) and were similar to values previously reported for the hippocampus (Kuppusamy, Lin et al. 1996).

Table 5 SS CBV values for each of the 5 regions of interest (ROI) for healthy controls and patients

	HF	Subiculum	CA1	CA2/3	DG
Control	3.37 ± 0.18	3.11 ± 0.60	2.67 ± 0.16	2.98 ± 0.23	3.18 ± 0.16
Schizophrenia	3.40 ± 0.28	3.29 ± 0.66	2.88 ± 0.15	2.82 ± 0.13	3.09 ± 0.24

CBV values (mean ± standard deviation; units = ml blood/ml parenchyma) averaged across hemisphere and along the long axis of the hippocampus for each manually segmented ROI. HF denotes hippocampal formation, and DG denotes dentate gyrus.

To test for anterior CA1 versus CA2/3 hyperactivity in schizophrenia, we performed a repeated-measures ANOVA. The resulting analysis showed a diagnosis-by-subfield interaction ($F(1,26) = 5.55$, $p < 0.05$, $d = 0.176$) and no main effect of subfield ($F(1,26) = 2.72$, $p > 0.10$). Healthy controls had significantly lower CBV in CA1 relative to CA2/3 (mean = 2.57 versus mean = 3.07; $F(1,13) = 12.04$, $p < 0.05$). Patients with schizophrenia failed to show this pattern ($p >$

0.10): CBV was similar in CA1 (mean = 2.90) and CA2/3 (mean = 2.81). *Post-hoc* one-tailed t-tests within the two subfields revealed a trend for patients with schizophrenia to have increased CBV relative to controls in CA1 ($t(26) = 1.60$, $p = 0.06$, $d = 0.63$; Figure 13). In contrast, CBV in CA2/3 was slightly decreased in patients with schizophrenia ($p = 0.14$, $d = 0.43$).

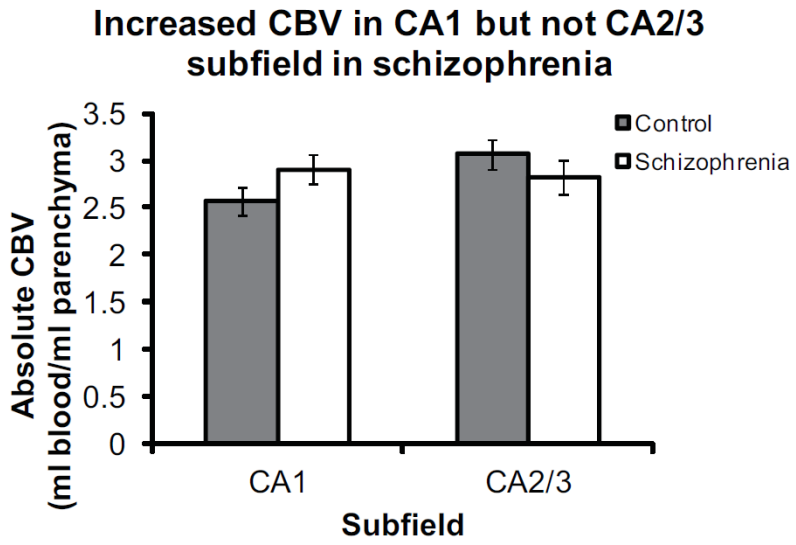

Figure 13 Increased SS CBV in the CA1 but not CA2/3 subfield in schizophrenia
For each subject, CA1 or CA2/3 CBV values were collapsed across hemisphere and anterior slices. A repeated-measures ANOVA illustrated a significant diagnosis by slice interaction ($p < 0.05$). A *post-hoc* one-tailed t-test shows a trend towards increased CBV in the CA1 subfield ($p = 0.06$) but not CA2/3 subfield ($p = 0.14$). Error bars denote standard error of the mean.

To determine whether the subfield-by-diagnosis difference was consistent across the anterior hippocampal formation, or localized within a specific slice, we performed two-sample, one-tailed t-tests within each of the three anterior slices. For the CA1 subfield, patients with schizophrenia had increased CBV relative to controls in two of the three slices (see Figure 14A): slice 2 (trend, $t(25) = 1.591$, $p = 0.06$) and slice 4 ($t(26) = 1.904$, $p < 0.05$). For the CA2/3

subfield, healthy controls had increased CBV relative to patients with schizophrenia in slice 4 (trend, t(26) = 1.553, p = 0.07, Figure 14B).

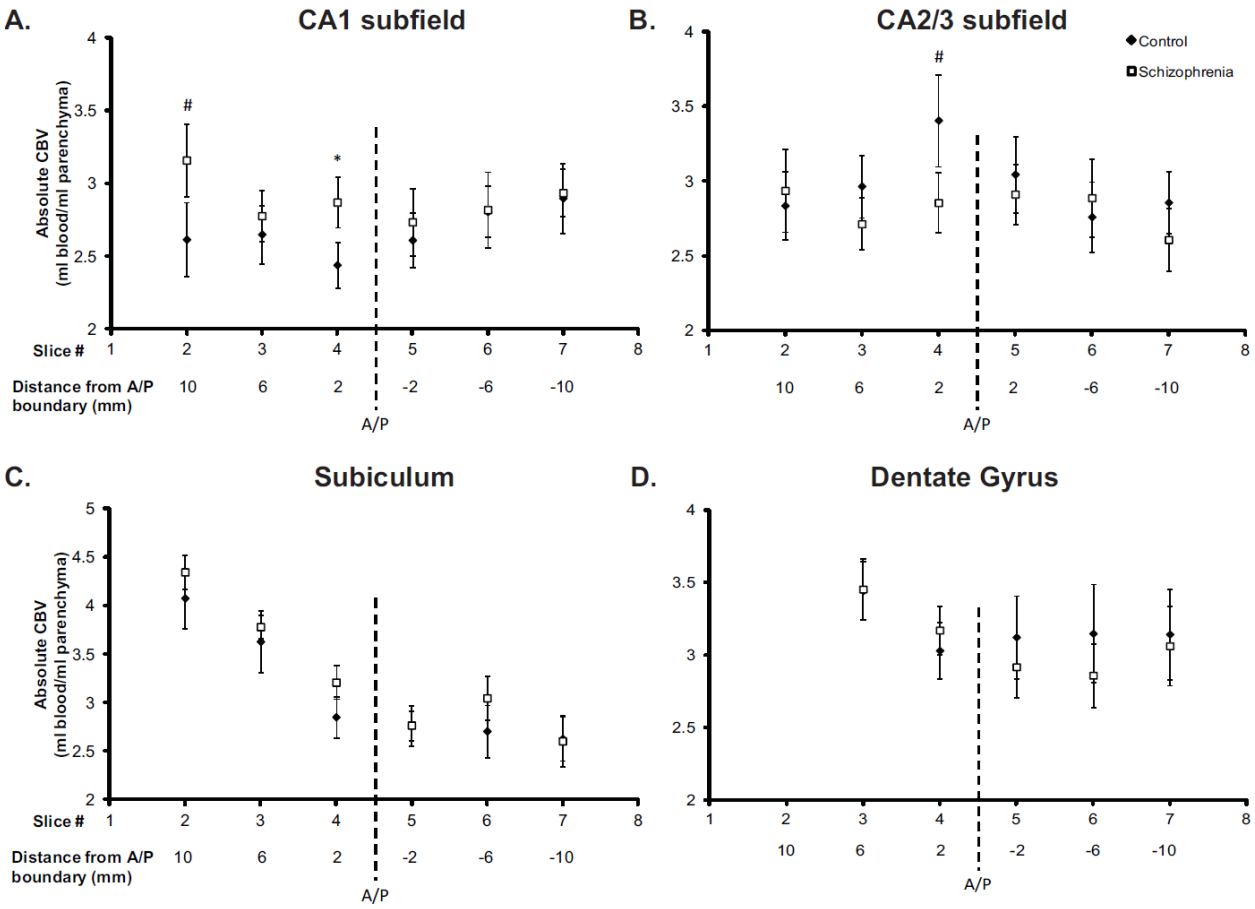

Figure 14 Increased SS CBV in the anterior CA1 in schizophrenia
For each subject, subfield CBV values were collapsed across hemisphere for each slice along the long axis of each subfield. *Post-hoc* one-tailed t-tests illustrate increased CA1 CBV in slices two (# p = 0.06) and four (* p < 0.05) (panel A) and decreased CA2/3 CBV in slice 4 (# p = 0.07) (panel B) in schizophrenia. There were no significant group CBV differences in the subiculum (panel C) and dentate gyrus (panel D). Error bars denote standard error of the mean. A/P refers to anterior/posterior boundary.

We then performed an exploratory investigation to test for group differences in the anterior subiculum and dentate gyrus. For the subiculum, healthy controls had an average CBV of 4.08, 3.63 and 2.85 for slices 2-4, while patients with schizophrenia had a mean CBV of 4.34, 3.78, and 3.21. *Post-hoc* two-tailed t-tests demonstrated no significant group differences (all p > 0.10; see Figure 14C). For the dentate gyrus, healthy controls had an average CBV of 3.44 and

3.03 for slices 2 and 3, while patients had a mean CBV of 3.45 and 3.17. There were no group differences in the dentate gyrus (all $p > 0.10$; see Figure 14D).

Finally, we tested whether the anterior CA1 CBV correlated with positive, negative, or general psychopathology, or the dose of antipsychotic medication. In the 14 patients, the anterior CA1 CBV did not correlate with positive ($r = 0.18$, $p = 0.53$), negative ($r = -0.12$, $p = 0.69$), or general ($r = -0.03$, $p = 0.91$) psychopathology as assessed by the PANSS. Three of the fourteen patients were not on antipsychotics or the chlorpromazine equivalent dose could not be calculated. Of the remaining 11 patients, there was no significant correlation between dose of antipsychotic medication and anterior CA1 ($r = 0.46$, $p = 0.16$).

Discussion

We used high resolution, steady state, contrast-enhanced T1-weighted imaging to test for anterior CA1 versus CA2/3 hippocampal subfield hyperactivity in schizophrenia. Here we report a significant diagnosis by subfield interaction due to the combined effect of a trend of increased CA1 CBV ($p = .06$) and non-significantly decreased CA2/3 CBV ($p=0.14$) in patients relative to healthy controls.

The hippocampal formation integrates multimodal information for the encoding of new and the retrieval of old memories. The entorhinal cortex sends glutamatergic fibers directly to the CA1 subfield (direct pathway) or indirectly to the CA1 subfield via the dentate gyrus and CA3 subfields (indirect pathway) (Amaral and Witter 1989). Any dysfunction along these two pathways could lead to increased CA1 CBV. Our results support the hypothesis of increased CA1 CBV in schizophrenia (Schobel, Lewandowski et al. 2009; Small, Schobel et al. 2011; Schobel,

Chaudhury et al. 2013), but do not support the hypothesis of increased CA3 metabolism in the context of dentate gyrus pathology in schizophrenia (Tamminga, Southcott et al. 2012). Schobel et al. reported increased CBV in the CA1 subfield, which was correlated with positive and negative symptoms of schizophrenia (Schobel, Lewandowski et al. 2009). In a follow up study, they showed that increased CBV was limited to a single slice in the left anterior CA1 in high-risk patients which spread to the subiculum after psychosis onset (Schobel, Chaudhury et al. 2013). We replicate the CBV increase in schizophrenia selectively in CA1, but do not find it to be limited to the left hemisphere and do not find it to be correlated to positive or negative symptoms.

Shape-based analyses also have reported structural findings in the CA1 subfield. One study in first-episode schizophrenia patients demonstrated regional volume reductions in the left anterior and midbody CA1 (Narr, Thompson et al. 2004). Another imaging study has linked left anterior CA1 deformity to antipsychotic dosage and symptom severity in a schizophrenia cohort (Zierhut, Grassmann et al. 2013). Together, these studies suggest structural and functional alterations in the anterior CA1 in schizophrenia. The CA1 subfield supports novelty detection by comparing information from the indirect pathway (i.e., entorhinal cortex to dentate gyrus to CA3 to CA1) to information received by the direct pathway (i.e., entorhinal cortex to CA1) (Knight 1996; Lisman and Otmakhova 2001; Vinogradova 2001; Li, Cullen et al. 2003). Hippocampal hyperactivity can lead to the formation of delusions and hallucinations through the incorrect formation and association of memories retrieved by the hippocampal formation (Lisman, Pi et al. 2010; Ewing and Winter 2013).

Several mechanisms of disease may lead to hippocampal hyperactivity in schizophrenia. Postmortem and imaging studies have provided support for N-methyl-D-aspartate receptor (NMDAR) hypofunction (Theberge, Bartha et al. 2002; Kristiansen, Huerta et al. 2007), dopamine dysregulation (Laruelle, Abi-Dargham et al. 1999; Abi-Dargham 2004), and gamma-aminobutyric acid- (GABA-) ergic interneuron loss (Zhang and Reynolds 2002; Akbarian and Huang 2006; Konradi, Yang et al. 2011; Nakazawa, Zsiros et al. 2012). These three mechanisms have been integrated into a comprehensive model of hippocampal dysfunction in schizophrenia (Lisman, Coyle et al. 2008). Hippocampal interneurons are more sensitive than pyramidal neurons to NMDAR blockade (Jones and Buhl 1993; Grunze, Rainnie et al. 1996; Lisman, Coyle et al. 2008; Bolton, Heaney et al. 2012). In addition, the number of fast-spiking parvalbumin-positive interneurons in CA1 are decreased in schizophrenia (Konradi, Yang et al. 2011). Since hippocampal pyramidal neurons are under tonic inhibition by this interneuron subtype, decreased interneuron function (either through cell loss or pyramidal cell-sensing activity via NMDAR hypofunction) results in the disinhibition of pyramidal neurons in CA1 (which can be registered as increased CBV). In animal models, hyperactivity of CA1 pyramidal neurons results in decreased inhibition of ventral tegmental area (VTA) neurons (Blaha, Yang et al. 1997; Legault and Wise 1999; Lodge and Grace 2011), which results in dopaminergic dysfunction and may lead to the positive and negative symptoms of schizophrenia. This prediction is consistent with the finding of CA1 CBV to be correlated positively with delusions and negatively to social dysfunction and avolition in a prodromal cohort (Schobel, Lewandowski et al. 2009). In addition, there is direct evidence that the experience of auditory hallucinations is linked to increased hippocampal activity (using BOLD fMRI (Dierks, Linden et al. 1999) and SPECT with a 99m-

Technetium exametazine radiotracer (Musalek, Podreka et al. 1989), for review see (Weiss and Heckers 1999).

We also studied CBV in the subiculum and the dentate gyrus. Since the subiculum serves as the main outflow of the hippocampus, an increase of CBV in CA1 could result in an increase of CBV in the subiculum. Schobel et al. reported increased subiculum CBV at psychosis onset (Schobel, Chaudhury et al. 2013) but, similar to our findings, did not report increased subiculum CBV in chronic schizophrenia patients (Schobel, Lewandowski et al. 2009). This set of results could be due to structural changes in the subiculum after psychosis onset (Rosoklija, Toomayan et al. 2000). We have recently demonstrated a significant anterior-posterior CBV gradient in the subiculum (Talati, Rane et al. 2014) and further studies are needed to elucidate the role of the subiculum in first-episode psychosis and chronic schizophrenia.

Small sample size is the main limitation of our study and the results should be considered preliminary. But the sample size is comparable to the original study of hippocampal CBV in schizophrenia (18 schizophrenia patients and 18 healthy controls), and we confirm the original finding of increased CA1 CBV (Schobel, Lewandowski et al. 2009) in schizophrenia. We were able to match the control group to the patient group on several parameters, including age, race, and parental education. Most of our patients were treated with antipsychotic medication at the time of the study. However, our studies are consistent with those by Schobel et al. and indicate that antipsychotic medications are not likely to affect resting-state CBV (Schobel, Lewandowski et al. 2009; Schobel, Chaudhury et al. 2013).

In conclusion, we report a subfield by diagnosis interaction due to the combined effect of a trend of increased CA1 CBV ($p = .06$) and non-significantly decreased CA2/3 CBV ($p=0.14$) in

patients relative to healthy controls. Future studies should investigate the evolution of hyperactivity in hippocampal subfields in the early stages of psychosis and their contribution to the generation of the signs and symptoms of psychosis.

CHAPTER IV

INCREASED HIPPOCAMPAL BLOOD VOLUME AND NORMAL BLOOD FLOW IN SCHIZOPHRENIA

Introduction

The hippocampus is abnormal in schizophrenia (Heckers and Konradi 2010). Studies of the underlying cellular and molecular mechanisms have illustrated N-methyl-D-aspartate (NMDA) receptor hypofunction (Olney, Newcomer et al. 1999) and reduced gamma-aminobutyric acid- (GABA-) ergic interneuron density (Benes, Kwok et al. 1998), especially in fast-spiking, parvalbumin-containing cells (Zhang and Reynolds 2002; Konradi, Yang et al. 2011). These molecular changes may lead to excitation-inhibition imbalances (Lisman, Coyle et al. 2008; Heckers and Konradi 2014), which can be indirectly assessed through perfusion imaging methods. Initial positron emission tomography (PET) and single photon emission computed tomography (SPECT) studies measured cerebral blood flow (CBF) or volume (CBV). These studies failed to achieve a general consensus: some reported increases in baseline hippocampal activity (Friston, Liddle et al. 1992; Heckers, Rauch et al. 1998; Malaspina, Harkavy-Friedman et al. 2004), while others illustrated decreases (Buchsbaum, Haier et al. 1992; Tamminga, Thaker et al. 1992; Nordahl, Kusubov et al. 1996) or no changes (Vita, Bressi et al. 1995). Due to radiation exposure and poor spatial resolution, these methods have fallen out of favor for comparable magnetic resonance imaging (MRI) methods (Small, Schobel et al. 2011).

Recently implemented MRI-based methods require an endogenous (blood water) or exogenous (paramagnetic) contrast agent to generate CBV or CBF maps. Arterial spin labeling uses blood water magnetization as an endogenous contrast to analyze a single hemodynamic parameter, i.e., CBF, in the brain. This method has provided mixed results, reporting increases

(Pinkham, Loughead et al. 2011), decreases (Scheef, Manka et al. 2010; Walther, Federspiel et al. 2011; Kindler, Jann et al. 2013), or no changes (Horn, Federspiel et al. 2009; Ota, Ishikawa et al. 2014) in medial temporal lobe CBF in schizophrenia. More recently, contrast-enhanced, high resolution (submillimeter) steady state imaging has been used to investigate CBV changes in schizophrenia. Though few in number, these initial studies support increased hippocampal Cornu Ammonis 1 (CA1) CBV (Schobel, Lewandowski et al. 2009; Schobel, Chaudhury et al. 2013; Talati, Rane et al. 2014). Importantly, this method also characterizes a single hemodynamic parameter, i.e., CBV, to make inferences about basal metabolism. Dynamic susceptibility contrast- (DSC-) MRI may be able to resolve these mixed findings of hippocampal activity across different modalities due to its ability to assess *several* hemodynamic parameters, including CBV, CBF, and mean transit time (MTT) (Perkio, Aronen et al. 2002).

Even though DSC-MRI has been used extensively to investigate metabolism and perfusion abnormalities in neurological disorders such as tumors and strokes, very few studies have implemented this technique to study psychiatric illnesses including schizophrenia (Renshaw, Levin et al. 1997). As recently reviewed by Théberge in 2008, only five articles have been published using this method in schizophrenia research (Theberge 2008). Since the review, there have been two additional studies of bolus-tracking perfusion imaging with a paramagnetic agent in schizophrenia (Bellani, Peruzzo et al. 2011; Peruzzo, Rambaldelli et al. 2011). Together, these studies illustrate several findings in schizophrenia: low and inverse hemispheric CBV as indirectly measured through contrast enhancement (CE) (Brambilla, Cerini et al. 2007); increased CBV in the cerebellum (Loeber, Sherwood et al. 1999), caudate, and occipital cortex (Cohen, Yurgelun-Todd et al. 1995); no alterations in CBV, CBF, or MTT in

cerebrum or cerebellum (Bellani, Peruzzo et al. 2011); decreased frontal cortex CBV and CBF only when using a best predictor model containing clinical state, age, and length of illness (Peruzzo, Rambaldelli et al. 2011); variable time-to-peak (TTP) in the caudate (Fabene, Farace et al. 2007); and increased perfusion in the prefrontal cortex, temporal lobe, and posterior parietal cortices after dopamine receptor D1 agonist administration (Mu, Johnson et al. 2007). Importantly, none of these studies used a region of interest-based analysis to report hemodynamic properties in the hippocampus in schizophrenia, even though functional abnormalities have been reported in this medial temporal lobe structure.

In this study, we used DSC-MRI to specifically study hippocampal perfusion properties (CBV, CBF, and MTT) in 15 patients with chronic schizophrenia and matched controls. Based on a previous report on this cohort using steady state CBV imaging (Talati, Rane et al. 2014), we hypothesized increased hippocampal perfusion, as measured by CBV and CBF.

Methods

Participants

15 patients with schizophrenia or schizoaffective disorder (age range: 20-54 years) and 15 matched healthy controls (age range: 22-53 years) provided informed consent in a manner approved by the Vanderbilt Institutional Board. Both groups were matched across several demographics, including age, race, and gender (Table 6). Subjects were recruited from the Vanderbilt Psychotic Disorders Program or the local community; they were paid for their participation. We used the Structured Clinical Interview for DSM-IV Axis I disorders (SCID, (First 2002)) to establish all diagnoses and the Positive and Negative Syndrome Scale (Kay, Fiszbein et

al. 1987) to assess the clinical status of the patients. 12 of the 15 patients were treated with antipsychotic medication and their chlorpromazine equivalent dosages (Gardner, Murphy et al. 2010) are listed in Table 6. History of major neurological or medical illness was an exclusion criterion. Since nephrogenic systemic fibrosis is a rare adverse effect of gadolinium-containing contrast, we required a normal serum creatinine value for study eligibility and confirmed normal values again after study completion.

Table 6 DSC subject demographics

	Controls (n = 15)	**Schizophrenia (n = 15)**	**Statistic**	**p-value**
Age (yrs)	34.27 ± 9.06	36.20 ± 12.59	t(25.43) = -0.483	0.63
Males	10	10	X(1) = 0	1.00
Race (W/B)	11/4	10/5	X(1) = 0.159	0.69
Subject edu. (yrs)	15.53 ± 2.77	14.20 ± 2.51	t(28) = 1.38	0.18
Avg. parental edu. (yrs)	14.40 ± 1.91	14.19 ± 2.03	t(28) = 0.30	0.77
Duration of Illness (yrs)		10.55 ± 8.86		
CPZ equivalent (mg/day)		352.50 ± 160.35		
PANSS		Positive: 15.47 ± 7.10 Negative: 17.47 ± 7.22 General: 28.07 ± 8.56		

Healthy control and chronic schizophrenia subject demographics. Groups are matched on age, gender, race, and subject and parental education. Values are reported as mean ± st dev. The chlorpromazine (CPZ) equivalent doses could not be calculated for two subjects who were off medication at the time of the study and for one subject who was taking asenapine. PANSS denotes the positive and negative syndrome scale.

Dynamic susceptibility contrast imaging

Imaging was performed using a Phillips 3T Achieva scanner with an 8 channel SENSE head coil. T2*-weighted echo planar images were acquired perpendicular to the long axis of the hippocampus for accurate segmentation using the following sequence parameters: TR = 1600 ms, TE = 54 ms, Field-of-View (FOV) = 240 x 240 mm^2, spatial resolution: 1.5 mm^3 isotropic, slices = 15, dynamics = 120. 14 dynamics were collected before gadopentetate dimeglumine

(Magnevist®, Bayer Schering Pharma, Germany, 0.1 mmol/kg) was injected at a constant rate of 5ml/sec through an 18G intravenous catheter in the antecubital vein via an MRI-compatible power injector (Medrad®, PA, USA). The bolus of contrast was immediately followed by a 40 mL saline flush at the same rate. The intravenous catheter was removed after the completion of the scan. To allow for accurate segmentation of the hippocampal formation (Moreno, Wu et al. 2007), high-resolution T1-weighted pre-contrast images were also acquired perpendicular to the long axis of the hippocampus using the following scan parameters: TR = 20 ms, TE = 3.41 ms, FOV = 256 x 256 mm^2, slices = 15.

Analysis

CBV, CBF, and MTT calculations: AFNI (3dvolreg) (Cox 1996) was used to correct for subject motion during the dynamic scans, and all images were registered to the first dynamic scan. First, voxel-wise signal contrast variations due to injection of gadolinium were converted to a concentration-time curve using Equation (8) (Ostergaard 2004):

$$\Delta R_2^*(t) = \frac{-log\left(\frac{S(t)}{S_0}\right)}{TE} \qquad \textbf{(8)}$$

where ΔR_2^* is the change in transverse relaxation rate (i.e., $1/T_2^*$); *TE* is the echo time; *S(t)* is the signal intensity at a time *t*; and S_0 is the baseline signal intensity at a voxel, calculated as the mean signal intensity at that voxel over the first 10 dynamic scans before contrast administration. Voxels located near the M1 segment of the middle cerebral artery were used to evaluate the arterial input function (AIF). Care was taken to place the voxels adjacent to the vessel to avoid susceptibility effects and signal cutoff as outlined by (van Osch, van der Grond et al. 2005). CBV, CBF, and MTT were calculated using singular value decomposition (SVD) with

block circulant matrices (Ostergaard, Sorensen et al. 1996; Ostergaard, Weisskoff et al. 1996). The threshold for the diagonal matrix generated using SVD was set to 0.15 in order to reduce oscillations of the derived tissue residue function. This threshold was chosen based on the high resolution and low signal-to-noise ratio of the images (SNR = 7.60±2.02). Regional CBF value was calculated as the peak value of the deconvolved tissue impulse response. Regional CBV was the ratio of the area under the tissue ΔR_2^* curve to the area under the AIF ΔR_2^* curve. Mean transit time (MTT) was calculated using Equation (9):

$$MTT = \frac{CBV}{CBF} \qquad \textbf{(9)}$$

Finally, a normal appearing white matter region of interest was chosen in the parietal region for each subject. Assuming a white matter CBF of 22 ml/100gm/min and a CBV of 2 ml/100gm (Ostergaard, Sorensen et al. 1996), the regional values were scaled to obtain absolute CBF and CBV measures. Matlab (version 7.13.0.564, The MathWorks Inc, Natick, Massachusetts) was used to generate an in-house script to obtain the CBV, CBF, and MTT values.

Hippocampal segmentation: The T1-weighted pre-contrast image was used for blind, manual segmentation of the hippocampal formation by one rater (PT) and verified by another rater (SR). If there were any discrepancies, the region of interest (ROI) was drawn by both raters until a consensus was reached. Manual segmentation of each subject's hippocampus generated 15 hippocampal ROIs for each hemisphere for a total of 30 hippocampal ROIs (15 left and 15 right). Hippocampal ROIs were downsampled to reach the same spatial resolution of the T2*-weighted images.

Statistics: CBF, CBV, and MTT values across all posterior hippocampal slices were averaged for each hemisphere for each subject. This method produced 6 values for each subject: left and right hippocampal CBV, left and right hippocampal CBF, and left and right hippocampal MTT.

Because of no *a priori* hypothesis about hemispheric lateralization, we performed an exploratory analysis testing for hemisphere effects. A repeated-measures analysis of variance (ANOVA) with hemisphere as a within-subject factor and group as a between-subject factor illustrated no main effect of hemisphere and no hemisphere by diagnosis interaction for CBV (*F(1,28) = 1.83, p = 0.19*; *F(1,28) = 0.62, p = 0.44*, respectively), CBF (*F(1,28) = 2.17, p = 0.15*; *F(1,28)=0.11, p = 0.74*, respectively), and MTT (*F(1,28) = 0.76, p = 0.39*; *F(1,28) = 0.56, p = 0.46*, respectively). Therefore, the primary analysis for each hemodynamic parameter (CBV, CBF, and MTT) was a between-group independent samples *t*-test after collapsing across hemisphere (average left/right). Because groups were well matched, age, gender, and race were not included as covariates in the analysis. Correlation analyses are reported using Pearson's correlation. Statistical analyses were performed using The Statistical Package for Social Sciences software (SPSS version 20, Armonk, NY: IBM Corp http://www.spss.com).

Results

Figure 15 depicts the ΔR_2^* changes before, during, and after gadolinium-contrast administration. Injection with a gadolinium bolus causes predominant R_2^* shortening, resulting in a loss of signal. As the contrast agent recirculates, the bolus diffuses and equilibrates with

the blood in the microvasculature, allowing the tissue R_2* to recover to nearly its pre-contrast value (shown in Figure 16).

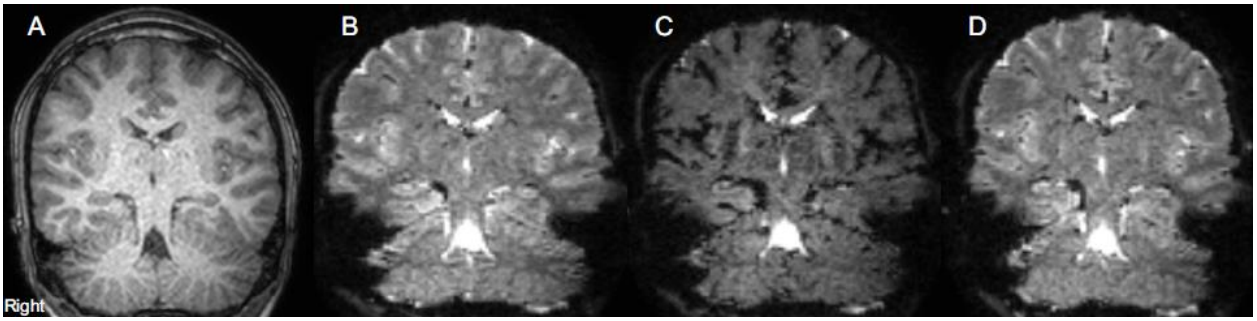

Figure 15 T1- and T2*-weighted dynamic scans in radiological orientation for a representative control subject with DSC imaging
A: T1-weighted structural image. B: T2*-weighted dynamic scan before contrast administration. C: Loss of signal intensity on T2*-weighted images during contrast administration. D: Recovery of signal intensity after contrast administration.

Whole brain CBV-, CBF-, and MTT-weighted maps were generated for each subject (see Figure 17) to extract hippocampal CBV, CBF, and MTT values. For healthy controls, hippocampal CBV (units = ml blood/100gm parenchyma) ranged from 2.69 to 5.32. Patients had a wider hippocampal CBV range (2.80 to 8.48). Hippocampal CBF (units = ml blood/100gm parenchyma per minute) ranged from 27.75 to 76.71 in healthy controls and 35.39 to 84.65 in patients. Finally, healthy control hippocampal MTT (units = seconds) ranged from 3.28 to 7.30 and patient hippocampal MTT ranged from 4.09 to 8.14. These values are similar to those previously published for medial temporal lobe CBF (Li, Sarkar et al. 2013) and CBV (Schobel, Lewandowski et al. 2009; Talati, Rane et al. 2014) and comparable to contrast-enhanced steady state CBV values in the same cohort (Talati, Rane et al. 2014).

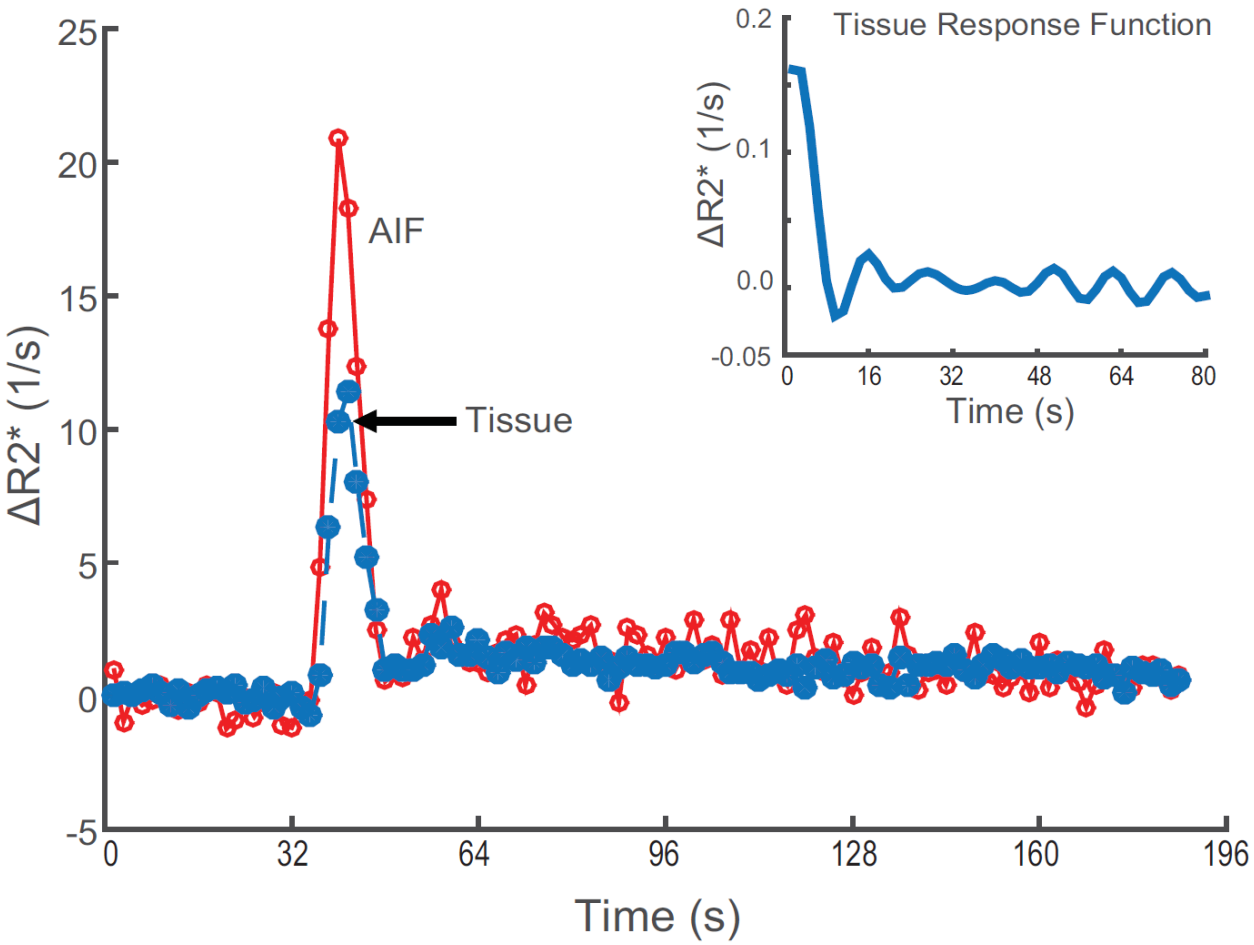

Figure 16 R_2* signal recovery after gadolinium bolus passage in two different brain regions of a control subject
After a gadolinium bolus, R_2* signal changes are evident across 120 dynamic scans (192 seconds) in select voxels near the M1 segment of the middle cerebral artery for the arterial input function (AIF, open circles connected by a solid line) and gray matter tissue (filled circles connected by a dashed line). The figure inset indicates the tissue response function obtained after deconvolution.

We first tested the hypothesis of increased hippocampal metabolism, as measured by CBV and CBF, in schizophrenia. Hippocampal CBV (mean ± stdev) was increased in patients with schizophrenia compared to healthy controls (4.57 ± 1.41 vs. 3.79 ± 0.86, one-tailed t-test, *t(28) = 1.83, p = 0.039*, Cohen's *d = 0.67*, Figure 18A), when averaged across hemispheres. However, there were no group differences in CBF (one-tailed t-test, *t(28) = -0.63, p = 0.28*, *d = 0.21*, Figure 18B). We then investigated whether hippocampal MTT was altered in schizophrenia and found no differences (two-tailed t-test, *t(28) = -1.23, p = 0.22*, *d = 0.46*), as illustrated in Figure 18C.

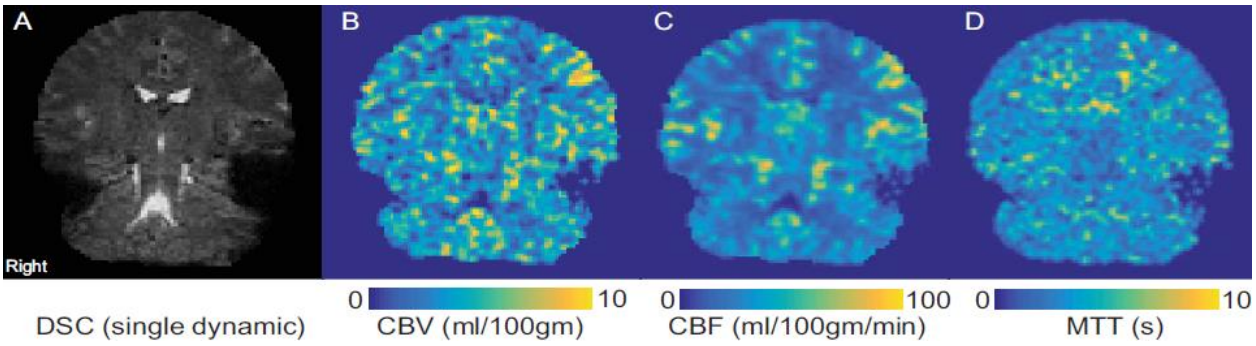

Figure 17 Hemodynamic maps for a representative control subject in radiological orientation for DSC-MRI
A: T2*-weighted dynamic susceptibility contrast (DSC) dynamic scan. B-D: cerebral blood volume- (CBV-), cerebral blood flow- (CBF-), and mean transit time- (MTT-) weighted maps, respectively. Color bar denotes values for each hemodynamic map, with lighter colors corresponding to larger values.

We explored whether increased CBV in schizophrenia correlated with duration of illness, dose of antipsychotic medication, or psychopathology as assessed by the Positive and Negative Syndrome Scale (PANSS). Hippocampal CBV did not correlate with duration of illness (*r = -0.28, p = 0.31*), positive symptoms (*r = -0.13, p = 0.65*), negative symptoms (*r = -0.43, p = 0.11*), or general psychopathology (*r = 0.001, p = 1.00*) in the patient group. Three patients' chlorpromazine (CPZ) equivalents could not be calculated because there was either no

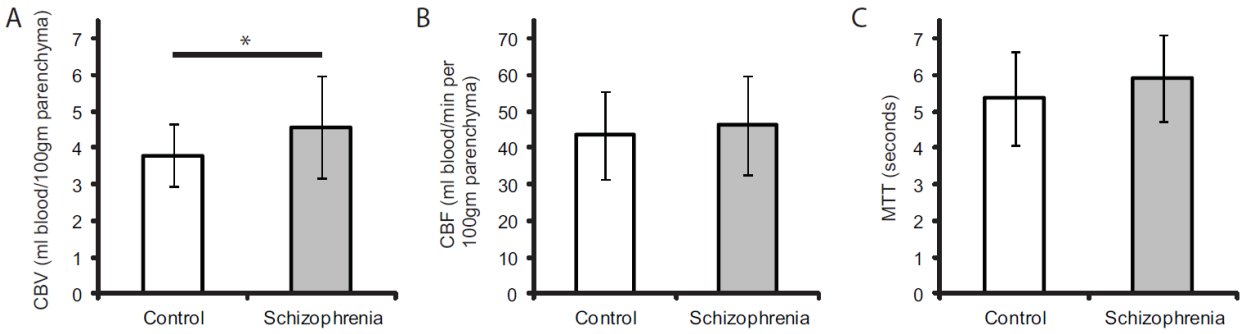

Figure 18 Increased hippocampal blood volume, but not flow, in schizophrenia using DSC-MRI
Hemodynamic parameters (mean ± st. dev) for healthy controls and patients with schizophrenia generated from dynamic susceptibility contrast- (DSC)-MRI for the hippocampus. These values are averaged across hemisphere and slice along the long axis of the hippocampus. Figure 4A illustrates increased hippocampal cerebral blood volume (CBV) in schizophrenia (one-tailed t-test, *t(28) = 1.831, p = 0.039*). Figure 4B illustrates no group differences in hippocampal cerebral blood flow (CBF, one-tailed t-test, *t(28) = -0.629, p = 0.28*), and Figure 4C illustrates no difference in hippocampal mean transit time (MTT) in schizophrenia (two-tailed t-test, *t(28) = -1.230, p = 0.22*). *p < 0.05

chlorpromazine equivalent dose (n=1) or they were not taking any medication at the time of the study (n=2). For the remaining 12 patients, antipsychotic medication dose did not correlate with hippocampal CBV (*r = 0.43, p = 0.16*).

Discussion

This is the first study to utilize DSC-MRI to study hippocampal perfusion in schizophrenia. We report increased hippocampal CBV in chronic schizophrenia, similar to our previous study using steady state imaging in the same cohort (Talati, Rane et al. 2014). However, we did not find increased hippocampal CBF or MTT in schizophrenia.

Because of the well-established relationship between CBV and CBF (Grubb, Raichle et al. 1974), many studies report CBV *or* CBF changes as a marker of basal activity. Here we report a novel finding in schizophrenia: increased hippocampal blood volume in the context of normal hippocampal blood flow. Our finding of increased hippocampal CBV is consistent with other gadolinium-enhanced studies (Schobel, Lewandowski et al. 2009; Schobel, Chaudhury et al. 2013). We did not observe increased hippocampal CBF using DSC-MRI, similar to what has been reported using arterial spin labeling (Horn, Federspiel et al. 2009; Ota, Ishikawa et al. 2014) and nuclear medicine techniques (Vita, Bressi et al. 1995). Even with the large variance in our dataset, the calculated effect sizes are larger for CBV (*d = 0.67*) than CBF (*d = 0.21*), suggesting that CBF changes may be more difficult to detect.

There might be several reasons for the finding of increased CBV in the context of normal CBF. First, previous studies have shown that antipsychotic medications do not affect hippocampal CBV (Schobel, Lewandowski et al. 2009; Schobel, Chaudhury et al. 2013; Talati,

Rane et al. 2014) but that they lower CBF in many brain regions (Miller, Andreasen et al. 1997; Novak, Milcinski et al. 2005; Ertugrul, Volkan-Salanci et al. 2009), including the hippocampus (Medoff, Holcomb et al. 2001; Lahti, Holcomb et al. 2003). Second, hippocampal excitation-inhibition imbalances (Lisman, Coyle et al. 2008; Heckers and Konradi 2014) in the prodromal or early stage of psychosis may lead to increased CBF to meet greater hippocampal metabolic demand. Increased CBF demands are mediated by increases in CBV via complex myogenic, chemical, neuronal, or metabolic autoregulatory mechanisms. Such CBV-CBF coupling occurs only when cerebral perfusion pressure remains unchanged. Therefore, a lack of CBF increase is likely due to a reduction in the cerebral perfusion pressure (Heilbrun, Jorgensen et al. 1972; Chan, Miller et al. 1992). Finally, instead of microvascular dilation, increased CBV can be secondary to angiogenesis (Swain, Harris et al. 2003), which could be assessed via hemodynamic response imaging (i.e., carbogen challenge (95%O_2+5%CO_2) that vasodilates all functional blood vessels and a hypercapnic challenge (95%air+5%CO_2) that only vasodilates mature blood vessels (Ben Bashat, Artzi et al. 2012).

A major goal in schizophrenia research is to link brain function with clinical features of the disease. Many perfusion imaging studies have quantified a single hemodynamic index (e.g., CBV or CBF) and correlated abnormal perfusion with psychopathology. For example, increased medial temporal lobe CBF has been associated with more severe general psychopathology (Friston, Liddle et al. 1992) and positive symptoms (Liddle, Friston et al. 1992; Lahti, Weiler et al. 2006), while increased hippocampal CBV has been associated with positive and negative symptoms (Schobel, Lewandowski et al. 2009) (see (Tregellas 2013) for a review). Furthermore, increased CBF in the superior temporal gyrus predicted a reduction of auditory hallucinations

after treatment with transcranial magnetic stimulation (Homan, Kindler et al. 2012), suggesting that decreased perfusion in this region may predict which patients are likely to respond to this treatment. However, not all studies using CBV or CBF have supported correlations between brain function and positive/negative symptoms (Kawasaki, Suzuki et al. 1992; Talati, Rane et al. 2014).

There are several assumptions that commonly underlie the DSC-MRI data analysis (Calamante, Gadian et al. 2002). First, there is an assumption of linearity between tissue contrast agent concentration and changes in the R_2* relaxation rate (Equation (8)). This assumption has been validated (Boxerman, Hamberg et al. 1995; Simonsen, Ostergaard et al. 1999) and likely holds true. Second, the arterial input function is presumed to represent the exact input to the tissue of interest (in this case, the hippocampus). The hippocampus has a differential blood supply, with the anterior region supplied by anterior hippocampal branch of the posterior cerebral artery (PCA) and anterior choroidal artery and the posterior region supplied by the middle and posterior hippocampal branches of the PCA (Huang and Okudera 1997). In practice, however, the M1 segment of the MCA is used and has generated reliable CBF values when compared with PET studies (Zaro-Weber, Moeller-Hartmann et al. 2012). Furthermore, we manually selected the AIF to avoid partial volume effects that can lead to under- or overestimation of the contrast agent concentration (van Osch, van der Grond et al. 2005). Other assumptions include constant capillary hematocrit and vascular permeability across brain regions and between subjects, which are not necessarily true.

The ideal imaging experiment to interrogate hippocampal hyperactivity would utilize a reliable, non-invasive imaging technique to longitudinally follow high-risk individuals who

eventually convert to psychosis. Arterial spin labeling (ASL) is one such non-invasive method that has been shown to be reliable with-in and between scanning sessions (Parkes, Rashid et al. 2004; Petersen, Mouridsen et al. 2010; Xu, Rowley et al. 2010; Gevers, van Osch et al. 2011; Donahue, Faraco et al. 2014). Even though ASL is gaining popularity due to increased signal-to-noise ratio at higher magnetic fields (e.g. 3T) and ease of implementation, there are some drawbacks to this method: the reproducibility is quite variable in different brain regions (Wu, Lou et al. 2014), it has worse spatial and temporal resolution than DSC-MRI (Wintermark, Sesay et al. 2005), the validity of the reported values varies depending on disease conditions (Tanaka, Nagaoka et al. 2011; Zaharchuk, El Mogy et al. 2012; Choi, Kim et al. 2013; Nael, Meshksar et al. 2013; Jiang, Zhao et al. 2014; White, Pope et al. 2014), and it is unclear how antipsychotic medication affects CBF values. Newer variants of arterial spin labeling acquire data over multiple post-labeling delays to assess several hemodynamic parameters (eg. CBV and CBF) and have been shown to correlate with DSC-MRI (Wang, Alger et al. 2013). However, the spatial resolution still may lead to some challenges in interpreting CBF and CBV values in small structures like the hippocampus.

This study has a few limitations. The sample size is small but consistent with other CBV imaging studies of schizophrenia patients (Schobel, Lewandowski et al. 2009; Talati, Rane et al. 2014). Most of our patients were treated with antipsychotic medication, which can affect hippocampal hemodynamic parameters such as CBF (see above). Furthermore, this method does not provide enough spatial resolution for subfield-specific investigation. While the in-plane resolution is 1.5 mm isotropic, the actual in-plane resolution is closer to 2 mm when considering the point-spread function degradation due to the paramagnetic bolus passage

(Wintermark, Sesay et al. 2005). Therefore, subfield-specific testing (Small, Schobel et al. 2011) was not feasible in this dataset.

In conclusion, we report increased hippocampal CBV, but not CBF, in chronic schizophrenia. Future studies need to incorporate several complementary imaging modalities to better characterize hippocampal dysfunction in schizophrenia.

CHAPTER V

HIPPOCAMPAL VOLUME, BLOOD FLOW, AND BLOOD VOLUME IN EARLY PSYCHOSIS

Introduction

While meta-analyses have consistently reported a smaller hippocampus in schizophrenia (Nelson, Saykin et al. 1998; Adriano, Caltagirone et al. 2012), the timing of hippocampal structural and functional changes remain uncertain. The literature on hippocampal volume in the early stage of psychosis ('first-episode psychosis') is mixed. Some report reduced volume (Velakoulis, Wood et al. 2006; Watson, Bai et al. 2012) while others do not (Laakso, Tiihonen et al. 2001; Smith, Lang et al. 2003; Williams, Avery et al. 2012). Two meta-analyses both illustrate reduced hippocampal volume in first-episode psychosis (Steen, Mull et al. 2006; Vita, De Peri et al. 2006). However, the authors caution that these meta-analyses are confounded by medication effects and different duration of undiagnosed illness. Another recent meta-analysis emphasized the negative association between duration of illness before baseline scan and the effect size of the group difference in the hippocampus (Olabi, Ellison-Wright et al. 2011), highlighting the importance of duration of illness in hippocampal pathology.

Multi-modal hippocampal imaging can provide a comprehensive profile of baseline hippocampal hemodynamics in a patient population. One recent method that has gained a lot of attention is contrast-enhanced steady-state cerebral blood volume (CBV) mapping (Moreno, Wu et al. 2007). This method uses high resolution imaging to obtain hippocampal CBV, a measure of basal metabolism (Small, Schobel et al. 2011). This method acquires images before and after injection with a paramagnetic agent. The difference image is then normalized by a region of pure blood to develop absolute CBV maps of various brain regions, including the

hippocampus. Several studies using this method have localized CBV changes to the anterior hippocampus in chronic patients (Schobel, Lewandowski et al. 2009; Talati, Rane et al. 2014) and in the early stage of psychosis (Schobel, Lewandowski et al. 2009; Schobel, Chaudhury et al. 2013). These studies have been interpreted in the context of an underlying hippocampal excitation-inhibition imbalance in schizophrenia (Heckers and Konradi 2014).

In addition to blood volume, studies need to incorporate measures of blood flow to provide a comprehensive assessment of hemodynamic status in patients. A popular non-invasive method called arterial spin labeling (ASL) measures tissue perfusion through cerebral blood flow (CBF). Briefly, the ASL method uses blood as an endogenous tracer to track magnetically labeled blood water as it reaches a tissue of interest, such as the hippocampus. In order to distinguish between static tissue and labeled blood water, a second image is acquired that does not label the blood water. The difference between the two images (control-label) is related to tissue perfusion. Several publications have used ASL to study the hippocampus in schizophrenia (Horn, Federspiel et al. 2009; Scheef, Manka et al. 2010; Pinkham, Loughead et al. 2011; Walther, Federspiel et al. 2011; Kindler, Jann et al. 2013; Ota, Ishikawa et al. 2014). One study has shown increased hippocampal CBF in unmediated patients (Scheef, Manka et al. 2010), and another has reported reduced hippocampal CBF in medicated patients (Walther, Federspiel et al. 2011), with the remaining studies reporting no group hippocampal CBF differences. To date, this method has not been used to study patients in early psychosis.

These two functional methods, together with structural imaging, can allow for interrogation of hemodynamic changes in the anterior and posterior hippocampus in the early stage of psychosis. This is important given a recent finding that the two hemodynamic

parameters may not be coupled in the disease process (Talati, Rane et al. 2015). Therefore, in this study, we used ASL, contrast-enhanced CBV, and structural imaging to study hippocampal structure and function in the early stage of psychosis. Based on previous work from our lab, we hypothesized no group differences in anterior hippocampal volume and CBF, but increased anterior hippocampal CBV.

Methods

Participants

28 patients in the early stage of psychosis (age range: 18-29 years) and 26 matched healthy controls (age range: 18-27 years) provided informed consent in a manner approved by the Vanderbilt Institutional Board. Our criterion for the early stage of psychosis was confined to the first two years of psychotic illness from our best estimated date of onset. Patients were matched with controls across several demographics, including age, race, and gender (Table 7). Subjects were recruited from the Vanderbilt Psychotic Disorders Program or the local community and were paid for their participation. We used the Structural Clinical Interview for DSM-IV Axis I disorders (SCID, (First 2002)) to establish all diagnoses and the Positive and Negative Syndrome Scale (PANSS) (Kay, Fiszbein et al. 1987) to assess patient clinical status. 26 of 28 patients were treated with antipsychotic medication, with chlorpromazine (CPZ) equivalent dosages (Gardner, Murphy et al. 2010) listed in Table 7. Three subjects were taking medications (lithium, valproate) with no CPZ equivalent. Subjects were excluded for any history of major neurological or medical illness or for a WTAR score < 70.

Table 7 Healthy control and early psychosis subject demographics

	Controls (n = 26)	First Episode Psychosis (n = 28)	Statistic	p-value
Age (yrs)	22.31±2.41	21.82±3.28	t(52) = 0.62	0.54
Males	23/3	23/5	χ (1) = 0.43	0.51
Race (W/B/O)	22/3/1	21/6/1	χ (2) = 0.95	0.62
Subject edu. (yrs)	14.90±1.89	13.48±1.94	t(52) = 2.73	0.009
Parental edu. (yrs)	14.54±1.82	15.03±2.48	t(52) = 0.82	0.42
WTAR	111.81±11.47	102.43±13.72	t(52) = 2.72	0.009
Duration of Illness (mo)		7.99±6.63		
CPZ equivalent (mg/day)[a]		344.93±213.18		
PANSS		Pos: 13.50±6.26		
		Neg: 17.11±8.83		
		Gen: 28.82±7.57		

Healthy control and first episode psychosis subject demographics. Groups are matched on age, gender, race, and parental education, with values reported as mean ± st dev. Patients had a lower WTAR and subject education compared to healthy controls.

[a]Calculated for 23 patients. Two patients were not on medications at the time of the study, and CPZ equivalents were not available for three patients.

Structural and Functional Imaging

Structural Imaging: Acquisition

A Phillips 3T MRI Achieva scanner (Best, The Netherlands) with a 32 channel SENSE head coil reception was used for imaging. The high-resolution T1-weighted fast field echo (FFE) structural scan was acquired as part of a larger imaging protocol. This comprised of 170 sagittal slices with the following scan parameters: spatial resolution = 1.0 mm^3 isotropic, TR/TE = 8.0/3.7 ms.

Hippocampal Morphometry Analysis

Hippocampal manual segmentation was completed by one rater (PT) using the modified Pruessner segmentation protocol (described in (Pruessner, Li et al. 2000)) using the program 3DSlicer (version 3.4). The program can view and trace a brain structure in three different

orientations (coronal, sagittal, and axial) and automatically calculate the volumes of manually segmented structures. A standardized hippocampal segmentation method was used across all subjects, as published in (Woolard and Heckers 2012). Briefly, the sagittal orientation was used to segment the right, then left, hippocampus in a lateral to medial fashion. The sagittal outlines were refined in the coronal plane in a posterior to anterior fashion. The anterior hippocampus contained more than one cut through the uncus in the coronal view (Duvernoy and Bourgouin 1998; Woolard and Heckers 2012). This method generated four hippocampal regions of interest (ROIs): right anterior (RA), right posterior (RP), left anterior (LA), and left posterior (LP). The intra- and inter-rater reliability of the volumes was > 0.90 for each hippocampal ROI.

Arterial Spin Labeling (ASL): Acquisition

The pseudocontinuous ASL (pCASL) sequence was not preceded by a functional task and was acquired in the same scanning session as the structural image with the following parameters: spatial resolution = 3 x 3 x 7 mm^3, 0.5 mm slice gap, TE = 13 ms, TR = 4000 ms, SENSE factor = 2, flip angle = 90^o, labeling duration = 1650 ms train of 0.5 ms Hanning pulses, and post-labeling delay = 1600 ms. The echo-planar imaging sequence acquired 30 paired (label, unlabeled) dynamics covering 17 axial slices and utilized two background suppression pulses at 1710 and 2860 ms to suppress static tissue signal over a wide range of T1s. An additional M0 ASL scan was acquired for baseline magnetization and for coregistration to the structural image. This scan had identical geometry and parameters as the pCASL scan except the TR = 20 s and the spin labeling pulse train was turned off.

ASL Preprocessing and CBF Analysis

Control and label maps were motion-corrected to the first control image using SPM8 (http://www.fil.ion.ucl.ac.uk/spm). Difference images (control-label) were then averaged across dynamics and fit to Buxton's kinetic model (Buxton, Frank et al. 1998), with appropriate parameters recommended by the ISMRM perfusion study group (Alsop, Detre et al. 2014) to generate CBF maps. These maps were corrected for slice labeling delay (calculated at 23 ms) and partial-volume effects using segmented gray matter, white matter, and CSF tissue classes generated from the voxel-based morphometry (VBM) 8.0 toolbox for SPM8 (http://dbm.neuro.uni-jena.de/vbm). It was assumed that the gray matter to white matter CBF ratio was 2.5 (Buxton, Frank et al. 1998). Hippocampal ROIs were resampled into the CBF map space to extract blood flow values.

Steady State CBV (SS CBV): Acquisition

14 patients and 20 healthy controls completed a second, contrast-enhanced scan on a different day (average interscan duration (± stdev): 25.29±37.23 days). A 3D T1 FFE sequence (Lin, Celik et al. 1999) was implemented to acquire T1-weighted pre- and post-contrast images with the following parameters: TR = 20ms, TE = 3.98 ms, field-of-view = 256 x 256 mm^2, spatial resolution = 0.80 x 0.80 x 4 mm^3, slices = 30, SENSE factor = 2.5, flip angle = 25. A power injector (Medrad®, PA, USA) was used for contrast administration (Magnevist ® - Gadopentetate dimeglumine, Bayer Schering Pharma, Germany, 0.1 mmol/kg) and subsequent 40 mL saline flush through an 18G needle in the antecubital vein. After contrast administration, post-contrast images were acquired approximately 4 minutes later. Images were acquired

perpendicular to the long axis of the hippocampus. We compared the fractional increase in tissue signal after the contrast agent had thorougly perfused the microvasculature and equilibrated in the blood.

SS CBV Analysis

AFNI (Cox 1996) was used to correct for subject motion in pre- and post-contrast steady state images. Absolute CBV (units = ml blood/ml parenchyma) was calculated using the following equation:

$$CBV = \frac{S_{par,post} - S_{par,pre}}{S_{ss,post} - S_{ss,pre}} * 100 \qquad \textbf{(10)}$$

where $S_{par,post} - S_{par,pre}$ is the difference between the post- and pre-contrast signal in the parenchyma and $S_{ss,post} - S_{ss,pre}$ denotes the difference between the post- and pre-contrast signal in the superior sagittal sinus (Lin, Celik et al. 1999). To minimize contribution from large epicortical vessels, a 10% regional CBV threshold was used (i.e., voxels with CBV values greater than 10 were excluded) (Lin, Celik et al. 1999). The CBV maps were coregistered to the T1 structural data using FSL's FLIRT (Jenkinson and Smith 2001; Jenkinson, Bannister et al. 2002), and the inverse transform was used to bring the hippocampal ROIs into the CBV space.

Statistics

The primary analyses for hippocampal volume, blood flow, and blood volume was a repeated-measures ANOVA with hemisphere (right, left) and region (anterior, posterior) as the repeated-measures and diagnosis as a between-group factor. Since groups were well matched on age, gender, and race, these were not included as covariates in the analysis. T-tests and chi-

squared tests were performed where appropriate (subject demographics, post-hoc tests). Spearman correlations are reported. Log transform of the CBF and CBV data was necessary for correlation analyses based on the power relationship between the two variables (Grubb, Raichle et al. 1974). Statistical analyses were performed using The Statistical Package for Social Sciences software (SPSS version 20, Armonk, NY: IBM Corp http://www.spss.com).

Results

We first investigated hippocampal volume in the early stage of psychosis. In healthy controls, the anterior was larger than the posterior hippocampus bilaterally (t-test, $p<0.001$ each), as expected (Figure 19). In patients, the right anterior hippocampus was larger than the right posterior hippocampus (t-test, $p<0.001$), although this was not true for the left hippocampus (t-test, $p = 0.16$). Between group comparison using a repeated-measures ANOVA illustrated a significant region by diagnosis interaction ($F_{1,52} = 5.93$, $p = 0.018$). Post-hoc t-tests illustrated no group differences in the right anterior ($t(52) = 1.45$, $p = 0.15$), right posterior ($t(52) = 1.961$, $p = 0.055$), left anterior ($t(52) = 1.53$, $p = 0.13$), and left posterior ($t(52) = 1.14$, $p = 0.26$) hippocampus after correcting for multiple comparisons. This region by diagnosis interaction is likely due to the combined effect of a trend towards a smaller anterior hippocampus and larger posterior hippocampus in patients compared to healthy controls.

We then investigated whether hippocampal excitation-inhibition imbalances would result in a differential CBF pattern in patients in the early stage of psychosis. Figure 20A shows an axial series from a representative subject that contained the anterior and posterior hippocampal ROIs. Blood flow in healthy controls and patients was bilaterally higher in the

posterior compared to the anterior hippocampus (t-test, $p < 0.003$ each, Figure 20B). CBF values were within the expected range for the anterior and posterior hippocampus (Li, Sarkar et al. 2013). We found that there were no group differences in hippocampal CBF when tested with a repeated-measures ANOVA (main effect of diagnosis: $F_{1,52} = 0.48$, $p = 0.49$; diagnosis by region interaction: $F_{1,52} = 2.16$, $p = 0.15$; diagnosis by hemisphere: $F_{1,52} = 0.17$, $p = 0.68$; and diagnosis by region by hemisphere: $F_{1,52} = 0.42$, $p = 0.52$).

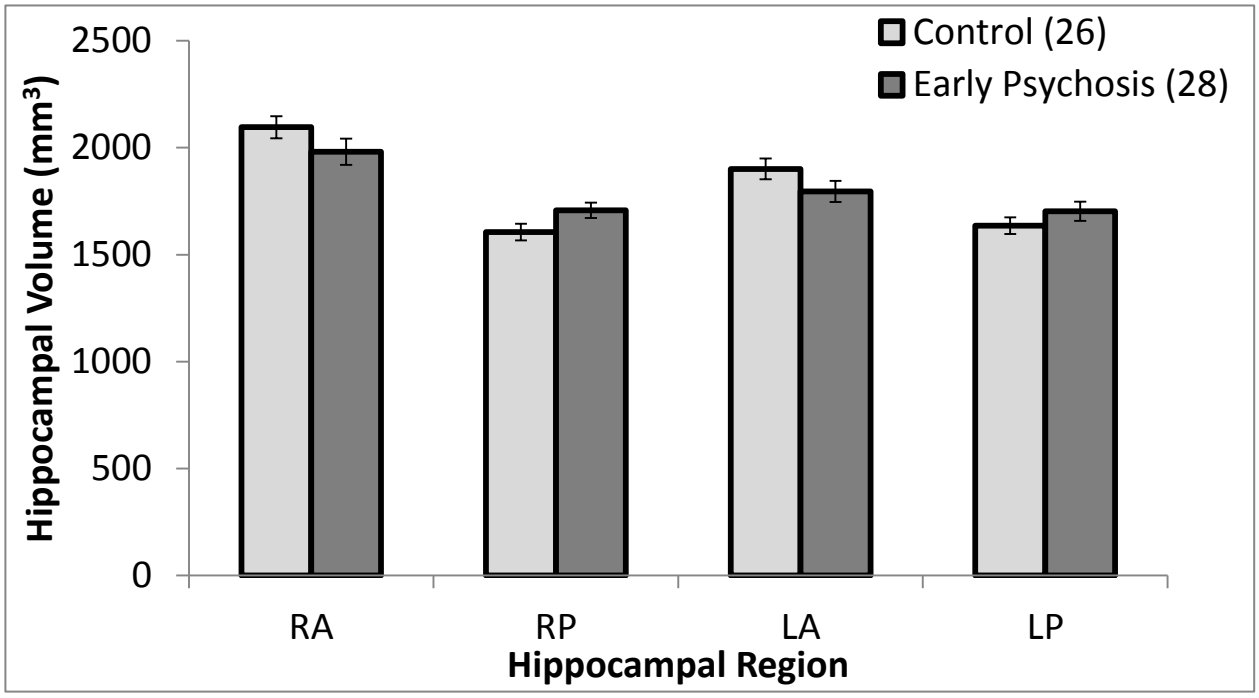

Figure 19 Hippocampal volume in early psychosis
A repeated-measures ANOVA illustrated a significant region by diagnosis interaction ($p = 0.018$). Post-hoc t-tests illustrated no regional differences after correcting for multiple comparisons. The region by diagnosis interaction is due to a trend towards a smaller anterior and larger posterior hippocampus in patients compared to controls.

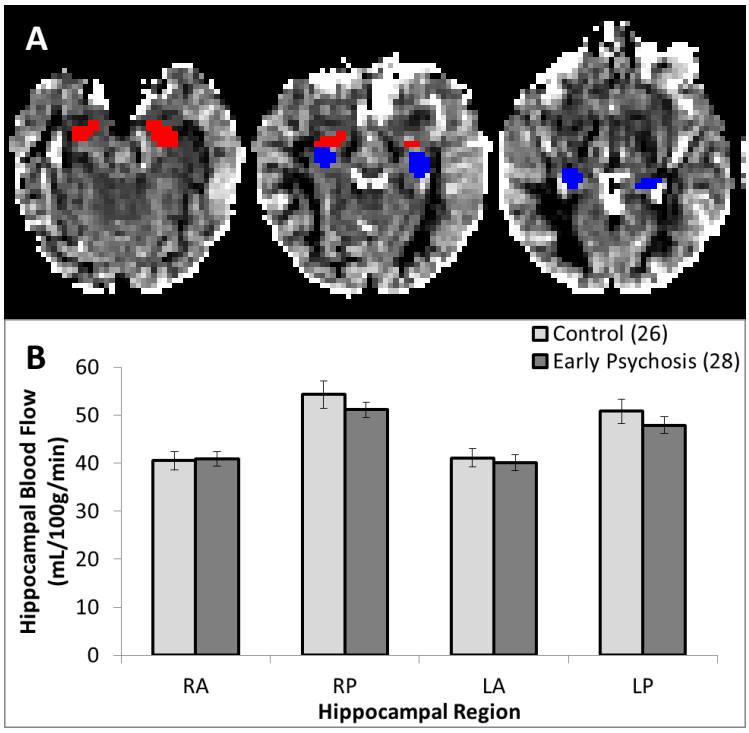

Figure 20 Hippocampal blood flow in early psychosis from pCASL
Figure 20A shows the anterior (red) and posterior (blue) hippocampal ROIs generated from manual segmentation overlaid on the CBF map. Figure 20B is the group quantification of blood flow in the anterior and posterior left and right hippocampus. A repeated-measures ANOVA found no main effect of group or interaction terms with group.

In a subgroup of individuals who underwent a contrast-enhanced imaging, we next tested whether patients in the early stage of psychosis had increased anterior hippocampal CBV. CBV values were in the expected ranges reported for the hippocampus (Talati, Rane et al. 2014). A repeated-measures ANOVA illustrated a significant main effect of diagnosis ($F_{1,32}$ = 4.71, p = 0.038). However, there was no interaction between diagnosis and hemisphere ($F_{1,32}$ = 0.42, p = 0.52), diagnosis and region ($F_{1,32}$ = 0.60, p = 0.23), and diagnosis by hemisphere by region ($F_{1,32}$ = 0.54, p = 0.47). Based on our previous work finding increased anterior hippocampal CBV in schizophrenia (Talati, Rane et al. 2014), we investigated CBV differences in this region. There was a trend towards increased right anterior hippocampal CBV (t(17.07) =

2.130, p = 0.048, Figure 21) but not left anterior hippocampal CBV (t(32) = 1.53, p = 0.14) after correcting for multiple comparisons (corrected alpha = 0.025). Hippocampal volume and blood flow in the subgroup did not differ from the larger dataset (all p>0.50).

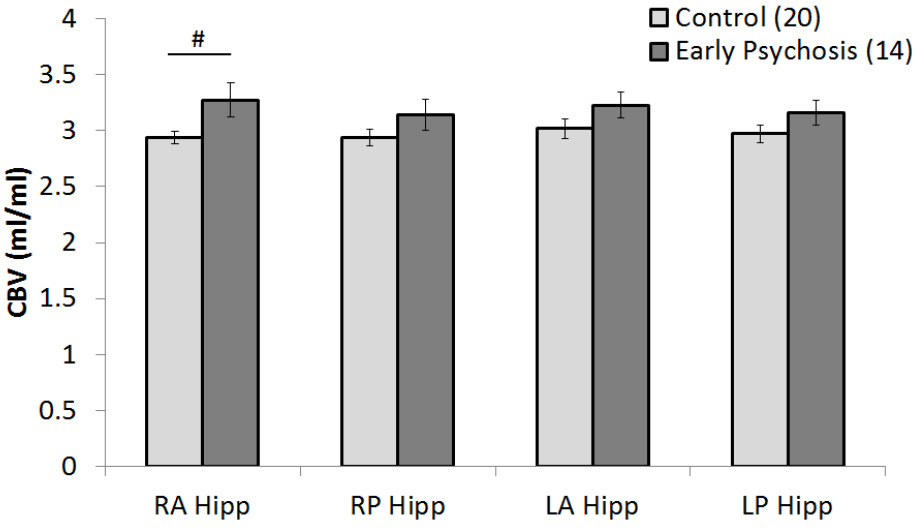

Figure 21 Hippocampal CBV from SS CBV method in early psychosis
Contrast-enhanced steady state imaging was used to obtain hippocampal CBV. A repeated-measures ANOVA illustrated a significant main effect of diagnosis, and post-hoc t-tests illustrate a trend towards increased right anterior hippocampal CBV ($^{\#}p = 0.048$) but not left anterior hippocampal CBV (p = 0.14) after correcting for multiple comparisons (corrected alpha = 0.025).

We then performed additional analyses to characterize the relationship between anterior hippocampal volume, blood flow, and blood volume. Right hippocampal blood flow did not correlate with right hippocampal volume in healthy controls (r = 0.010, p = 0.96). The same was true for the left hippocampus (r = -0.23, p = 0.27). However, in patients, we found a strong, inverse correlation between volume and blood flow in the right (r = -0.54, p = 0.003) and left (r = -0.59, p = 0.001) hippocampus after correcting for multiple comparisons (Figure 22). There

was a group difference in correlation coefficients for the right ($p = 0.034$) but not left ($p = 0.12$) anterior hippocampus. We did not find a relationship between left and right anterior hippocampal CBV and hippocampal volume ($p > 0.30$ each) and left and right anterior hippocampal CBV and CBF ($p > 0.10$ each) for both controls and patients.

Finally, we explored whether anterior hippocampal CBF or CBV related to patient psychopathology. Left and right anterior hippocampal CBF did not correlate with any measures on the PANSS (all $p > 0.30$), medication dose ($p > 0.35$), or duration of illness ($p > 0.30$). This was also true for correlations between left and right anterior hippocampal CBV and the PANSS (all $p > 0.10$), medication dose ($p > 0.15$), and duration of illness ($p > 0.75$).

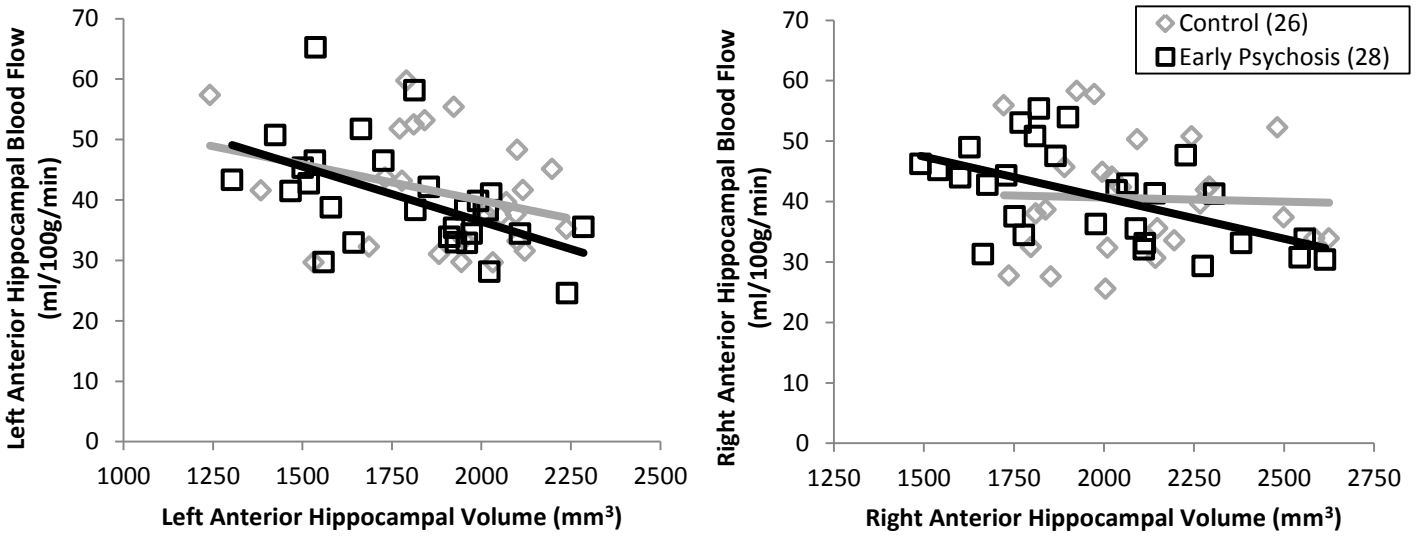

Figure 22 Correlations between anterior hippocampal volume and blood flow

Figure 22 shows scatterplots between hippocampal volume and blood flow for the left and right anterior hippocampus for patients (black squares) and controls (gray diamonds). Blood flow did not correlate with volume in controls for the right ($p = 0.96$) and left ($p = 0.27$) hippocampus. However, there was a strong, inverse correlation between volume and blood flow in the bilateral anterior hippocampus ($p < 0.003$ each). There was a group difference in correlation coefficients for the right ($p = 0.034$) but not left ($p = 0.12$) anterior hippocampus.

Discussion

To our knowledge, this is the first study to use multi-modal imaging to study the hippocampal formation in the early stage of psychosis. While we do not find group differences in hippocampal volume and blood flow, we report a trend toward increased right anterior hippocampal CBV and a strong inverse correlation between anterior hippocampal volume and blood flow in early psychosis.

The finding of no group differences in hippocampal volume is consistent with a study by Velakoulis et al., which found a smaller left hippocampus in patients with first-episode schizophrenia but no volume changes in first-episode schizophreniform disorder (Velakoulis, Wood et al. 2006). The patient groups only differed in duration of illness, which suggested that a longer duration of illness could account for hippocampal volume changes. This idea is supported by a recent meta-analysis that noted a positive relationship between the magnitude of group hippocampal volume differences and duration of illness (Olabi, Ellison-Wright et al. 2011). Since our patient cohort has an average of eight months of duration of illness from our best estimated onset, we could be capturing these patients quite early on before hippocampal volume changes have occurred. Longitudinal studies are currently underway in this patient cohort to test this hypothesis.

In order to test the hypothesis of hippocampal excitation-inhibition imbalance in schizophrenia, we collected blood flow and blood volume data. In contrast to another published study on early psychosis that found increased CBV in the anterior hippocampus (Schobel, Chaudhury et al. 2013), we only found this to be a trend in the anterior hippocampus. A *post-hoc* power analysis based on the between-group effect size observed in this finding (d =

0.80), approximately 52 total subjects are needed to have 80% power at alpha = 0.05 to detect group differences. Interestingly, we do not find increased CBF in this same region in patients. While preliminary studies suggest that medications do not affect CBV (Schobel, Lewandowski et al. 2009; Schobel, Chaudhury et al. 2013; Talati, Rane et al. 2014), they may differentially affect CBF (Medoff, Holcomb et al. 2001; Lahti, Holcomb et al. 2003; Lahti, Weiler et al. 2006), which could explain such uncoupling (Talati, Rane et al. 2015). Neither of these parameters correlated with duration of illness or measures of psychopathology. While there has been a great need to tie together brain structure or function with clinical outcomes, we were not able to do so with this dataset.

The most robust finding from this data was the negative, inverse relationship between anterior hippocampal volume and blood flow in patients. This regional phenomenon was not seen in the anterior hippocampus in controls or posterior hippocampus in patients (data not shown). This suggests a localized, pathological finding that needs further discussion. If blood flow is coupled to metabolism in this patient population, it would be expected that CBF serves as a secondary readout of underlying glutamate dysregulation. While this dataset did not include spectroscopy data to measure glutamate levels, a recent finding in unmedicated first episode patients revealed a similar inverse correlation between glutamate levels and hippocampal volume (Kraguljac, White et al. 2013), which would support this hypothesis. In our dataset, we did not find a correlation between patient CBV, which serves as a marker of basal metabolism based on PET studies (Small, Schobel et al. 2011), and CBF. This suggests a potential decoupling between metabolism and blood flow. In this context, CBF may be less specific to hippocampal gray matter, similar to what has been reported in Alzheimer's disease (Alsop,

Casement et al. 2008). That is, factors outside of the hippocampus, such as nitric oxide signaling, could influence hippocampal blood flow by modulating glutamatergic N-methyl-D-aspartate (NMDA) receptors (Brenman and Bredt 1997; Hu and Zhu 2014). This is a plausible hypothesis in light of studies illustrating disruptions in nitric oxide signaling in schizophrenia (Kristofikova, Kozmikova et al. 2008; Nasyrova, Ivashchenko et al. 2015). Finally, another potential alternative could be that this correlation is driven predominantly by treatment response. Patients who do not respond well to antipsychotic treatment may have higher hippocampal CBF than those who respond well to pharmacotherapy. This has been shown in O^{15}-PET studies investigating changes in regional hippocampal CBF (Lahti, Weiler et al. 2009), and this medication effect may also explain why our CBF values do not correlate well with CBV values. It can be inferred that those patients with a poorer treatment response have a much smaller hippocampus due to a longer duration of (poorly treated) illness. This can be easily investigated in a follow up visit with these patients.

This study has a couple of limitations. First, this data was collected over two scanning sessions. The average inter-scan range was less than a month, and ASL reproducibility studies have been shown to be reliable over this time period (Jiang, Kim et al. 2010), although there are still some concerns about the long term reproducibility (Parkes, Rashid et al. 2004; Petersen, Mouridsen et al. 2010). Recent studies suggest that ASL reproducibility may be dependent on the post-labeling delay, so incorporating multiple post-labeling delays (instead of a single one as in this study) may be a suitable alternative to reliably assess hippocampal CBF (Wu, Lou et al. 2014). Second, baseline CBV is a proxy for brain metabolism and can be used to measure slower changes associated with aging and disease (Small, Schobel et al. 2011). As such, correlations

between these two methods should be robust. However, this data must be interpreted with caution, as we were unable to confirm the established relationship between CBV and CBF (Grubb, Raichle et al. 1974) in healthy controls, even after the analyses were rerun on unthresholded CBV data (not shown).

In conclusion, we do not find changes in hippocampal volume or blood flow in early psychosis patients. We report a trend towards increased hippocampal CBV, and a strong negative correlation between the anterior hippocampal blood flow and volume exclusively in patients. The relationship between these hippocampal hemodynamic imaging methods needs to be better understood before making strong inferences about the hippocampus in the early stage of psychosis.

CHAPTER VI

HIPPOCAMPAL ARTERIAL CEREBRAL BLOOD VOLUME IN EARLY PSYCHOSIS

Introduction

Recent evidence implicates hippocampal excitation-inhibition imbalances in schizophrenia (Heckers and Konradi 2014). While neurovascular coupling has allowed for the examination of hippocampal cerebral blood flow (CBF) and blood volume (CBV) as proxies for neural activity, CBF may not be a good surrogate in medicated patients because antipsychotic medications can 'normalize' blood flow in the hippocampus (Medoff, Holcomb et al. 2001; Lahti, Weiler et al. 2006; Lahti, Weiler et al. 2009). Some initial studies suggest that CBV is not affected by antipsychotic medications (Schobel, Lewandowski et al. 2009; Talati, Rane et al. 2014), which may explain uncoupling between these two hemodynamic parameters in schizophrenia (Talati, Rane et al. 2015).

Anterior hippocampal CBV is consistently increased in schizophrenia. Contrast-enhanced steady state CBV mapping has illustrated increased anterior hippocampal CBV in chronic patients (Schobel, Lewandowski et al. 2009; Talati, Rane et al. 2014) and early psychosis (Schobel, Chaudhury et al. 2013). A preliminary study suggests that increased CBV *precedes* volumetric changes in the anterior hippocampus in early psychosis (Schobel, Chaudhury et al. 2013), which may allow it to serve as a biomarker for schizophrenia. For this to occur, a method must be noninvasive yet sensitive enough to generate CBV maps that can distinguish between groups.

Arterial CBV (aCBV) comprises approximately 20-30% of total CBV (Ito, Kanno et al. 2001; Kim, Hendrich et al. 2007) and is under direct regulation of precapillary sphincters that adjust blood flow into capillary beds. It has been shown that this vascular compartment experiences the most changes after neural stimulation (Hillman, Devor et al. 2007; Kim, Hendrich et al. 2007; Chen, Bouchard et al. 2011), with the venous compartment experiencing slower, less specific changes after neural activity. Arterial CBV is therefore more sensitive to neural activity than total CBV.

Current imaging methods that measure aCBV may have great utility in biomarker development. One method is inflow-based vascular-space-occupancy with dynamic subtraction (iVASO-DS). It was reproducible over time (Rane 2015) in a group of young, healthy individuals, making it a good candidate for longitudinal studies. This single-slice method acquires a series of paired (control, label) dynamics in a brain region of interest, such as the hippocampus. The control image contains signal from blood and tissue while the label image is acquired precisely when the inflowing arterial blood water magnetization is zero (hence also called the nulled image) and contains only tissue signal. The difference between the images (control – null) contains signal from arterial blood. We have shown recently that the hippocampal aCBV values have higher reproducibility at shorter inversion times (ie, TI < 1000 ms) and is optimized for the hippocampus at TI = 725 ms (Rane 2015).

In this study, we used iVASO-DS to study hippocampal aCBV in 17 patients with early psychosis and 25 group-matched controls with TI = 725 ms. Based on the existing literature of increased hippocampal CBV (Schobel, Lewandowski et al. 2009; Small, Schobel et al. 2011;

Schobel, Chaudhury et al. 2013; Talati, Rane et al. 2014; Talati, Rane et al. 2015), we hypothesized increased anterior hippocampal aCBV in the early stage of psychosis.

Methods

Participants

17 patients in the early stage of psychosis (age range: 18-29 years) and 25 matched healthy controls (age range: 19-27 years) provided informed consent in a manner approved by the Vanderbilt Institutional Board. Our criterion for the early stage of psychosis was confined to the first two years of psychotic illness from our best estimated date of onset, with the average duration of illness of 7.6 months. Both groups were matched across several demographics, including age, race, and gender (Table 8). Subjects were recruited from the Vanderbilt Psychotic Disorders Program or the local community and were paid for their participation. We used the Structural Clinical Interview for DSM-IV Axis I disorders (SCID, (First 2002)) to establish all diagnoses and the Positive and Negative Syndrome Scale (PANSS) (Kay, Fiszbein et al. 1987) to assess patient clinical status. 13 of the 17 patients were treated with antipsychotic medication, with chlorpromazine equivalent dosages (Gardner, Murphy et al. 2010) listed in Table 8. Subjects were excluded for any history of major neurological or medical illness or a WTAR < 70.

Structural and Functional Imaging

iVASO acquisition

A Phillips 3T MRI Achieva scanner (Best, The Netherlands) with a 32 channel SENSE head coil reception was used for imaging. The high-resolution T1-weighted fast field echo (FFE)

Table 8 iVASO subject demographics

	Controls (n = 25)	First Episode Psychosis (n = 17)	Statistic	p-value
Age (yrs)	22.7±2.4	21.9±3.4	t(40) = 0.823	0.42
Males	22/3	13/4	X(1) = 0.97	0.33
Race (W/B)	21/3/1	11/5/1	X(2) = 2.18	0.34
Subject edu. (yrs)	15.0±1.83	13.4±2.1	t(40) = 2.70	0.01
Avg. parental edu. (yrs)	14.5±1.8	15.1±2.0	t(40) = 1.06	0.30
WTAR	112.6±11.0	105.7±12.6	t(40) = 1.88	0.07
Duration of Illness (mo)		7.6±6.1		
CPZ equivalent (mg/day)[a]		339.7±235.3		
PANSS		Pos: 13.6±6.7		
		Neg: 15.5±8.7		
		Gen: 28.1±6.7		

Healthy control and early psychosis subject demographics. Groups are matched on age, gender, race. Values are reported as mean ± st dev.
[a]13 out of 17 patients had CPZ equivalents

structural scan was acquired as part of a larger imaging protocol and comprised of 170 sagittal slices with the following scan parameters: spatial resolution = 1.0 mm^3 isotropic, TR/TE = 8.0/3.7 ms. For the single slice structural image, the data were resliced in an oblique angle along the long axis of both hippocampus (resolution = 1x1x4 mm^3). The iVASO sequence was a single-shot gradient-echo, echo-planar imaging acquisition with the following parameters: spatial resolution = 2.5 × 2.5 × 4 mm^3, TE = 15 ms, TR = 500, 1000, 1492, 2000, 5000 ms corresponding to TI = 429, 725, 914, 1034, 1191 ms, respectively. Alternating control and null images (30 each) were acquired for a total of 60 dynamics. Slice placement was determined from the angulations of the oblique anatomical slice. No parallel acceleration was used. Five averages of an equilibrium magnetization (TR = 6000 ms) image with the same slice geometry and acquisition scheme but in the absence of iVASO preparation pulses were also acquired. For the null image, the inversion volume, along the slice-select direction for non-selective inversion, extended above the imaging slice, similar to Seq IIa, in (Hua, Qin et al. 2011; Rane 2015). For

the control image acquisition, two slice-selective inversion pulses were used, as proposed by Donahue et al. (Donahue, Sideso et al. 2010). The shim volume was extended well-below the imaging slice to improve homogenous labeling of incoming blood water magnetization through the carotid and basilar arteries.

iVASO pre-processing and analysis

iVASO images at each TR/TI were motion corrected using FSL's MCFLIRT (Jenkinson, Bannister et al. 2002). aCBV was calculated using the following equation (Donahue, Sideso et al. 2010):

$$aCBV \approx \frac{\Delta S}{AC_b\left(\frac{TI}{\tau}\right)M_b^0 E1E2} \quad \textbf{(11)}$$

where ΔS is the difference signal between the control and the null image, A is a constant dependent on the scanner gain, C_b is the blood water density (0.87ml/ml) (Herscovitch and Raichle 1985), TI is the inversion time, τ is the arterial arrival time (time for inverted blood water to reach the capillary exchange site), $M^0{}_b$ is the steady state magnetization of blood water, $E1 = 1 - e^{(-TR/T1b)}$, and $E2 = e^{(-TE/R2^*b)}$ where $R2^*{}_b$ is the R2* of blood water. Note that E1 accounts for the effect of excitation pulse which was erroneously omitted in (Donahue, Sideso et al. 2010). $T1_b$ = $T1$ of blood water 1.627s, τ = 500 ms for the hippocampus, R2* of arterial blood water = $16s^{-1}$ and of venous blood water = $21s^{-1}$. The product $AM^0{}_b$ was calculated from the first control image for each TR/TI combination using a sagittal sinus region of interest (ROI) and a correction for differences between arterial and venous $R2^*$ as outlined by Petersen et al. (Petersen, Lim et al. 2006). Signal in the sagittal sinus was calculated from the control image as follows:

$$S_c = S_{venous\ blood} \quad \textbf{(12)}$$

$$S_c = AM_b^0 C_b E1E2 \quad \textbf{(13)}$$

$$AM_b^0 = \frac{S_c}{C_b E1E2} \quad \textbf{(14)}$$

For each subject, the bilateral two regions (anterior, posterior) were manually segmented on a high spatial resolution anatomical image to generate four ROIs. The anatomical image was then skull-stripped and co-registered (downsampled) to the iVASO images. The transformation matrix was then applied to the four ROIs to bring them into the iVASO space. Mean aCBV values were recorded for each region at each TI. Macrovascular aCBV contributions from the middle hippocampal artery (Duvernoy 2013) were minimized by excluding voxels with aCBV > 5 ml/100g.

Analysis

The primary analysis was conducted at TI = 725 based on our previously published work that optimized this parameter for the hippocampus in healthy controls. Furthermore, this time point is also likely valid for schizophrenia because of no differences in hippocampal blood flow or mean transit time (Talati, Rane et al. 2015). To account for individual differences in arterial arrival time in the hippocampus, a secondary analysis was performed that determined the best inversion time for each subject based on the maximum difference signal between the control and null images. Using this criteria, 14 out of 25 controls and 10 out of 17 patients had the maximum difference signal at TI = 725 ms. Mean aCBV values for that inversion time were then used for group analyses. Matlab (version 7.13.0.564, The MathWorks Inc, Natick, Massachusetts) was used to generate an in-house script to obtain aCBV values.

Statistics

The primary analysis was a repeated-measures ANOVA to investigate between group aCBV differences, with region (anterior, posterior) and hemisphere as the repeated measures. Two-sided t-tests and chi-square tests were performed on clinical information where appropriate. Because groups were well matched, age, gender, and race were not included as covariates in the analysis. Statistical analyses were performed using The Statistical Package for Social Sciences software (SPSS version 20, Armonk, NY: IBM Corp http://www.spss.com).

Results

The top panel of Figure 23 illustrates the single slice structural (Figure 23A), sample iVASO image (Figure 23B), and arterial CBV map (Figure 23C) containing the long axis of the right and left hippocampus. The right anterior and posterior hippocampal overlays on the

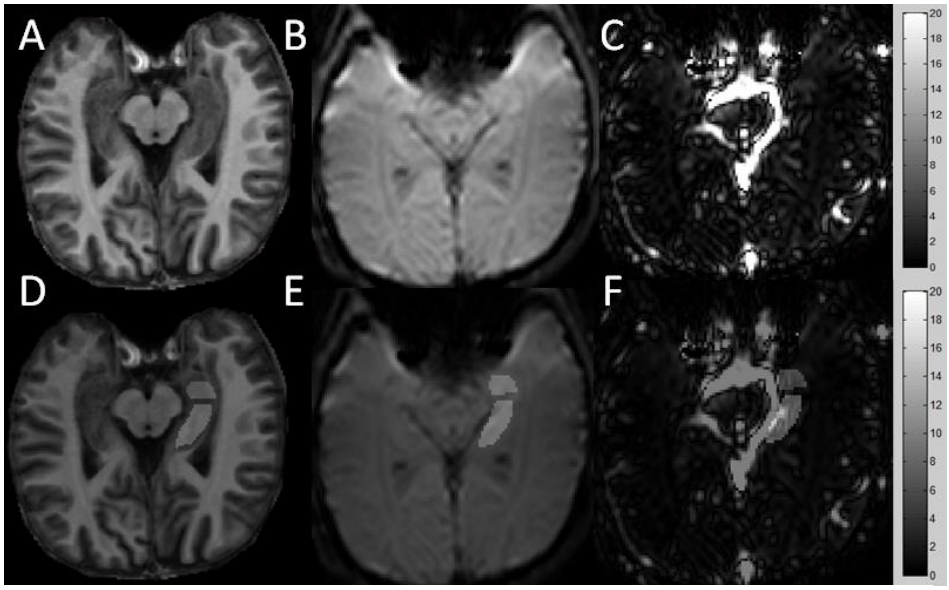

Figure 23 iVASO slice planning
Figure 23A illustrates a T1-weighted structural image. Figure 23B shows a control iVASO image (TI = 725 ms) after coregistration, and Figure 23C is an arterial CBV map thresholded between 0 and 20. Right anterior and posterior hippocampal ROIs are overlaid on the structural (Figure 23D), control iVASO (Figure 23E) and aCBV map (Figure 23F). Note that the macrovasculature is white with aCBV values > 20.

structural (Figure 23D), iVASO (Figure 23E) and aCBV map (Figure 23F) are shown in the bottom panel.

In order to test the hypothesis of increased arterial CBV in early psychosis, aCBV values were quantified at TI = 725 ms for the right anterior (RA), right posterior (RP), left anterior (LA), and left posterior (LP) hippocampus. Healthy controls had aCBV values (mean ± st error) of 2.02 ± 0.098 ml/100g in the anterior and 2.30 ± 0.060 ml/100g in the posterior hippocampus. These values are comparable with reported values in the literature for hippocampal arterial CBV with some inclusion of capillary CBV (due to uncertainties in arterial arrival time) (Hua, Qin et al. 2011; Rane 2015). Healthy controls had significantly higher aCBV in the RP compared to RA hippocampus (2.24 ± 0.10 ml/100g vs 1.90 ± 0.13 ml/100g, t-test, $p = 0.039$). However, this was not seen in patients with early psychosis (t-test, $p > 0.10$, Figure 24). Furthermore, there were no regional aCBV differences in the left hippocampus in both groups (t-test, $p > 0.10$). A repeated measures ANOVA illustrated no main effect of hemisphere ($F_{1,33} = 0.816$, $p = 0.373$), region ($F_{1,33} = 2.140$, $p = 0.153$) or significant interactions with diagnosis (all $p > 0.10$).

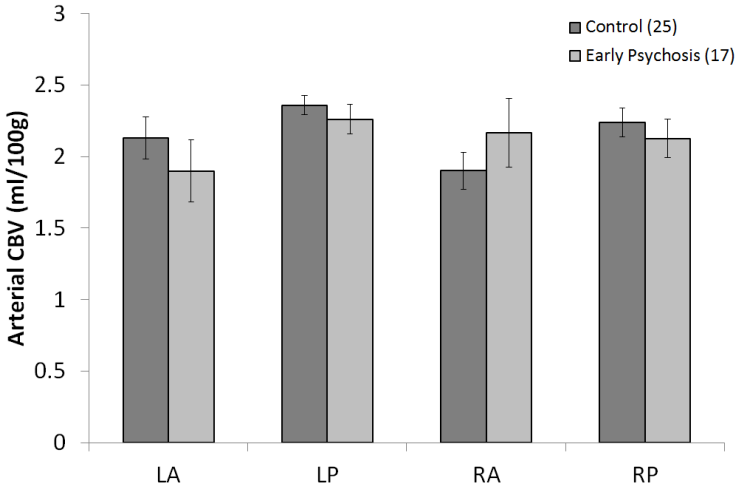

Figure 24 aCBV values in hippocampal ROIs at TI = 725 ms
Figure 24 illustrates aCBV values in patients and healthy controls at TI = 725 ms for the left and right anterior and posterior regions (LA, LP, RA, RP). Error bars denote standard error of the mean.

To account for individual physiological differences in arterial arrival time, we also generated aCBV values by using the best inversion time for each subject. The results from this analysis also illustrate no group differences for each of the ROIs investigated (Figure 25).

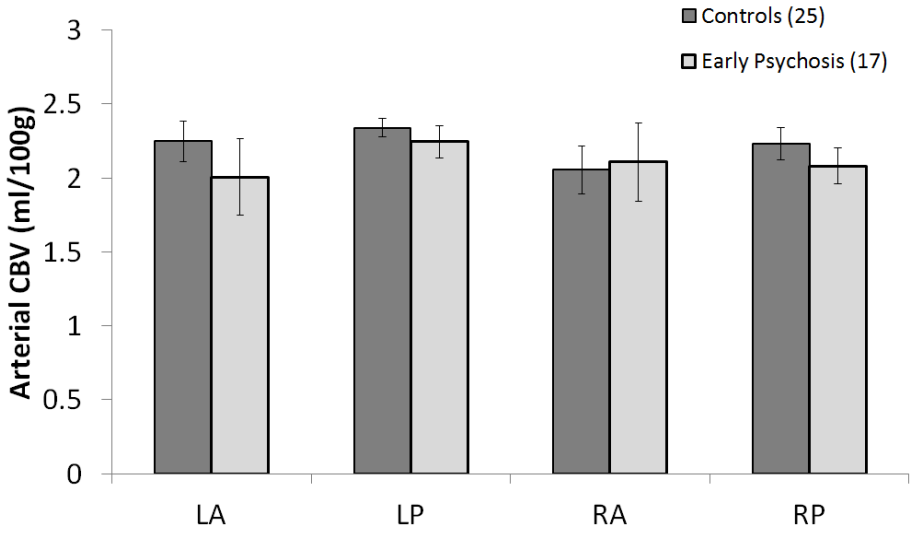

Figure 25: aCBV values in hippocampal ROIs based on the best inversion time for each subject
Figure 25 illustrates aCBV values in patients and healthy controls for the left and right anterior and posterior regions (LA, LP, RA, RP). Error bars denote standard error of the mean.

Discussion

To our knowledge, this is the first study to use inflow-based-vascular-space-occupancy with dynamic subtraction (iVASO-DS) to study the hippocampal formation in the early stage of psychosis. We failed to reject the null hypothesis of no group differences in arterial CBV in the hippocampus in the early stage of psychosis.

There is a great need for non-invasive brain biomarkers to diagnosis neuropsychiatric conditions (Tregellas 2014). While total hippocampal CBV is increased in individuals who convert to psychosis, this method will be difficult to implement in biomarker imaging due to its invasive nature (intravenous access and contrast administration). Our current study failed to

find group differences in aCBV, even though this vascular compartment experiences robust changes in response to neural stimulation (Hillman, Devor et al. 2007; Kim, Hendrich et al. 2007; Chen, Bouchard et al. 2011). We need to explain our current findings of normal aCBV in the context of previous findings of increased total CBV in prodromal, early psychosis, and chronic schizophrenia patients. These results can be interpreted in a new working model: acute excitation-inhibition imbalances can lead to marked aCBV changes, while chronic imbalances could restore aCBV and increase venous CBV. Currently, a few sequences exist to test this hypothesis directly, including a hyperoxic gas challenge (Blockley, Griffeth et al. 2013), venous refocusing for volume estimation (VERVE (Stefanovic and Pike 2005)), and subtraction of contrast-enhanced total CBV from aCBV (Kim and Kim 2011). Unfortunately, we were not able to collect such data in the current cohort.

There are some limitations to this method. First, we assumed that the consecutive inversion pulses in both the control and null images were identical, in line with previous studies (Hua, Qin et al. 2011; Hua, Qin et al. 2011). Our previous work has shown that this assumption does not significantly alter aCBV values and hence will not affect the outcome of this work (Donahue, Sideso et al. 2010; Rane 2015). Second, advanced models can be used for multi-TI iVASO data, which will likely improve the result. However, insufficient data points in our work prevent us from applying this method here. Third, the 4 mm thick imaging slice included the hippocampal formation and could partial volume with white matter, which would confound our aCBV results. Finally, based on the spatial resolution of this data, subfield-specific testing (Small, Schobel et al. 2011) was not feasible in this dataset.

In conclusion, we could not identify clear distinctions in hippocampal aCBV in the early stage of psychosis. Further studies are needed to better understand the vascular compartment that underlies total CBV differences in the hippocampus in schizophrenia.

CHAPTER VII

CONCLUSIONS AND FUTURE DIRECTIONS

Introduction

Progress in imaging science is being made on several fronts. First, advances in hardware now allow for reduced scanning time with multi-band and multi-slice imaging (Feinberg and Setsompop 2013). This is the most exciting advancement because it will allow researchers to reduce scanning time by a factor of two to four with minimal loss in SNR. This can facilitate multi-modal imaging to provide comprehensive characterization of the same patient in a single scanning session. Second, higher magnetic field imaging (e.g. 7T MRI) is becoming a popular method to study the brain. This is already being used to investigate hippocampal structure (Thomas, Welch et al. 2008) and function (Suthana, Donix et al. 2015) along the longitudinal and transverse axes. It is the hope that higher resolution data may be able to clarify the literature on mixed findings in neuropsychiatric diseases. Finally, researchers are constantly developing new, non-invasive sequences that hold great promise in replacing conventional, invasive methods. Arterial spin labeling (ASL) is perhaps the best example. It is now considered a clinical method and had advanced from a single post-labeling delay that measures CBF to incorporating multiple post-labeling delays for measuring CBF, aCBV, and arterial arrival time.

The work presented in this study incorporated different structural and functional techniques to examine the hippocampus in a clinical population. There are several findings that deserve further investigation. First, this study found no changes in hippocampal volume in early psychosis. This may be because the patients recruited in this study had an average duration of illness of around eight months, considerably shorter than most other studies reporting on this

patient population. Second, we found a trend towards increased anterior hippocampal CBV in early psychosis and report increased CA1 CBV in chronic patients. This suggests the emergence of abnormal hippocampal metabolism that may indeed precede volumentric changes over time. We failed to find group differences in arterial CBV, which suggests that venous CBV may be increased in schizophrenia. Finally, we did not find group CBF differences in the early psychosis and chronic schizophrenia, which suggests that antipsychotic medications may indeed affect hippocampal hemodynamics. These findings lead to important, testable hypotheses in future studies.

Broader implications

There is a great interest in applying currently available imaging methods to find disease signatures or biomarkers. While invasive methods such as SS CBV may be able to lay the groundwork for this objective, they will never be viable in this setting by design. Wide scale implementation of biomarker imaging will only emerge from non-invasive, reproducible imaging with sufficient spatial and temporal resolution to address the given need. For example, in the hippocampus, progress must be made to interrogate along the long axis of each subfield. Equally important is to recognize the limitations of imaging. Referring back to the hippocampus example, there is a proximal to distal connectivity gradient along the transverse axis of the CA1 subfield (Igarashi, Ito et al. 2014), but there may never be sufficient resolution to investigate this *in vivo*.

In addition to finding disease signatures, imaging can also be used to test mechanisms in animal models. Based on the synthesis of post-mortem, molecular, cellular and imaging data in

human subjects, hypotheses can be generated to test in animal models, especially now that methods exist to knock in/out and modify genes. For example, if hippocampal excitation-inhibition imbalances are due to interneuron dysfunction in schizophrenia, mouse models can be developed and imaged to test this hypothesis. An expected imaging phenotype would lend support to the hypothesis while unexpected phenotypes would have to be reconciled.

Finally, imaging can be used to monitor clinical outcomes. Current imaging methods are used for a variety of clinical reasons, including monitoring vascular disease and tumor progression. It may be not too far in the distant future that an imaging test can tell whether someone with a neuropsychiatric disease is responsive to a certain medication or treatment based on patterns in blood flow or volume in a certain region of the brain. This could very well be the case for pharmacotherapy response and hippocampal blood flow in schizophrenia, which would make imaging an important component in personalized medicine.

In closing, imaging methods hold a lot of promise for biomarker development, mechanism testing, and outcome monitoring. With new imaging technology, we will continue to learn more about the brain and develop sophisticated imaging tools to better understand brain structure and function.

REFERENCES

Abi-Dargham, A. (2004). "Do we still believe in the dopamine hypothesis? New data bring new evidence." The international journal of neuropsychopharmacology / official scientific journal of the Collegium Internationale Neuropsychopharmacologicum **7 Suppl 1**: S1-5.

Adriano, F., C. Caltagirone, et al. (2012). "Hippocampal volume reduction in first-episode and chronic schizophrenia: a review and meta-analysis." The Neuroscientist : a review journal bringing neurobiology, neurology and psychiatry **18**(2): 180-200.

Akbarian, S. and H. S. Huang (2006). "Molecular and cellular mechanisms of altered GAD1/GAD67 expression in schizophrenia and related disorders." Brain research reviews **52**(2): 293-304.

Aleman, A., R. Hijman, et al. (1999). "Memory impairment in schizophrenia: a meta-analysis." The American journal of psychiatry **156**(9): 1358-1366.

Alsop, D. C., M. Casement, et al. (2008). "Hippocampal hyperperfusion in Alzheimer's disease." NeuroImage **42**(4): 1267-1274.

Alsop, D. C., J. A. Detre, et al. (2014). "Recommended implementation of arterial spin-labeled perfusion MRI for clinical applications: A consensus of the ISMRM perfusion study group and the European consortium for ASL in dementia." Magnetic resonance in medicine : official journal of the Society of Magnetic Resonance in Medicine / Society of Magnetic Resonance in Medicine.

Altshuler, L. L., G. Bartzokis, et al. (2000). "An MRI study of temporal lobe structures in men with bipolar disorder or schizophrenia." Biological psychiatry **48**(2): 147-162.

Amaral, D. G. and M. P. Witter (1989). "The three-dimensional organization of the hippocampal formation: a review of anatomical data." Neuroscience **31**(3): 571-591.

Andersen, P. (2007). The hippocampus book. Oxford ; New York, Oxford University Press.

Andersen, P., T. V. Bliss, et al. (1971). "Lamellar organization of hippocampal pathways." Experimental brain research. Experimentelle Hirnforschung. Experimentation cerebrale **13**(2): 222-238.

Armstrong, K., L. E. Williams, et al. (2012). "Revised associative inference paradigm confirms relational memory impairment in schizophrenia." Neuropsychology **26**(4): 451-458.

Arthurs, O. J. and S. Boniface (2002). "How well do we understand the neural origins of the fMRI BOLD signal?" Trends in neurosciences **25**(1): 27-31.

Ashton, D., J. Van Reempts, et al. (1989). "Dorsal-ventral gradient in vulnerability of CA1 hippocampus to ischemia: a combined histological and electrophysiological study." Brain research **487**(2): 368-372.

Attwell, D., A. M. Buchan, et al. (2010). "Glial and neuronal control of brain blood flow." Nature **468**(7321): 232-243.

Ball, M. J., M. Fisman, et al. (1985). "A new definition of Alzheimer's disease: a hippocampal dementia." Lancet **1**(8419): 14-16.

Bangen, K. J., K. Restom, et al. (2009). "Differential age effects on cerebral blood flow and BOLD response to encoding: associations with cognition and stroke risk." Neurobiology of aging **30**(8): 1276-1287.

Bannerman, D. M., J. N. Rawlins, et al. (2004). "Regional dissociations within the hippocampus--memory and anxiety." Neuroscience and biobehavioral reviews **28**(3): 273-283.

Bellani, M., D. Peruzzo, et al. (2011). "Cerebellar and lobar blood flow in schizophrenia: a perfusion weighted imaging study." Psychiatry Research **193**(1): 46-52.

Ben Bashat, D., M. Artzi, et al. (2012). "Hemodynamic response imaging: a potential tool for the assessment of angiogenesis in brain tumors." PloS One **7**(11): e49416.

Benes, F. M., E. W. Kwok, et al. (1998). "A reduction of nonpyramidal cells in sector CA2 of schizophrenics and manic depressives." Biological Psychiatry **44**(2): 88-97.

Blaha, C. D., C. R. Yang, et al. (1997). "Stimulation of the ventral subiculum of the hippocampus evokes glutamate receptor-mediated changes in dopamine efflux in the rat nucleus accumbens." The European journal of neuroscience **9**(5): 902-911.

Blockley, N. P., V. E. Griffeth, et al. (2013). "An analysis of the use of hyperoxia for measuring venous cerebral blood volume: comparison of the existing method with a new analysis approach." NeuroImage **72**: 33-40.

Bolton, M. M., C. F. Heaney, et al. (2012). "Deficits in emotional learning and memory in an animal model of schizophrenia." Behavioural brain research **233**(1): 35-44.

Boxerman, J. L., L. M. Hamberg, et al. (1995). "MR contrast due to intravascular magnetic susceptibility perturbations." Magnetic Resonance in Medicine **34**(4): 555-566.

Braak, H., E. Braak, et al. (1996). "Pattern of brain destruction in Parkinson's and Alzheimer's diseases." Journal of neural transmission **103**(4): 455-490.

Brambilla, P., R. Cerini, et al. (2007). "Assessment of cerebral blood volume in schizophrenia: A magnetic resonance imaging study." Journal of Psychiatric Research **41**(6): 502-510.

Brenman, J. E. and D. S. Bredt (1997). "Synaptic signaling by nitric oxide." Current opinion in neurobiology **7**(3): 374-378.

Brickman, A. M., Y. Stern, et al. (2011). "Hippocampal subregions differentially associate with standardized memory tests." Hippocampus **21**(9): 923-928.

Buchsbaum, M. S., R. J. Haier, et al. (1992). "Frontostriatal disorder of cerebral metabolism in never-medicated schizophrenics." Archives of General Psychiatry **49**(12): 935-942.

Buxton, R. B., L. R. Frank, et al. (1998). "A general kinetic model for quantitative perfusion imaging with arterial spin labeling." Magnetic resonance in medicine : official journal of the Society of Magnetic Resonance in Medicine / Society of Magnetic Resonance in Medicine **40**(3): 383-396.

Calamante, F. (2013). "Arterial input function in perfusion MRI: a comprehensive review." Progress in nuclear magnetic resonance spectroscopy **74**: 1-32.

Calamante, F., D. G. Gadian, et al. (2002). "Quantification of perfusion using bolus tracking magnetic resonance imaging in stroke: assumptions, limitations, and potential implications for clinical use." Stroke **33**(4): 1146-1151.

Chan, K. H., J. D. Miller, et al. (1992). "The effect of changes in cerebral perfusion pressure upon middle cerebral artery blood flow velocity and jugular bulb venous oxygen saturation after severe brain injury." Journal of Neurosurgery **77**(1): 55-61.

Chen, B. R., M. B. Bouchard, et al. (2011). "High-speed vascular dynamics of the hemodynamic response." NeuroImage **54**(2): 1021-1030.

Choi, Y. J., H. S. Kim, et al. (2013). "Pseudoprogression in patients with glioblastoma: added value of arterial spin labeling to dynamic susceptibility contrast perfusion MR imaging." Acta Radiologica **54**(4): 448-454.

Cobb, S. R., E. H. Buhl, et al. (1995). "Synchronization of neuronal activity in hippocampus by individual GABAergic interneurons." Nature **378**(6552): 75-78.

Cohen, B. M., D. Yurgelun-Todd, et al. (1995). "Abnormalities of regional distribution of cerebral vasculature in schizophrenia detected by dynamic susceptibility contrast MRI." The American Journal of Psychiatry **152**(12): 1801-1803.

Cohen, J. (1988). Statistical power analysis for the behavioral sciences. Hillsdale, N.J., L. Erlbaum Associates.

Cox, R. W. (1996). "AFNI: software for analysis and visualization of functional magnetic resonance neuroimages." Computers and Biomedical Research, an international journal **29**(3): 162-173.

DeLisi, L. E., M. S. Buchsbaum, et al. (1989). "Increased temporal lobe glucose use in chronic schizophrenic patients." Biological psychiatry **25**(7): 835-851.

Demaster, D., T. Pathman, et al. (2013). "Structural Development of the Hippocampus and Episodic Memory: Developmental Differences Along the Anterior/Posterior Axis." Cerebral cortex.

Dierks, T., D. E. Linden, et al. (1999). "Activation of Heschl's gyrus during auditory hallucinations." Neuron **22**(3): 615-621.

Donahue, M. J., C. C. Faraco, et al. (2014). "Bolus arrival time and cerebral blood flow responses to hypercarbia." Journal of Cerebral Blood Flow and Metabolism **34**(7): 1243-1252.

Donahue, M. J., E. Sideso, et al. (2010). "Absolute arterial cerebral blood volume quantification using inflow vascular-space-occupancy with dynamic subtraction magnetic resonance imaging." Journal of cerebral blood flow and metabolism : official journal of the International Society of Cerebral Blood Flow and Metabolism **30**(7): 1329-1342.

Driscoll, I., D. A. Hamilton, et al. (2003). "The aging hippocampus: cognitive, biochemical and structural findings." Cerebral cortex **13**(12): 1344-1351.

Dunn, J. F., M. A. Roche, et al. (2004). "Monitoring angiogenesis in brain using steady-state quantification of DeltaR2 with MION infusion." Magnetic Resonance in Medicine **51**(1): 55-61.

Duvernoy, H. M. and P. Bourgouin (1998). The human hippocampus : functional anatomy, vascularization and serial sections with MRI. Berlin ; New York, Springer.

Duvernoy, H. M., Cattin, Françoise, Risold, Pierre-Yves. (2013). The human hippocampus : functional anatomy, vascularization and serial sections with MRI, Springer.

Eichenbaum, H. (2004). "Hippocampus: cognitive processes and neural representations that underlie declarative memory." Neuron **44**(1): 109-120.

Ertugrul, A., B. Volkan-Salanci, et al. (2009). "The effect of clozapine on regional cerebral blood flow and brain metabolite ratios in schizophrenia: relationship with treatment response." Psychiatry Research **174**(2): 121-129.

Ewing, S. G. and C. Winter (2013). "The ventral portion of the CA1 region of the hippocampus and the prefrontal cortex as candidate regions for neuromodulation in schizophrenia." Medical hypotheses **80**(6): 827-832.

Fabene, P. F., P. Farace, et al. (2007). "Three-dimensional MRI perfusion maps: a step beyond volumetric analysis in mental disorders." Journal of Anatomy **210**(1): 122-128.

Fanselow, M. S. and H. W. Dong (2010). "Are the dorsal and ventral hippocampus functionally distinct structures?" Neuron **65**(1): 7-19.

Feinberg, D. A. and K. Setsompop (2013). "Ultra-fast MRI of the human brain with simultaneous multi-slice imaging." Journal of magnetic resonance **229**: 90-100.

Fellini, L., C. Florian, et al. (2009). "Pharmacological intervention of hippocampal CA3 NMDA receptors impairs acquisition and long-term memory retrieval of spatial pattern completion task." Learning & memory **16**(6): 387-394.

First, M. B., Spitzer, Robert L, Gibbon Miriam, and Williams, Janet B.W, Ed. (2002). Structured Clinical Interview for DSM-IV-TR Axis I Disorders, Research Version, Patient Edition With Psychotic Screen (SCID-I/P W/ PSY SCREEN), New York: Biometrics Research, New York State Psychiatric Institute.

Friston, K. J., P. F. Liddle, et al. (1992). "The left medial temporal region and schizophrenia. A PET study." Brain : a journal of neurology **115 (Pt 2)**: 367-382.

Friston, K. J., P. F. Liddle, et al. (1992). "The left medial temporal region and schizophrenia. A PET study." Brain **115 (Pt 2)**: 367-382.

Galvin, J. E., K. Uryu, et al. (1999). "Axon pathology in Parkinson's disease and Lewy body dementia hippocampus contains alpha-, beta-, and gamma-synuclein." Proceedings of the National Academy of Sciences of the United States of America **96**(23): 13450-13455.

Gardner, D. M., A. L. Murphy, et al. (2010). "International consensus study of antipsychotic dosing." The American Journal of Psychiatry **167**(6): 686-693.

Gevers, S., M. J. van Osch, et al. (2011). "Intra- and multicenter reproducibility of pulsed, continuous and pseudo-continuous arterial spin labeling methods for measuring cerebral perfusion." Journal of Cerebral Blood Flow and Metabolism **31**(8): 1706-1715.

Gloor, P. (1997). The temporal lobe and limbic system. New York, Oxford University Press.

Gonzalez, R. G., A. J. Fischman, et al. (1995). "Functional MR in the evaluation of dementia: correlation of abnormal dynamic cerebral blood volume measurements with changes in cerebral metabolism on positron emission tomography with fludeoxyglucose F 18." AJNR. American journal of neuroradiology **16**(9): 1763-1770.

Grace, A. A. (2010). "Dopamine system dysregulation by the ventral subiculum as the common pathophysiological basis for schizophrenia psychosis, psychostimulant abuse, and stress." Neurotoxicity research **18**(3-4): 367-376.

Grubb, R. L., Jr., M. E. Raichle, et al. (1974). "The effects of changes in PaCO2 on cerebral blood volume, blood flow, and vascular mean transit time." Stroke **5**(5): 630-639.

Grunze, H. C., D. G. Rainnie, et al. (1996). "NMDA-dependent modulation of CA1 local circuit inhibition." The Journal of neuroscience : the official journal of the Society for Neuroscience **16**(6): 2034-2043.

Gur, R. E., P. D. Mozley, et al. (1995). "Resting cerebral glucose metabolism in first-episode and previously treated patients with schizophrenia relates to clinical features." Archives of general psychiatry **52**(8): 657-667.

Heckers, S. (2001). "Neuroimaging studies of the hippocampus in schizophrenia." Hippocampus **11**(5): 520-528.

Heckers, S. and C. Konradi (2010). "Hippocampal pathology in schizophrenia." Current Topics in Behavioral Neurosciences **4**: 529-553.

Heckers, S. and C. Konradi (2014). "GABAergic mechanisms of hippocampal hyperactivity in schizophrenia." Schizophrenia Research.

Heckers, S., S. L. Rauch, et al. (1998). "Impaired recruitment of the hippocampus during conscious recollection in schizophrenia." Nature Neuroscience **1**(4): 318-323.

Heilbrun, M. P., P. B. Jorgensen, et al. (1972). "Relationships between cerebral perfusion pressure and regional cerebral blood flow in patients with severe neurological disorders." Stroke **3**(2): 181-195.

Heinrichs, R. W. and K. K. Zakzanis (1998). "Neurocognitive deficit in schizophrenia: a quantitative review of the evidence." Neuropsychology **12**(3): 426-445.

Helgeland, M. I. and S. Torgersen (2005). "Stability and prediction of schizophrenia from adolescence to adulthood." European child & adolescent psychiatry **14**(2): 83-94.

Herman, J. P., N. K. Mueller, et al. (2004). "Role of GABA and glutamate circuitry in hypothalamo-pituitary-adrenocortical stress integration." Annals of the New York Academy of Sciences **1018**: 35-45.

Herscovitch, P. and M. E. Raichle (1985). "What is the correct value for the brain--blood partition coefficient for water?" Journal of cerebral blood flow and metabolism : official journal of the International Society of Cerebral Blood Flow and Metabolism **5**(1): 65-69.

Hillman, E. M., A. Devor, et al. (2007). "Depth-resolved optical imaging and microscopy of vascular compartment dynamics during somatosensory stimulation." NeuroImage **35**(1): 89-104.

Homan, P., J. Kindler, et al. (2012). "Cerebral blood flow identifies responders to transcranial magnetic stimulation in auditory verbal hallucinations." Translational Psychiatry **2**: e189.

Honea, R., T. J. Crow, et al. (2005). "Regional deficits in brain volume in schizophrenia: a meta-analysis of voxel-based morphometry studies." The American journal of psychiatry **162**(12): 2233-2245.

Horn, H., A. Federspiel, et al. (2009). "Structural and metabolic changes in language areas linked to formal thought disorder." The British Journal of Psychiatry **194**(2): 130-138.

Howarth, C. (2014). "The contribution of astrocytes to the regulation of cerebral blood flow." Frontiers in neuroscience **8**: 103.
Hu, Y. and D. Y. Zhu (2014). "Hippocampus and nitric oxide." Vitamins and hormones **96**: 127-160.
Hua, J., Q. Qin, et al. (2011). "Inflow-based vascular-space-occupancy (iVASO) MRI." Magnetic resonance in medicine : official journal of the Society of Magnetic Resonance in Medicine / Society of Magnetic Resonance in Medicine **66**(1): 40-56.
Hua, J., Q. Qin, et al. (2011). "Measurement of absolute arterial cerebral blood volume in human brain without using a contrast agent." NMR in biomedicine **24**(10): 1313-1325.
Huang, Y. P. and T. Okudera (1997). "Arterial supply to the hippocampal formation." Neuroimaging Clinics of North America **7**(1): 31-50.
Hyman, B. T., G. W. Van Hoesen, et al. (1984). "Alzheimer's disease: cell-specific pathology isolates the hippocampal formation." Science **225**(4667): 1168-1170.
Igarashi, K. M., H. T. Ito, et al. (2014). "Functional diversity along the transverse axis of hippocampal area CA1." FEBS letters **588**(15): 2470-2476.
Insausti, R. (1993). "Comparative anatomy of the entorhinal cortex and hippocampus in mammals." Hippocampus **3 Spec No**: 19-26.
Ito, H., I. Kanno, et al. (2001). "Arterial fraction of cerebral blood volume in humans measured by positron emission tomography." Annals of nuclear medicine **15**(2): 111-116.
Jenkinson, M., P. Bannister, et al. (2002). "Improved optimization for the robust and accurate linear registration and motion correction of brain images." NeuroImage **17**(2): 825-841.
Jenkinson, M. and S. Smith (2001). "A global optimisation method for robust affine registration of brain images." Medical image analysis **5**(2): 143-156.
Jiang, J., L. Zhao, et al. (2014). "Comparative analysis of arterial spin labeling and dynamic susceptibility contrast perfusion imaging for quantitative perfusion measurements of brain tumors." International Journal of Clinical and Experimental Pathology **7**(6): 2790-2799.
Jiang, L., M. Kim, et al. (2010). "Reliability and reproducibility of perfusion MRI in cognitively normal subjects." Magnetic resonance imaging **28**(9): 1283-1289.
Jones, R. S. and E. H. Buhl (1993). "Basket-like interneurones in layer II of the entorhinal cortex exhibit a powerful NMDA-mediated synaptic excitation." Neuroscience letters **149**(1): 35-39.
Kawasaki, Y., M. Suzuki, et al. (1992). "Regional cerebral blood flow in patients with schizophrenia. A preliminary report." European Archives of Psychiatry and Clinical Neuroscience **241**(4): 195-200.
Kay, S. R., A. Fiszbein, et al. (1987). "The positive and negative syndrome scale (PANSS) for schizophrenia." Schizophrenia Bulletin **13**(2): 261-276.
Kesner, R. P. and E. T. Rolls (2015). "A computational theory of hippocampal function, and tests of the theory: new developments." Neuroscience and biobehavioral reviews **48**: 92-147.
Kim, T., K. S. Hendrich, et al. (2007). "Arterial versus total blood volume changes during neural activity-induced cerebral blood flow change: implication for BOLD fMRI." Journal of cerebral blood flow and metabolism : official journal of the International Society of Cerebral Blood Flow and Metabolism **27**(6): 1235-1247.
Kim, T. and S. G. Kim (2011). "Temporal dynamics and spatial specificity of arterial and venous blood volume changes during visual stimulation: implication for BOLD quantification." Journal of cerebral blood flow and metabolism : official journal of the International Society of Cerebral Blood Flow and Metabolism **31**(5): 1211-1222.
Kindler, J., K. Jann, et al. (2013). "Static and Dynamic Characteristics of Cerebral Blood Flow During the Resting State in Schizophrenia." Schizophrenia Bulletin.
King, K. G., L. Glodzik, et al. (2008). "Anteroposterior hippocampal metabolic heterogeneity: three-dimensional multivoxel proton 1H MR spectroscopic imaging--initial findings." Radiology **249**(1): 242-250.

Kjelstrup, K. G., F. A. Tuvnes, et al. (2002). "Reduced fear expression after lesions of the ventral hippocampus." Proceedings of the National Academy of Sciences of the United States of America **99**(16): 10825-10830.
Knight, R. (1996). "Contribution of human hippocampal region to novelty detection." Nature **383**(6597): 256-259.
Konradi, C., C. K. Yang, et al. (2011). "Hippocampal interneurons are abnormal in schizophrenia." Schizophrenia Research **131**(1-3): 165-173.
Kraguljac, N. V., D. M. White, et al. (2013). "Increased hippocampal glutamate and volumetric deficits in unmedicated patients with schizophrenia." JAMA psychiatry **70**(12): 1294-1302.
Kristiansen, L. V., I. Huerta, et al. (2007). "NMDA receptors and schizophrenia." Current opinion in pharmacology **7**(1): 48-55.
Kristofikova, Z., I. Kozmikova, et al. (2008). "Lateralization of hippocampal nitric oxide mediator system in people with Alzheimer disease, multi-infarct dementia and schizophrenia." Neurochemistry international **53**(5): 118-125.
Kuppusamy, K., W. Lin, et al. (1996). "In vivo regional cerebral blood volume: quantitative assessment with 3D T1-weighted pre- and postcontrast MR imaging." Radiology **201**(1): 106-112.
Laakso, M. P., J. Tiihonen, et al. (2001). "A morphometric MRI study of the hippocampus in first-episode, neuroleptic-naive schizophrenia." Schizophrenia research **50**(1-2): 3-7.
Lahti, A. C., H. H. Holcomb, et al. (2003). "Functional effects of antipsychotic drugs: comparing clozapine with haloperidol." Biological Psychiatry **53**(7): 601-608.
Lahti, A. C., M. A. Weiler, et al. (2006). "Correlations between rCBF and symptoms in two independent cohorts of drug-free patients with schizophrenia." Neuropsychopharmacology : official publication of the American College of Neuropsychopharmacology **31**(1): 221-230.
Lahti, A. C., M. A. Weiler, et al. (2006). "Correlations between rCBF and symptoms in two independent cohorts of drug-free patients with schizophrenia." Neuropsychopharmacology **31**(1): 221-230.
Lahti, A. C., M. A. Weiler, et al. (2009). "Modulation of limbic circuitry predicts treatment response to antipsychotic medication: a functional imaging study in schizophrenia." Neuropsychopharmacology : official publication of the American College of Neuropsychopharmacology **34**(13): 2675-2690.
Laruelle, M., A. Abi-Dargham, et al. (1999). "Increased dopamine transmission in schizophrenia: relationship to illness phases." Biological psychiatry **46**(1): 56-72.
Ledoux, A. A., J. L. Phillips, et al. (2013). "Decreased fMRI activity in the hippocampus of patients with schizophrenia compared to healthy control participants, tested on a wayfinding task in a virtual town." Psychiatry research **211**(1): 47-56.
Legault, M. and R. A. Wise (1999). "Injections of N-methyl-D-aspartate into the ventral hippocampus increase extracellular dopamine in the ventral tegmental area and nucleus accumbens." Synapse **31**(4): 241-249.
Lesack, K. and C. Naugler (2011). "An open-source software program for performing Bonferroni and related corrections for multiple comparisons." Journal of pathology informatics **2**: 52.
Li, S., W. K. Cullen, et al. (2003). "Dopamine-dependent facilitation of LTP induction in hippocampal CA1 by exposure to spatial novelty." Nature neuroscience **6**(5): 526-531.
Li, X., S. N. Sarkar, et al. (2013). "Anteroposterior perfusion heterogeneity in human hippocampus measured by arterial spin labeling MRI." NMR in Biomedicine **26**(6): 613-621.
Liddle, P. F., K. J. Friston, et al. (1992). "Cerebral blood flow and mental processes in schizophrenia." Journal of the Royal Society of Medicine **85**(4): 224-227.
Lin, W., A. Celik, et al. (1999). "Regional cerebral blood volume: a comparison of the dynamic imaging and the steady state methods." Journal of magnetic resonance imaging : JMRI **9**(1): 44-52.

Lisman, J. E., J. T. Coyle, et al. (2008). "Circuit-based framework for understanding neurotransmitter and risk gene interactions in schizophrenia." Trends in Neurosciences **31**(5): 234-242.
Lisman, J. E. and A. A. Grace (2005). "The hippocampal-VTA loop: controlling the entry of information into long-term memory." Neuron **46**(5): 703-713.
Lisman, J. E. and N. A. Otmakhova (2001). "Storage, recall, and novelty detection of sequences by the hippocampus: elaborating on the SOCRATIC model to account for normal and aberrant effects of dopamine." Hippocampus **11**(5): 551-568.
Lisman, J. E., H. J. Pi, et al. (2010). "A thalamo-hippocampal-ventral tegmental area loop may produce the positive feedback that underlies the psychotic break in schizophrenia." Biological psychiatry **68**(1): 17-24.
Lodge, D. J. and A. A. Grace (2011). "Hippocampal dysregulation of dopamine system function and the pathophysiology of schizophrenia." Trends in pharmacological sciences **32**(9): 507-513.
Loeber, R. T., A. R. Sherwood, et al. (1999). "Differences in cerebellar blood volume in schizophrenia and bipolar disorder." Schizophrenia Research **37**(1): 81-89.
Lopez, A. D., C. D. Mathers, et al. (2006). Measuring the Global Burden of Disease and Risk Factors, 1990-2001. Global Burden of Disease and Risk Factors. A. D. Lopez, C. D. Mathers, M. Ezzati, D. T. Jamison and C. J. L. Murray. Washington (DC).
Lowry, C. A. (2002). "Functional subsets of serotonergic neurones: implications for control of the hypothalamic-pituitary-adrenal axis." Journal of neuroendocrinology **14**(11): 911-923.
Malaspina, D., J. Harkavy-Friedman, et al. (2004). "Resting neural activity distinguishes subgroups of schizophrenia patients." Biological Psychiatry **56**(12): 931-937.
Manji, H., T. Kato, et al. (2012). "Impaired mitochondrial function in psychiatric disorders." Nature reviews. Neuroscience **13**(5): 293-307.
Markram, H., M. Toledo-Rodriguez, et al. (2004). "Interneurons of the neocortical inhibitory system." Nature reviews. Neuroscience **5**(10): 793-807.
Medoff, D. R., H. H. Holcomb, et al. (2001). "Probing the human hippocampus using rCBF: contrasts in schizophrenia." Hippocampus **11**(5): 543-550.
Miller, D. D., N. C. Andreasen, et al. (1997). "Effect of antipsychotics on regional cerebral blood flow measured with positron emission tomography." Neuropsychopharmacology **17**(4): 230-240.
Moreno, H., W. E. Wu, et al. (2007). "Imaging the Abeta-related neurotoxicity of Alzheimer disease." Archives of Neurology **64**(10): 1467-1477.
Morris, R. G., P. Garrud, et al. (1982). "Place navigation impaired in rats with hippocampal lesions." Nature **297**(5868): 681-683.
Moser, E., M. B. Moser, et al. (1993). "Spatial learning impairment parallels the magnitude of dorsal hippocampal lesions, but is hardly present following ventral lesions." The Journal of neuroscience : the official journal of the Society for Neuroscience **13**(9): 3916-3925.
Moser, M. B. and E. I. Moser (1998). "Functional differentiation in the hippocampus." Hippocampus **8**(6): 608-619.
Mouritzen Dam, A. (1979). "The density of neurons in the human hippocampus." Neuropathology and applied neurobiology **5**(4): 249-264.
Mu, Q., K. Johnson, et al. (2007). "A single 20 mg dose of the full D1 dopamine agonist dihydrexidine (DAR-0100) increases prefrontal perfusion in schizophrenia." Schizophrenia Research **94**(1-3): 332-341.
Musalek, M., I. Podreka, et al. (1989). "Regional brain function in hallucinations: a study of regional cerebral blood flow with 99m-Tc-HMPAO-SPECT in patients with auditory hallucinations, tactile hallucinations, and normal controls." Comprehensive psychiatry **30**(1): 99-108.

Nael, K., A. Meshksar, et al. (2013). "Periprocedural arterial spin labeling and dynamic susceptibility contrast perfusion in detection of cerebral blood flow in patients with acute ischemic syndrome." Stroke **44**(3): 664-670.
Nakazawa, K., V. Zsiros, et al. (2012). "GABAergic interneuron origin of schizophrenia pathophysiology." Neuropharmacology **62**(3): 1574-1583.
Narr, K. L., P. M. Thompson, et al. (2004). "Regional specificity of hippocampal volume reductions in first-episode schizophrenia." NeuroImage **21**(4): 1563-1575.
Nasyrova, R. F., D. V. Ivashchenko, et al. (2015). "Role of nitric oxide and related molecules in schizophrenia pathogenesis: biochemical, genetic and clinical aspects." Frontiers in physiology **6**: 139.
Nelson, M. D., A. J. Saykin, et al. (1998). "Hippocampal volume reduction in schizophrenia as assessed by magnetic resonance imaging: a meta-analytic study." Archives of general psychiatry **55**(5): 433-440.
Nordahl, T. E., N. Kusubov, et al. (1996). "Temporal lobe metabolic differences in medication-free outpatients with schizophrenia via the PET-600." Neuropsychopharmacology **15**(6): 541-554.
Nordahl, T. E., N. Kusubov, et al. (1996). "Temporal lobe metabolic differences in medication-free outpatients with schizophrenia via the PET-600." Neuropsychopharmacology : official publication of the American College of Neuropsychopharmacology **15**(6): 541-554.
Novak, B., M. Milcinski, et al. (2005). "Early effects of treatment on regional cerebral blood flow in first episode schizophrenia patients evaluated with 99Tc-ECD-SPECT." Neuroendocrinology Letters **26**(6): 685-689.
O'Mara, S. (2005). "The subiculum: what it does, what it might do, and what neuroanatomy has yet to tell us." Journal of anatomy **207**(3): 271-282.
Olabi, B., I. Ellison-Wright, et al. (2011). "Are there progressive brain changes in schizophrenia? A meta-analysis of structural magnetic resonance imaging studies." Biological psychiatry **70**(1): 88-96.
Olney, J. W., J. W. Newcomer, et al. (1999). "NMDA receptor hypofunction model of schizophrenia." Journal of Psychiatric Research **33**(6): 523-533.
Ongur, D., T. J. Cullen, et al. (2006). "The neural basis of relational memory deficits in schizophrenia." Archives of general psychiatry **63**(4): 356-365.
Ostergaard, L. (2004). "Cerebral perfusion imaging by bolus tracking." Topics in Magnetic Resonance Imaging **15**(1): 3-9.
Ostergaard, L. (2004). "Cerebral perfusion imaging by bolus tracking." Topics in magnetic resonance imaging : TMRI **15**(1): 3-9.
Ostergaard, L., A. G. Sorensen, et al. (1996). "High resolution measurement of cerebral blood flow using intravascular tracer bolus passages. Part II: Experimental comparison and preliminary results." Magnetic Resonance in Medicine **36**(5): 726-736.
Ostergaard, L., R. M. Weisskoff, et al. (1996). "High resolution measurement of cerebral blood flow using intravascular tracer bolus passages. Part I: Mathematical approach and statistical analysis." Magnetic Resonance in Medicine **36**(5): 715-725.
Ostojic, J., D. Kozic, et al. (2010). "Three-dimensional multivoxel spectroscopy of the healthy hippocampus-are the metabolic differences related to the location?" Clinical radiology **65**(4): 302-307.
Ota, M., M. Ishikawa, et al. (2014). "Pseudo-continuous arterial spin labeling MRI study of schizophrenic patients." Schizophrenia Research **154**(1-3): 113-118.
Parkes, L. M., W. Rashid, et al. (2004). "Normal cerebral perfusion measurements using arterial spin labeling: reproducibility, stability, and age and gender effects." Magnetic Resonance in Medicine **51**(4): 736-743.

Perala, J., J. Suvisaari, et al. (2007). "Lifetime prevalence of psychotic and bipolar I disorders in a general population." Archives of general psychiatry **64**(1): 19-28.
Perkio, J., H. J. Aronen, et al. (2002). "Evaluation of four postprocessing methods for determination of cerebral blood volume and mean transit time by dynamic susceptibility contrast imaging." Magnetic Resonance in Medicine **47**(5): 973-981.
Peruzzo, D., G. Rambaldelli, et al. (2011). "The impact of schizophrenia on frontal perfusion parameters: a DSC-MRI study." Journal of Neural Transmission **118**(4): 563-570.
Petersen, E. T., T. Lim, et al. (2006). "Model-free arterial spin labeling quantification approach for perfusion MRI." Magnetic resonance in medicine : official journal of the Society of Magnetic Resonance in Medicine / Society of Magnetic Resonance in Medicine **55**(2): 219-232.
Petersen, E. T., K. Mouridsen, et al. (2010). "The QUASAR reproducibility study, Part II: Results from a multi-center Arterial Spin Labeling test-retest study." NeuroImage **49**(1): 104-113.
Pinkham, A., J. Loughead, et al. (2011). "Resting quantitative cerebral blood flow in schizophrenia measured by pulsed arterial spin labeling perfusion MRI." Psychiatry Research **194**(1): 64-72.
Poppenk, J. and M. Moscovitch (2011). "A hippocampal marker of recollection memory ability among healthy young adults: contributions of posterior and anterior segments." Neuron **72**(6): 931-937.
Preston, A. R., D. Shohamy, et al. (2005). "Hippocampal function, declarative memory, and schizophrenia: anatomic and functional neuroimaging considerations." Current neurology and neuroscience reports **5**(4): 249-256.
Pruessner, J. C., L. M. Li, et al. (2000). "Volumetry of hippocampus and amygdala with high-resolution MRI and three-dimensional analysis software: minimizing the discrepancies between laboratories." Cerebral cortex **10**(4): 433-442.
Ragland, J. D., R. C. Gur, et al. (2001). "Effect of schizophrenia on frontotemporal activity during word encoding and recognition: a PET cerebral blood flow study." The American journal of psychiatry **158**(7): 1114-1125.
Rane, S., Talati, P., Donahue, MJ., Heckers SH. (2015). "iVASO reproducibility of the hippocampus and cortex at different blood water nulling times." Magnetic Resonance in Medicine **In press.**
Renshaw, P. F., J. M. Levin, et al. (1997). "Dynamic susceptibility contrast magnetic resonance imaging in neuropsychiatry: present utility and future promise." European Radiology **7 Suppl 5**: 216-221.
Restom, K., K. J. Bangen, et al. (2007). "Cerebral blood flow and BOLD responses to a memory encoding task: a comparison between healthy young and elderly adults." NeuroImage **37**(2): 430-439.
Rosoklija, G., G. Toomayan, et al. (2000). "Structural abnormalities of subicular dendrites in subjects with schizophrenia and mood disorders: preliminary findings." Archives of general psychiatry **57**(4): 349-356.
Rusinek, H., M. Brys, et al. (2011). "Hippocampal blood flow in normal aging measured with arterial spin labeling at 3T." Magnetic resonance in medicine : official journal of the Society of Magnetic Resonance in Medicine / Society of Magnetic Resonance in Medicine **65**(1): 128-137.
Sakaie, K. E., W. Shin, et al. (2005). "Method for improving the accuracy of quantitative cerebral perfusion imaging." Journal of magnetic resonance imaging : JMRI **21**(5): 512-519.
Scheef, L., C. Manka, et al. (2010). "Resting-state perfusion in nonmedicated schizophrenic patients: a continuous arterial spin-labeling 3.0-T MR study." Radiology **256**(1): 253-260.
Schmidt, B., D. F. Marrone, et al. (2012). "Disambiguating the similar: the dentate gyrus and pattern separation." Behavioural brain research **226**(1): 56-65.
Schobel, S. A., N. H. Chaudhury, et al. (2013). "Imaging patients with psychosis and a mouse model establishes a spreading pattern of hippocampal dysfunction and implicates glutamate as a driver." Neuron **78**(1): 81-93.

Schobel, S. A., N. M. Lewandowski, et al. (2009). "Differential targeting of the CA1 subfield of the hippocampal formation by schizophrenia and related psychotic disorders." Archives of General Psychiatry **66**(9): 938-946.
Schwarzbauer, C., J. Syha, et al. (1993). "Quantification of regional blood volumes by rapid T1 mapping." Magnetic resonance in medicine : official journal of the Society of Magnetic Resonance in Medicine / Society of Magnetic Resonance in Medicine **29**(5): 709-712.
Shenton, M. E., C. C. Dickey, et al. (2001). "A review of MRI findings in schizophrenia." Schizophrenia research **49**(1-2): 1-52.
Shiroishi, M. S., G. Castellazzi, et al. (2015). "Principles of T2 *-weighted dynamic susceptibility contrast MRI technique in brain tumor imaging." Journal of magnetic resonance imaging : JMRI **41**(2): 296-313.
Simic, G., I. Kostovic, et al. (1997). "Volume and number of neurons of the human hippocampal formation in normal aging and Alzheimer's disease." The Journal of comparative neurology **379**(4): 482-494.
Simonsen, C. Z., L. Ostergaard, et al. (1999). "CBF and CBV measurements by USPIO bolus tracking: reproducibility and comparison with Gd-based values." Journal of Magnetic Resonance Imaging **9**(2): 342-347.
Small, S. A., S. A. Schobel, et al. (2011). "A pathophysiological framework of hippocampal dysfunction in ageing and disease." Nature reviews. Neuroscience **12**(10): 585-601.
Small, S. A., S. A. Schobel, et al. (2011). "A pathophysiological framework of hippocampal dysfunction in ageing and disease." Nature Reviews: Neuroscience **12**(10): 585-601.
Smith, G. N., D. J. Lang, et al. (2003). "Developmental abnormalities of the hippocampus in first-episode schizophrenia." Biological psychiatry **53**(7): 555-561.
Snyder, J. S., R. Radik, et al. (2009). "Anatomical gradients of adult neurogenesis and activity: young neurons in the ventral dentate gyrus are activated by water maze training." Hippocampus **19**(4): 360-370.
Stafstrom, C. E. (2005). "The role of the subiculum in epilepsy and epileptogenesis." Epilepsy currents / American Epilepsy Society **5**(4): 121-129.
Steen, R. G., C. Mull, et al. (2006). "Brain volume in first-episode schizophrenia: systematic review and meta-analysis of magnetic resonance imaging studies." The British journal of psychiatry : the journal of mental science **188**: 510-518.
Stefanovic, B. and G. B. Pike (2005). "Venous refocusing for volume estimation: VERVE functional magnetic resonance imaging." Magnetic Resonance in Medicine **53**(2): 339-347.
Stewart, G. N. (1893). "Researches on the Circulation Time in Organs and on the Influences which affect it: Parts I.-III." The Journal of physiology **15**(1-2): 1-89.
Styner, M., I. Oguz, et al. (2006). "Framework for the Statistical Shape Analysis of Brain Structures using SPHARM-PDM." The insight journal(1071): 242-250.
Suthana, N. A., M. Donix, et al. (2015). "High-resolution 7T fMRI of Human Hippocampal Subfields during Associative Learning." Journal of cognitive neuroscience **27**(6): 1194-1206.
Swain, R. A., A. B. Harris, et al. (2003). "Prolonged exercise induces angiogenesis and increases cerebral blood volume in primary motor cortex of the rat." Neuroscience **117**(4): 1037-1046.
Szaflarski, J. P., S. K. Holland, et al. (2004). "High-resolution functional MRI at 3T in healthy and epilepsy subjects: hippocampal activation with picture encoding task." Epilepsy & behavior : E&B **5**(2): 244-252.
Talati, P., S. Rane, et al. (2014). "Increased hippocampal CA1 cerebral blood volume in schizophrenia." NeuroImage: Clinical **5**: 359-364.
Talati, P., S. Rane, et al. (2014). "Anterior-Posterior Cerebral Blood Volume Gradient in Human Subiculum." Hippocampus **24**(5): 503-509.

Talati, P., S. Rane, et al. (2015). "Increased hippocampal blood volume and normal blood flow in schizophrenia." Psychiatry research **232**(3): 219-225.
Tamminga, C. A., S. Southcott, et al. (2012). "Glutamate dysfunction in hippocampus: relevance of dentate gyrus and CA3 signaling." Schizophrenia bulletin **38**(5): 927-935.
Tamminga, C. A., A. D. Stan, et al. (2010). "The hippocampal formation in schizophrenia." The American journal of psychiatry **167**(10): 1178-1193.
Tamminga, C. A., G. K. Thaker, et al. (1992). "Limbic system abnormalities identified in schizophrenia using positron emission tomography with fluorodeoxyglucose and neocortical alterations with deficit syndrome." Archives of General Psychiatry **49**(7): 522-530.
Tanaka, Y., T. Nagaoka, et al. (2011). "Arterial spin labeling and dynamic susceptibility contrast CBF MRI in postischemic hyperperfusion, hypercapnia, and after mannitol injection." Journal of Cerebral Blood Flow and Metabolism **31**(6): 1403-1411.
Tandon, R., W. Gaebel, et al. (2013). "Definition and description of schizophrenia in the DSM-5." Schizophrenia research **150**(1): 3-10.
Theberge, J. (2008). "Perfusion magnetic resonance imaging in psychiatry." Topics in Magnetic Resonance Imaging **19**(2): 111-130.
Theberge, J., R. Bartha, et al. (2002). "Glutamate and glutamine measured with 4.0 T proton MRS in never-treated patients with schizophrenia and healthy volunteers." The American journal of psychiatry **159**(11): 1944-1946.
Thomas, B. P., E. B. Welch, et al. (2008). "High-resolution 7T MRI of the human hippocampus in vivo." Journal of magnetic resonance imaging : JMRI **28**(5): 1266-1272.
Thomas, D. L., M. F. Lythgoe, et al. (2006). "Regional variation of cerebral blood flow and arterial transit time in the normal and hypoperfused rat brain measured using continuous arterial spin labeling MRI." Journal of cerebral blood flow and metabolism : official journal of the International Society of Cerebral Blood Flow and Metabolism **26**(2): 274-282.
Tregellas, J. R. (2013). "Neuroimaging Biomarkers for Early Drug Development in Schizophrenia." Biological Psychiatry.
Tregellas, J. R. (2014). "Neuroimaging biomarkers for early drug development in schizophrenia." Biological psychiatry **76**(2): 111-119.
Tregellas, J. R., J. Smucny, et al. (2014). "Intrinsic hippocampal activity as a biomarker for cognition and symptoms in schizophrenia." The American journal of psychiatry **171**(5): 549-556.
Tukey, J. W. (1977). Exploratory data analysis. Reading, Mass., Addison-Wesley Pub. Co.
van Osch, M. J., J. van der Grond, et al. (2005). "Partial volume effects on arterial input functions: shape and amplitude distortions and their correction." Journal of Magnetic Resonance Imaging **22**(6): 704-709.
Velakoulis, D., S. J. Wood, et al. (2006). "Hippocampal and amygdala volumes according to psychosis stage and diagnosis: a magnetic resonance imaging study of chronic schizophrenia, first-episode psychosis, and ultra-high-risk individuals." Archives of general psychiatry **63**(2): 139-149.
Vinogradova, O. S. (2001). "Hippocampus as comparator: role of the two input and two output systems of the hippocampus in selection and registration of information." Hippocampus **11**(5): 578-598.
Vita, A., S. Bressi, et al. (1995). "High-resolution SPECT study of regional cerebral blood flow in drug-free and drug-naive schizophrenic patients." The American Journal of Psychiatry **152**(6): 876-882.
Vita, A., L. De Peri, et al. (2006). "Brain morphology in first-episode schizophrenia: a meta-analysis of quantitative magnetic resonance imaging studies." Schizophrenia research **82**(1): 75-88.
Walther, S., A. Federspiel, et al. (2011). "Resting state cerebral blood flow and objective motor activity reveal basal ganglia dysfunction in schizophrenia." Psychiatry Research **192**(2): 117-124.

Wang, D. J., J. R. Alger, et al. (2013). "Multi-delay multi-parametric arterial spin-labeled perfusion MRI in acute ischemic stroke - Comparison with dynamic susceptibility contrast enhanced perfusion imaging." NeuroImage. Clinical **3**: 1-7.

Wang, D. J., J. R. Alger, et al. (2013). "Multi-delay multi-parametric arterial spin-labeled perfusion MRI in acute ischemic stroke - Comparison with dynamic susceptibility contrast enhanced perfusion imaging." NeuroImage: Clinical **3**: 1-7.

Wang, J., D. C. Alsop, et al. (2003). "Arterial transit time imaging with flow encoding arterial spin tagging (FEAST)." Magnetic resonance in medicine : official journal of the Society of Magnetic Resonance in Medicine / Society of Magnetic Resonance in Medicine **50**(3): 599-607.

Watson, D. R., F. Bai, et al. (2012). "Structural changes in the hippocampus and amygdala at first episode of psychosis." Brain imaging and behavior **6**(1): 49-60.

Weiss, A. P. and S. Heckers (1999). "Neuroimaging of hallucinations: a review of the literature." Psychiatry research **92**(2-3): 61-74.

Weiss, A. P., D. L. Schacter, et al. (2003). "Impaired hippocampal recruitment during normal modulation of memory performance in schizophrenia." Biological psychiatry **53**(1): 48-55.

White, C. M., W. B. Pope, et al. (2014). "Regional and voxel-wise comparisons of blood flow measurements between dynamic susceptibility contrast magnetic resonance imaging (DSC-MRI) and arterial spin labeling (ASL) in brain tumors." Journal of Neuroimaging **24**(1): 23-30.

Willard, S. L., D. P. Friedman, et al. (2009). "Anterior hippocampal volume is reduced in behaviorally depressed female cynomolgus macaques." Psychoneuroendocrinology **34**(10): 1469-1475.

Willard, S. L., D. R. Riddle, et al. (2013). "Cell Number and Neuropil Alterations in Subregions of the Anterior Hippocampus in a Female Monkey Model of Depression." Biological psychiatry.

Williams, L. E., S. N. Avery, et al. (2012). "Intact relational memory and normal hippocampal structure in the early stage of psychosis." Biological psychiatry **71**(2): 105-113.

Wintermark, M., M. Sesay, et al. (2005). "Comparative overview of brain perfusion imaging techniques." Stroke; a journal of cerebral circulation **36**(9): e83-99.

Wintermark, M., M. Sesay, et al. (2005). "Comparative overview of brain perfusion imaging techniques." Stroke **36**(9): e83-99.

Witter, M. P., F. G. Wouterlood, et al. (2000). "Anatomical organization of the parahippocampal-hippocampal network." Annals of the New York Academy of Sciences **911**: 1-24.

Woolard, A. A. and S. Heckers (2012). "Anatomical and functional correlates of human hippocampal volume asymmetry." Psychiatry research **201**(1): 48-53.

Wu, B., X. Lou, et al. (2014). "Intra- and interscanner reliability and reproducibility of 3D whole-brain pseudo-continuous arterial spin-labeling MR perfusion at 3T." Journal of Magnetic Resonance Imaging **39**(2): 402-409.

Xu, G., H. A. Rowley, et al. (2010). "Reliability and precision of pseudo-continuous arterial spin labeling perfusion MRI on 3.0 T and comparison with 15O-water PET in elderly subjects at risk for Alzheimer's disease." NMR in Biomedicine **23**(3): 286-293.

Zaharchuk, G., I. S. El Mogy, et al. (2012). "Comparison of arterial spin labeling and bolus perfusion-weighted imaging for detecting mismatch in acute stroke." Stroke **43**(7): 1843-1848.

Zaro-Weber, O., W. Moeller-Hartmann, et al. (2012). "Influence of the arterial input function on absolute and relative perfusion-weighted imaging penumbral flow detection: a validation with (1)(5)O-water positron emission tomography." Stroke **43**(2): 378-385.

Zhang, Z. J. and G. P. Reynolds (2002). "A selective decrease in the relative density of parvalbumin-immunoreactive neurons in the hippocampus in schizophrenia." Schizophrenia Research **55**(1-2): 1-10.

Zierhut, K. C., R. Grassmann, et al. (2013). "Hippocampal CA1 deformity is related to symptom severity and antipsychotic dosage in schizophrenia." Brain : a journal of neurology **136**(Pt 3): 804-814.